

This is to certify that the

dissertation entitled

A Tandem Time-of-Flight Mass Spectrometer: MS/MS on the Chromatographic Time Scale

presented by

Mary Ann Seeterlin

has been accepted towards fulfillment of the requirements for

Ph. D. degree in Chemistry

Major professor

Date 1/24/94

MSU is an Affirmative Action/Equal Opportunity Institution

0-12771



LIBRARY
Michigan State
University

PLACE IN RETURN BOX to remove this checkout from your record. TO AVOID FINES return on or before date due.

| DATE DUE | DATE DUE | DATE DUE |
|----------|----------|----------|
| | | |
| | | |
| | | |
| | | |
| | | |
| | | |
| | | |

MSU is An Affirmative Action/Equal Opportunity Institution

A TANDEM TIME-OF-FLIGHT MASS SPECTROMETER: MS/MS ON THE CHROMATOGRAPHIC TIME SCALE

Ву

Mary Ann Seeterlin

Advisor: Christie G. Enke

A DISSERTATION

Submitted to
Michigan State University
in partial fulfillment of the requirements
for the degree of

DOCTOR OF PHILOSOPHY

Department of Chemistry

ABSTRACT

A TANDEM TIME-OF-FLIGHT MASS SPECTROMETER: MS/MS ON THE CHROMATOGRAPHIC TIME SCALE

By

Mary A. Seeterlin

The tandem time-of-flight (TOF/TOF) instrument constructed has been designed to obtain complete MS/MS spectra from compounds eluting from a capillary gas chromatographic column, while maintaining unit mass resolution for both precursor ion selection and product ion analysis. To meet this goal, the instrument needs to acquire at least 10 product spectra per second. Such spectral generation rates require maximum utilization of sample molecules and ions, efficient fragmentation of precursor ions, and array detection of the product ions produced. The use of continuous electron impact ionization with ion storage between pulsed extractions, TOF separation and reflectron focusing of precursor ions, pulsed laser photo-induced dissociation (PID), TOF separation and reflectron focusing of product ions, and array detection of all products formed, meets each of these criteria.

The electron impact source designed for this instrument utilizes two opposing filaments which continuously emit electrons. Reduced ion loss rates achieved by this source yield a high density of ions in each parent ion packet. An extraction pulse applied to the rear electrode accelerates the ions out of the

ionization region. The spatial distribution of the ions in the source is focused at a space-focus plane just outside of the source [1].

Precursor ion packets are separated due to their mass dependent velocities. A grid-free reflectron [2] focuses the space-focus plane image at the interaction region. The timing of a 15 ns excimer laser pulse selects the desired precursor ion packet with unit mass resolution to 1000. The high degree of spatial and temporal overlap obtained by this instrument provides optimal photodissociation efficiency.

After fragmentation, acceleration of the ions just following the interaction region gives the product ions mass dependent velocities and reduces the relative range of the product ion kinetic energies. A second reflectron will focus the interaction region image at a detector.

This system is capable of generating 500 transients per second (limited by the laser). If approximately 50 transients are summed for each product spectrum, 10 product spectra per second will be produced. With this rate of acquisition a substantial amount of MS/MS information can be obtained for a chromatographically eluted component.

References

- B. A. Mamyrin, V. I. Krataev, K. V. Shmikk, and V. A. Zagulin, Sov. Phys. JETP, 1973, 37, 45.
- 2 R. Grix, U. Gruner, G. Li, H. Stroh, H. Wollnik, *Int J. Mass Spectrom. Ion Proc.*, **1989**, 93, 323.

flight - of - time

ACKNOWLEDGMENTS

Often, as I explained to friends and family my thesis work, they would say that it sounded much like a job. I must admit that some days it felt more like a job than school, but looking back at how I've grown over the last five years, I realize that the project itself was the means through which I was taught, like homework in a course. The product of this thesis is not simply an analytical instrument but rather my personal growth - in confidence, independence and critical thinking. I am indebted to many for my education. Foremost, I acknowledge and thank Dr. Enke. Always there at an impasse, and always far away when I struggled through the problems which I was capable of solving on my own. His guidance, enthusiasm and trust have been cherished. For my degree in philosophy, I couldn't have made a better choice of advisor.

Studying with others has always made learning not only much more enjoyable, but also much more efficient and insightful. In research, I found this to be equally true. Working with George Yefchak, Raimond Grix, Dave McLane, Ben Gardner, Paul Vlasak, Doug Beussman, Sherri Delbert and Qinchung Li has been great. Throwing ideas back and forth, no matter how undeveloped, between such receptive minds has been very stimulating, and has helped me to gain confidence with my ability to be creative.

This thesis is also the product of many people who enjoy learning so much that they want to share it. I have been lucky to have had Mr. Levigne, Mr. Oldham, Mr. Male, Mr. Burgett, Mr. Rule, Mr Stallcup, Dr. Blecker, Dr. Richardson, Dr. Kren, Dr. Salari and Dr. Cope, Dr. Crouch, Dr. Allison, Dr.

Reusch and Dr. Leroi. Every step in my career as a student, I have always had an inspiring guide. Luckier still am I to have learned with great friends. Jim Ridge, my study buddy, has taught me more than any other teacher. Learning together has been fun. Mark Cole, and his contagious enthusiasm for knowledge has taught me about science, politics, life and myself. I will always be thankful for this.

Last, but most important, I would like to acknowledge my family. They have and continue to give me encouragement and guidance in life and I could not have gotten here without them. My dad and mom showed me how to see my goal, see it finished, and make my work something to be proud of. They also showed me to enjoy life along the way. With my brothers I learned the secrets and joys of working with a team, and as I have been recently reminded, that a team members success is often twice as sweet. John, my husband and closest friend has shared and shares the joys, excitement and frustrations of life, making everything that much more worth doing.

Wonderful family, teachers, friends, health . . for these I thank God and trust him with my future.

Table of Contents

| Chapter 1: Introduction | 1 |
|---|----|
| 1.1 Tandem Mass Spectrometry (MS/MS) | 1 |
| 1.2 Mass Spectrometers | 4 |
| 1.3 Existing Instrumentation for MS/MS | 7 |
| 1.4 MS/MS on the Chromatographic Time Scale | 8 |
| 1.5 A Tandem Time-of-Flight Mass Spectrometer | 9 |
| Chapter 2: Time-of-Flight Mass Spectrometry | 16 |
| 2.1 Advantages of Time-of-Flight Analysis | 16 |
| 2.2 TOF Resolution - Problems | 20 |
| 2.3 TOF Resolution - Breakthroughs | 20 |
| 2.4 Time-Array Detection | 24 |
| Chapter 3: An Electron Impact Ionization Storage Source | 28 |
| 3.1 Ion Storage for TOFMS | 28 |
| 3.2 The Storage Well | 29 |
| 3.3 A Mathematical Model of Ion Storage | 35 |
| 3.4 Effects of Helium & High Frequency Field Modulation | 41 |
| 3.5 Effects of Source Design | 51 |
| 3.6 The TOF/TOF Source | 54 |
| Chapter 4: TOF/TOF Instrumentation | 59 |
| 4.1 Instrument Overview | 59 |
| 4.2 Description | 62 |
| 4.2.1 Vacuum Chamber | 62 |
| 4.2.2 Vacuum System | 64 |
| 4.2.3 Sample Introduction | 64 |
| 4.2.4 First TOF Analyzer | 65 |
| 4.2.4.1 Source Extraction | |
| 4.2.4.2 High Voltage Shield | |
| 4.2.4.3 Einzel Lens and Steering Plates | 66 |

| 4.2.4.4 First Reflectron | 68 |
|--|-----|
| 4.2.4.5 First Detector | 68 |
| 4.2.5 Interaction Region | 71 |
| 4.2.5.1 Optical Rail | 73 |
| 4.2.5.2 Gate | 73 |
| 4.2.5.3 Light Tube | 74 |
| 4.2.6 Second TOF Analyzer | 76 |
| 4.2.6.1 Post Acceleration | 76 |
| 4.2.6.2 Reflectron 2 | 76 |
| 4.2.6.3 Detector 2 | 76 |
| 4.3 Performance | 77 |
| 4.3.1 Resolution | 77 |
| 4.3.2 Beam Image | 77 |
| 4.3.3 Preliminary Gate Studies | 81 |
| Chapter 5: Photo-Induced Dissociation | 84 |
| 5.1 Introduction to Photo-Induced Dissociation | 84 |
| 5.2 PID in the TOF/TOF Instrument | 86 |
| 5.3 Results and Discussion | 87 |
| 5.3.1 Precursor Selection | 87 |
| 5.3.2 PID Efficiency | 89 |
| 5.3.3 Photoionization | 94 |
| Chapter 6: Product Ion Analysis | 99 |
| 6.1 Historical Use of TOF for Product Ion Analysis | 99 |
| 6.2 TOF Product Ion Analysis in the TOF/TOF Instrument | 100 |
| 6.3 Theoretically Modeled Resolution | 101 |
| 6.4 Performance | 103 |
| 6.5 The Second Reflectron | 105 |
| Chanter 7: Conclusions | 110 |

LIST OF FIGURES

| 1.1 | Schematic representation of the collection of an MS/MS product spectrum. | 3 |
|-----|---|----|
| 1.2 | Diagram of a time-of-flight mass spectrometer. Ions formed in the ion source are accelerated out periodically. Isomass ion packets separate in time due to their mass dependent velocities and are detected. | 6 |
| 1.3 | Schematic diagram of the tandem time-of-flight mass instrument | 12 |
| 2.1 | Diagram of a quadrupole mass spectrometer, demonstrating the filtering nature of mass analysis | 19 |
| 2.2 | Depiction of the ion spatial and energy effects on TOF resolution. lons in the source have a spatial and energy distribution which account for a distribution of arrival times at the detector. | 21 |
| 2.3 | Schematic representation of the energy focusing effect of the reflectron. Ions at the space-focus plane have a distribution of energies. An ion with more energy spends more time on the potential hill created by the reflectron than a slower ion. If the reflectron is tuned properly this extra time spent in the reflectron matches the difference in time the ions spend in the field free region, and they come to a temporal focus at the detector. | 23 |
| 3.1 | A 10,000 fold increase in peak detector current would be achieved in a TOF instrument capable of ion storage over an instrument which could detect all of the ions continuously extracted. | 30 |
| 3.2 | Diagram of the storage source developed in Professor Wollnik's laboratory. This source is rotationally symmetric about the ion optical axis. G ₄ -G ₁ are grided electrodes, for acceleration, and storage. Pu are "pusher" electrodes responsible for focusing the electrons generated by (K) the filament into the storage area | 31 |
| 3.3 | Graph of peak intensity (m/z = 18) versus the voltage applied to the center grid (G3) | 33 |
| 3.4 | Voltages applied to the source electrodes in both theoretical and experimental operation. | 34 |

| 3.5 | Theoretical graph of ion peak intensity versus the ionization time37 |
|------|---|
| 3.6 | Graph of peak intensity (m/z=44) versus ionization time |
| 3.7 | Predicted ion population growth curves for different analyte partial pressures |
| 3.8 | Effect of analyte pressure on the ion population growth curves of CHBr ₃ 40 |
| 3.9 | Normalized ion loss curves for ion s of different m/z42 |
| 3.10 | lon growth curves for a background analyte at different helium pressures |
| 3.11 | Visual model of the process of ion storage and the effect of the tremendous number of helium ions on the loss of analyte ions |
| 3.12 | Ion storage curve for m/z = 4 (He+)46 |
| 3.13 | Effect of source pressure (due to He flow) on analyte peak (m/z = 58) intensity |
| 3.14 | Simulated effect of a 2MHz, 30Vp-p ac voltage on the trajectory of ions with m/z=4,28,52, and 76. Ions, starting with 5 eV of kinetic energy and angle = 90 degrees, are oscillated from side to side in the source, causing ions of lower mass to be accelerated out |
| 3.15 | lon population growth curves with and without the application of an ac voltage |
| 3.16 | Background spectra with and without the application of an ac voltage. Note the increase in intensity for the higher massed ions when the ac voltage is applied |
| 3.17 | Two different source designs depicting the use of a circular cage, and a square cage |
| 3.18 | Schematic diagram of the TOF/TOF source55 |
| 3.19 | Ion population growth curve for the TOF/TOF source56 |
| 4.1 | Schematic diagram of the TOF/TOF instrument and control system60 |
| 4.2 | Blueprint of the TOF/TOF vacuum chamber63 |

| 4.3 | SIMION model of an Einzel lens system. Collimated ions of equal energy are focused to a point using an Einzel lens created by the voltages applied to three "washer" electrodes. The outer two electrodes are held at the same potential while the center electrode is held at a either a negative potential (in this case) or a positive potential with respect to the other two. | 67 |
|------|--|----|
| 4.4 | SIMION model of Wollnik's grid-free reflectron. The reflectron is made up of large "washer" electrodes which have voltages applied to them. Ions which enter the reflectron will travel up the potential field, stop, and be accelerated out. As depicted in this model ions of greater energy travel further into the reflectron than ions of lower energy. | 69 |
| 4.5 | SIMION model of the modified grid-free reflectron used in the first TOF analyzer. This reflectron does not have the "lips" in the Wollnik design, yet the contours are not significantly different | 70 |
| 4.6 | The top (A) and side (B) views of the ion trajectory through the TOF/TOF instrument. | 72 |
| 4.7 | SIMION model of the ion gate. This gate is made of fine wires (0.003" diameter). Alternate wires are held at +300V and -300V. The potential field generated by these alternating electrodes extends only a few millimeters. This short field allows for the selective gating of closely bunched ion packets and thus high resolution gating. | 75 |
| 4.8 | Mass spectrum of bromobenzene collected with a detector at the interaction region, showing resolution of 1500 (FWHM) for the molecular ion ($m/z = 156$ and 158). | 78 |
| 4.9 | Mass spectrum for the monoisotopic molecular ion (m/z = 158) of bromobenzene collected with a detector placed at the end of the second TOF analyzer, showing resolution greater than 1700 (FWHM). | 79 |
| 4.10 | Plot of the intensity of m/z = 18 as a function of the iris diaphragm aperture area. | 80 |
| 4.11 | Plot of ion intensity versus the potential difference applied between alternate wires of the deflection grid | 82 |
| 5.1 | Spectra of the molecular ion region of bromobenzene. a. Spectrum with the laser off. b-d. Spectra with the laser delay set at 86.40 µs, 86.70 µs and 86.97 µs, respectively | 88 |

| 5.2 | Diagram of the TOF/TOF instrument showing the location of the temporary detector approximately 12 inches after the interaction region | 91 |
|-----|---|-----|
| 5.3 | A product spectrum for the molecular ion (m/z = 156) of bromobenzene. | 92 |
| 5.4 | The spectrum resulting form the photoionization of residual gas molecules in the interaction region. | 96 |
| 6.1 | Simulated resolution of product ions for precursor ions with m/z = 500, 1000, and 2000. All fragment ions of precursor ions with m/z ≤ 1000 will have at least unit mass resolution | 104 |
| 6.2 | a. A spectrum of the molecular ion region of toluene obtained at the final detector. b. The spectrum of the molecular ion region of toluene when the laser is fired to interact with the molecular ion (m/z = 92). The peak at 109.4 μ s is m/z = 91 product ion | 106 |
| 6.3 | The bromobenzene product ion (m/z= 77) obtained after the second reflectron was retuned for lower kinetic energy ions | 107 |
| 6.4 | SIMION model of a hyperbolic reflectron. The two electrodes used to form this reflectron include a grid electrode and a hyperbolic electrode. In one model both of these electrodes extend perpendicular to this page and are of infinite length, in the other model these electrodes are symmetric about the x axis. Ions enter these mirrors at the origin of the grid electrode and travel towards the hyperbolic electrode with no y velocity component | 109 |
| 6.5 | Graph of the location an ion along the x axis versus time for ions with a large range of energies. The origin is located at $x = 75$. lons which have a wide range of different energies, and which are temporally focused at the origin when they enter the reflectron, exit the reflectron at the origin and are again in temporal focus. This simulation was performed on an extended monopole | 110 |
| 6.6 | Graph of the location an ion along the x axis versus time for ions with a large range of energies. The origin is located at $x = 75$. This simulation was performed on a conical reflectron. Ions which have a wide range of different energies, and which are temporally focused at the origin when they enter the reflectron, are not temporally focused with this reflectron. | 111 |

LIST OF TABLES

| 3.1 | lon storage time constants (1/kL) and ion formation rate constants (kF) for six different source designs | .53 |
|-----|--|-----|
| 5.1 | PID results for several precursor ion m/z values | 93 |

Chapter 1: Introduction

"... you can imagine my surprise when I arrived for work on my first day, to find on my desk a paper that read "Remit: Build a mass spectrometer.""

J. H. Beynon

1.1 Tandem Mass Spectrometry (MS/MS)

"I feel sure that there are many problems in Chemistry which could be solved with far greater ease by this than any other method. The method is surprisingly sensitive - more so even than that of spectrum analysis - requires an infinitesimal amount of material and does not require this to be specially purified:..."[1]

As the advantages of mass spectrometers impressed J. J. Thomson in 1913, the advantages of tandem mass spectrometers impress researchers today.

Since the introduction of tandem mass spectrometry in the 1970's, this technique has proven to be a valuable tool for an ever increasing number of analytical applications as well as for studies of fundamental phenomena. The analytical applications range from the analysis of relatively small organics such as environmental pollutants, industrial products, or food components to larger organic and bioorganic structures [2].

This multitude of applications stems from the variety of experiments possible with the many different MS/MS instruments available. Despite the differences, all MS/MS experiments involve the same fundamental elements: lonization of the sample is the first step and is most often accomplished using electron impact ionization. Bombarded by 70 eV electrons a neutral molecule in the vapor state obtains sufficient energy to eject one of its electrons thus becoming an ion. This ion typically has additional excess energy which results in fragmentation and the production of product ions of different m/z. A precursor m/z value is selected by the first mass analyzer in the MS/MS instrument. The selected precursor ions undergo a mass changing reaction in an interaction region, and lastly the ions formed in the interaction region are mass analyzed in the second stage of mass analysis. These steps are illustrated in Figure 1.1.

In contrast to a typical mass spectrum in which precursor ion/product ion relationships are unclear, MS/MS clearly establishes these relationships and is thus a valuable tool for structural elucidation of complex unknowns. A complete MS/MS data set contains a product spectrum for each ion present in the normal mass spectrum. Such data sets comprise all precursor-product reactions and are extremely useful for elucidating their structure. Although not currently available, libraries of MS/MS spectra would dramatically improve the accuracy of spectral searching techniques.

The widespread use of tandem mass spectrometry is due largely to its high sensitivity and selectivity [3]. Compared to a single mass analyzer, two analyzers in tandem eliminate a large percentage of chemical noise and dramatically lower the detection limits. In one type of experiment, the first mass analyzer performs a separation step while the second mass analyzer provides the data for compound identification. MS/MS also allows for trace analysis of target compounds in complex mixtures with minimal sample cleanup [4].

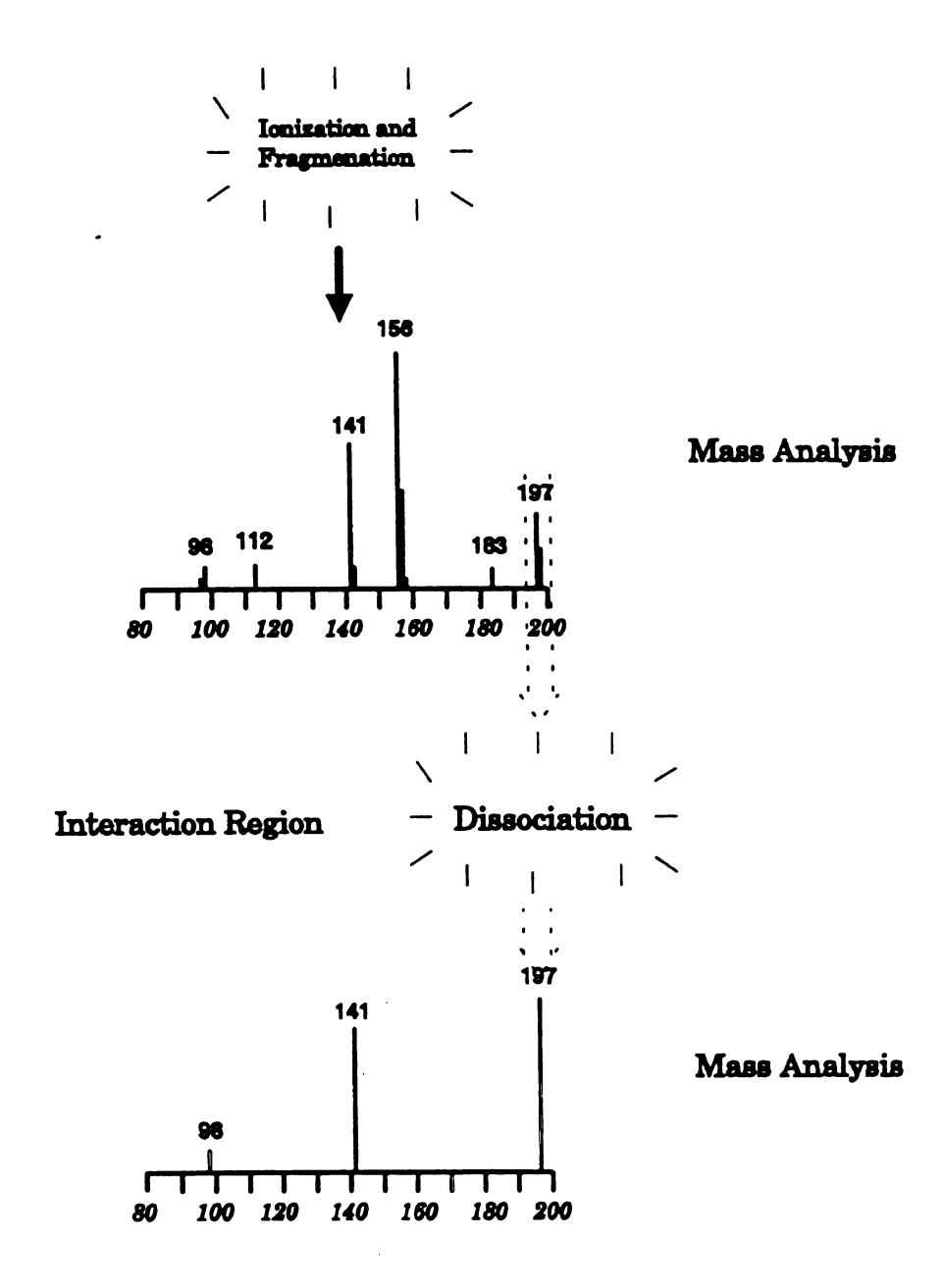


Figure 1.1 Schematic representation of the collection of an MS/MS product spectrum.

1.2 Mass Spectrometers

Mass analyzers measure the mass to charge ratio of ions. The flexibility and ease with which ions can be maneuvered with both electric and magnetic fields have led to many different mass analyzers. The magnetic sector, electric sector, quadrupole mass filter, Fourier transform-ion cyclotron resonance, ion trap and time-of-flight mass analyzers all are based on different principles of mass to charge separation or detection.

A magnetic sector uses a magnetic field to disperse ions according to their momentum [5]. In the presence of a magnetic field an ion travels in a circular path. The radius of this circular path is dependent on the momentum to charge ratio and the magnetic field strength. With a thin slit in front of a detector, a mass spectrum is obtained by scanning either the acceleration voltage of the source or the magnetic field.

In an electric sector [6] an ion travels in a circular path also. The radius of travel is dependent on the kinetic energy and the electric field strength. Used in conjunction with a magnetic sector and slits, the electric sector filters out all ions which fall outside a narrow spread of energies. This combination of devices provides very high resolution mass analysis. If, however, an ion fragments in the field-free region preceding the electric sector, it can act as a product ion mass analyzer by dispersing them according to their kinetic energy [7].

The quadrupole mass analyzer [8] consists of four symmetrically arranged parallel rods. Diagonally opposite rods are electrically connected and a combination of dc and rf potentials are applied to the rods. With the correct application of voltages, only ions with a narrow range of mass to charge ratio have stable trajectories through the quadrupole. Scanning these voltages allows sequential mass to charge values to pass, thus creating a mass spectrum.

Fourier transform-ion cyclotron resonance (FT-ICR) [9] and ion trap mass spectrometers (ITMS) differ from the previous instruments in that they are not beam instruments. Beam instruments form ions in one region, accelerate them into the scanning mass analyzer, and detect the ions allowed through. Each of these steps is performed in the same region of the ICR cell. This cell is located in a magnetic field. The ions formed by a pulse of electrons travel in a circular orbit with a frequency dependent upon the ion's mass-to-charge ratio and the magnetic field strength. A very fast rf sweep is made across a range of frequencies that corresponds to the desired mass range, causing the ions to travel together coherently. This coherent ion motion induces an image current in a set of receiver plates. The composite signal detected is due to the motion of all of the excited ions. The Fourier transform of this time domain spectrum yields a frequency domain spectrum which is can be relabeled as a mass spectrum after calibration.

The ITMS [10] is actually a three dimensional quadrupole, and the equations explaining the ion stability in the trap are very similar to the equations for stable ion trajectories in the quadrupole mass analyzer. In the most popular mode of operation, termed mass-selective instability, no dc potential is applied to the endcap electrode, producing an rf only quadrupole field. After an ionization period, all ions with m/z above a threshold value have stable trajectories within the trap. As the rf amplitude is increased, ions of increasing m/z value become sequentially unstable. These ions pass through holes in the endcaps and are detected.

Time-of-flight mass analysis [11], as depicted in Figure 1.2, is conceptually and mechanically very simple. Ions produced in the source are extracted with a high voltage pulse applied to the source backplate. All of the ions receive approximately the same kinetic energy. Ions of different mass to

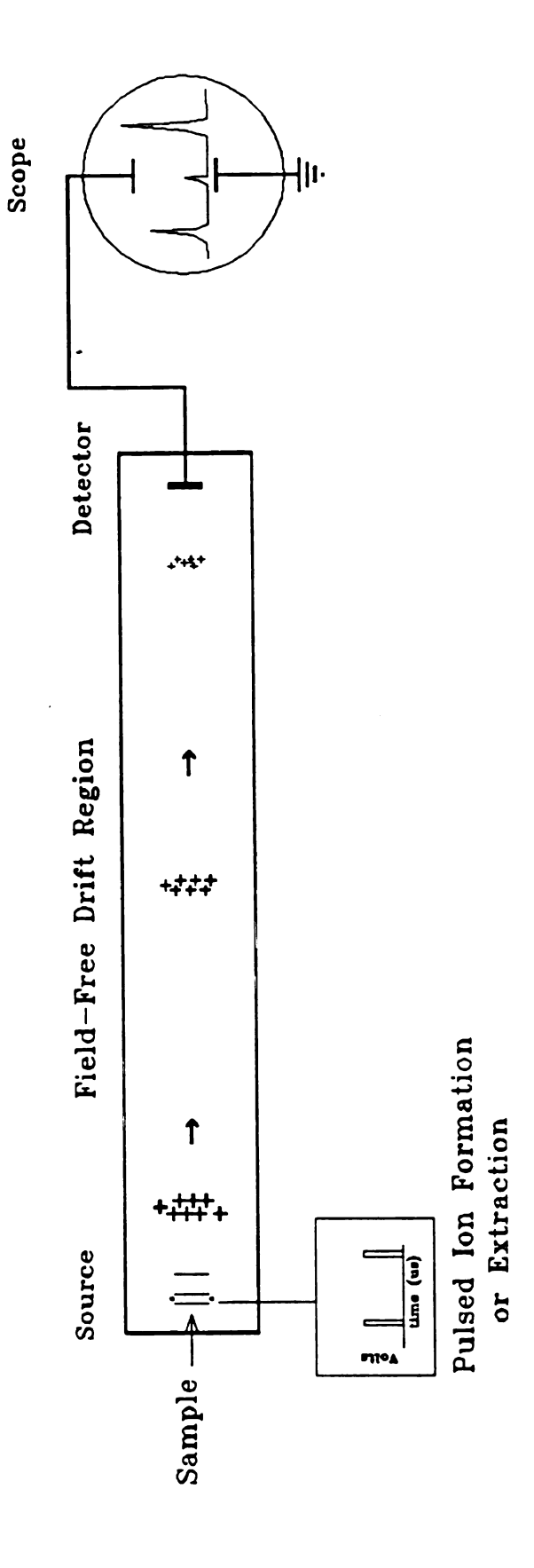


Figure 1.2 Diagram of a time-of-flight mass spectrometer. lons formed in the ion source are accelerated out periodically. Isomass ion packets separate in time due to their mass dependent velocities and are detected.

charge ratio have different velocities and isomass packets thus become separated in time as they travel down a field-free flight tube. These ion packets arrive at the detector at different times. A mass spectrum is created with each source extraction.

1.3 Existing Instrumentation for MS/MS

To obtain MS/MS spectra, two mass analyzers are typically used. As combinatorial mathematics would imply, this has led to a plethora of different instrument designs.

Sector based MS/MS instruments include single magnetic sector instruments which were used in the early stages of MS/MS work [12], two-sector instruments of the BE geometry [7] and the EB or "reverse" geometry [13] (where B and E refer to magnetic and electric sectors respectively) as well as three and four [14] sectored instruments. These instruments typically employ high energy collisional activation to induce fragmentation.

The first triple quadrupole instrument for MS/MS studies was introduced in 1978 [15]. This instrument has become very popular due to straightforward nature of the scanning procedures for product, precursor and neutral loss spectra, and the simplicity of operation especially under computer control. This instrument utilizes low energy collisions for precursor ion fragmentation.

Hybrid instruments, consisting of both sector and quadrupole instruments have also been developed [16]. These instruments take advantage of the different qualities of the analyzers and offer tremendous experimental versatility. The BEQQ instrument [17], for example, which incorporates a deceleration step before the first quadrupole, can yield both high and low energy fragmentation, as well as high resolution selection of precursor ions.

The two mass analysis stages of MS/MS can both be performed in the trapping FT-ICR [18] and ITMS [19] instruments. The ions produced in the ionization period are stored, as discussed earlier, in either a combination of magnetic and electric fields in a FT-ICR or with electric fields in an ITMS. Next, all ions except the desired precursor ions are scanned or ejected from the cell. The precursor ions of interest, left in the cell, are now excited enough to cause collisionally induced dissociation (CID) with background gas but not enough to be ejected from the cell. Product ions produced are then detected with the conventional methods. Multiple stages of MS (i.e., MSⁿ) are possible with both of these instruments.

1.4 MS/MS on the Chromatographic Time Scale

Chromatographic introduction of sample into an MS/MS instrument is routine. Experiments, however, typically involve monitoring a single reaction (SRM) or a few reactions [20] while the continuous chromatographic eluent flows into the source. Increasing the number of reactions monitored requires sacrificing ion statistics for each reaction due to the scanning nature of the second analyzer employed in most commercially available instrument.

To obtain a complete MS/MS data set from any commercially available instrument takes at least one minute. The speed of this acquisition is limited by the time it takes the second mass analyzer to scan the entire mass range while still producing product spectra with useful ion statistics. Modern chromatographic methods including gas chromatography (GC), high performance liquid chromatography (HPLC), and capillary zone electrophoresis (CZE), typically yield separated mixture components with peaks which are on the order of 1-5 seconds wide. Clearly, available MS/MS instrumentation is not able

to obtain complete MS/MS data set from such components because the components are not present in the source long enough. The design and construction of an instrument capable of obtaining complete MS/MS data set from compounds introduced chromatographically is the subject of this dissertation.

1.5 A Tandem Time-of-Flight Mass Spectrometer

In two sector MS/MS instruments and in triple quadrupole mass spectrometers, the acquisition of the product spectrum is the rate limiting step in the collection of a complete MS/MS data set. The choice of product ion mass analyzer is thus critical. The 100+ fold increase in acquisition speed needed from an MS/MS instrument compatible with chromatographic sample introduction requires that the second mass analyzer utilize array detection. Array detection has been demonstrated using a magnetic sector analyzer with multielement electrooptic ion array detection [21], a Fourier transform MS, and a time-of-flight mass spectrometer using array detection [22]. Using array detection the magnetic sector possesses only limited mass resolution when a large range of masses is studied. The FTMS requires successive, alternating introduction of the sample and the collision gas for each product spectrum and is therefore not a high speed technique. The time-of-flight mass analyzer, however, capable of producing thousands of transients per second, does not have these limitations and is thus a suitable candidate for array detection in an MS/MS instrument. Time-of-flight mass spectrometry will be examined more carefully in Chapter 2.

Time-of-flight mass analysis requires that ions start as discrete packets.

Techniques to produce such ion packets involve either deflecting a slice from a continuous beam or pulsing the source. For a time-of-flight analyzer to be used

for product ion analysis, the first mass analyzer for the new MS/MS instrument could therefore be a beam instrument (e.g., magnetic sector, quadrupole etc.) utilizing beam deflection to produce a discrete ion packet of precursor ions, or a time-of-flight instrument which produces temporally separated isomass ion packets. An instrument based upon a magnetic sector and time-of-flight instrument in tandem, and utilizing beam deflection was built in Dr. Enke's Using a technique termed time-resolved-ion-momentum mass laboratory. spectrometry (TRIMS) [23] a complete MS/MS spectrum could be obtained in 10 s. Although this is among the fastest speeds achieved to date, it is barely fast enough for the wide peaks obtained in packed column gas chromatography [24]. This instrument is limited by the inherently low scan rates of magnetic sectors since acquisition of the MS/MS spectra requires the scanning of the magnetic field. In addition, the poor duty cycle for the deflection technique wastes a large percentage of the ions.

We have chosen to use a time-of-flight mass analyzer for the first stage of mass analysis. By its nature a TOF analyzer yields discrete packets of separated isomass ions. In addition, the development of an electron impact source for TOF which stores the continuously generated ions between pulsed extraction, eliminates the waste of precursor ions. The characterization and improvement of this storage source for time-of-flight is detailed in Chapter 3.

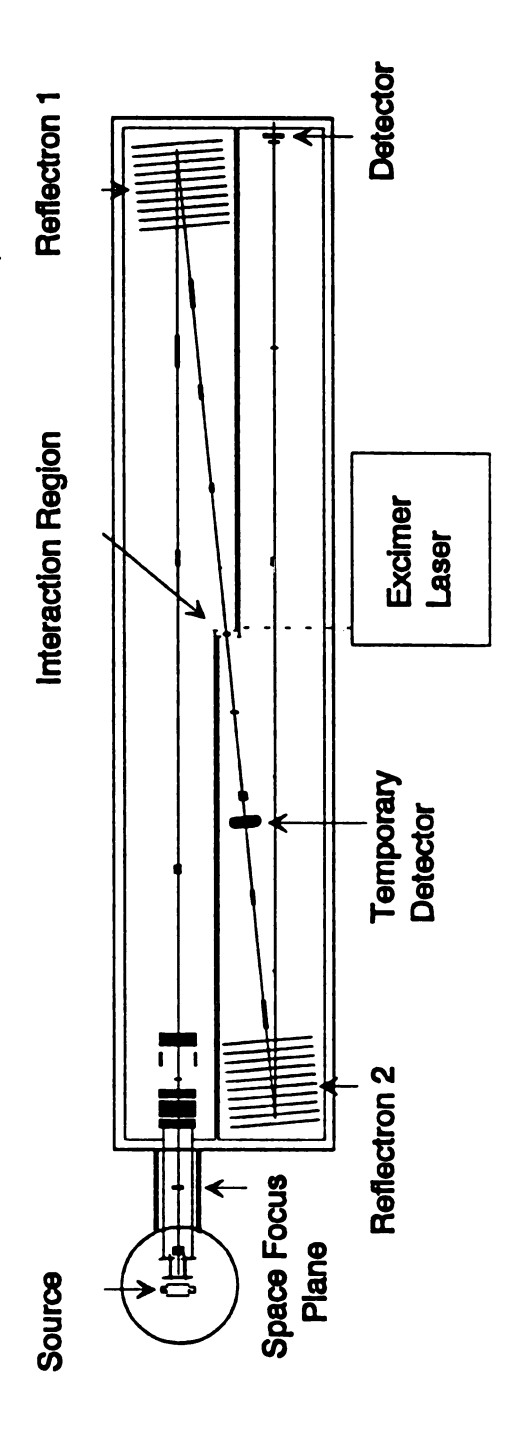
The choice of fragmentation technique was made on the basis of efficiency, ease, and minimum disruption of the ion kinetic energy distribution. Cornish and Cotter [25] have incorporated CID in their tandem time-of-flight mass spectrometer using a pulsed valve. This technique is a novel way to introduce collision gas into the ion path with minimal increase in the overall chamber gas pressure. Cooks [26] has used surface induced dissociation in his tandem time-of-flight instrument. Both of these methods yield useful

fragmentation but due to the collisional processes the resulting product ions possess a large range of kinetic energies which is detrimental to good resolution in TOF mass analysis. In addition, both rely upon a gate to select the desired precursor. This gating process results in limited mass resolution for precursor selection.

We have selected photo-induced dissociation (PID) as a means of fragmentation. PID has historically been plagued by low efficiency. This low efficiency has resulted from a very low interaction cross section and low ion densities. In the TOF/TOF instrument, however, the storage source together with time-of-flight produces a very high density of precursor ions at the interaction region. Combined with the high photon density of a high power laser, efficiency over 100% is theoretically possible. A more detailed description of the photo-induced dissociation process will be covered in Chapter 5.

Photo-induced dissociation with a pulsed laser also provides an excellent means for precursor m/z selection. The laser selected for this instrument provides pulses which are approximately 15-20 ns in duration. Focused to the width of the ion packets (approximately 1 mm), the dimensions of the laser pulse almost perfectly match those of the precursor ion packet. This ideal overlap results in precursor selection with resolution of approximately 1200. Laser selection of precursors, as well as demonstration of this efficient photo-induced dissociation will also be covered in Chapter 5.

The tandem time-of-flight instrument, depicted in Figure 1.3, was constructed in a stepwise manner. Chapter 4 contains a description of the instrumentation. The vacuum chamber and vacuum system, the TOF focusing elements necessary for both analyzers, the elements in the interaction region



Schematic diagram of the tandem time-of-flight mass instrument. Figure 1.3

will be as well as the resolving power and beam image produced by this instrument will be found in Chapter 4.

The second time-of-flight analyzer will be discussed in Chapter 6. A theoretical model of the expected resolution predicts unit mass resolution for precursors up to m/z = 1000. Preliminary experimental results of the second mass analyzer are also presented in Chapter 6.

References

- 1 Thomson, J. J., Rays of Positive Electricity and Their Applications to Chemical Analysis, Longmans: London, 1913.
- 2 K. L. Busch, G. L. Glish and S. A. McLuckey, *Mass Spectrometry/Mass Spectrometry: Techniques and Applications of Tandem Mass Spectrometry*, VCH Publishers Inc., New York, **1988**
- 3 J. V. Johnson, R. A Yost, *Anal. Chem.*, 57, 758A, 1985
- G. L. Glish, V. M. Shaddock, K. Harmon, R. G. Cooks, *Anal. Chem.*, 52,
 165, 1980
- 5 A. O. Nier, *Rev Sci. Instrum.*, 11, 212, **1940**
- H. E. Duckworth, S. N. Goshal, *Mass Spectrometry*, 1963, McGraw-Hill,
 New York, 201.
- M. Barber, R. M. Elliot, Presented at the ASTM E-14 Conference on Mass Spectrometry, Montreal, June 1964.
- P. H. Dawson, *Quadrupole Mass Spectrometry and Its Applications*, 1976, Elsevier, New York.

- 10 G. C. Stafford, P. E. Kelley, J. E. P. Syka, W. E. Reynolds, J. F. J. Todd, Int. J. Mass Spec. Ion Proc., 60, 85, 1984.
- 11 A. E. Cameron, D. F. Eggers Jr., Rev. Sci. Instrum, 19, 605, 1948.
- J. H. Beynon, J. W. Amy, W. E. Baitinger, *J. Chem. Soc Chem. Commun.*,1969, 723.
- 13 J. H. Beynon, R. M. Caprioli, T. Ast, *Org. Mass Spectrom.* 1971, 5, 229.
- F. W. McLafferty, P. J. Todd, D. C. McGilvery, M. A. Baldwin, J. Am Chem. Soc., 1980, 102, 3360.
- 15 R. A. Yost, C. G. Enke, *J. Am. Chem. Soc.*, **1978**, 100, 2274.
- 16 G. L. Glish, S. A. McLuckey, T. Y. Ridley, R. G. Cooks, *Int. J. Mass Spectrom. Ion Phys.*, 1982, 41, 157.
- 17 A. E. Schoen, J. W. Amy, J. D. Ciupek, R. G. Cooks, P. Dobberstein, G. Jung, *Int. J. Mass Spectrom. Ion Proc.* **1985**, 65, 125.
- 18 R. B. Cody, B. S. Freiser, *Int. J. Mass Spectrom. Ion Phys.*, **1982**, 41, 199.
- J. N. Louris, R. G. Cooks, J. E. P. Syka, P. E. Kelley, G. C. Stafford Jr., J.
 F. J. Todd, *Anal. Chem.* 1987, 59, 1677.
- 20 R. W. Kondrat, G. A. McClusky, R. G. Cooks, *Anal. Chem.* **1978**, 50, 2017.
- P. A. Leclercq, H. M. J. Snijders, C. A. Cramers, K. H. Maurer, U. Rapp, J. High Res. Chrom., 1989, 12, 652.

- E. D. Erickson, C. G. Enke, J. F. Holland, J. T. Watson, *Anal. Chem.*1990, 62, 1079.
- 23 J. T. Stults, C. G. Enke, J. F. Holland, *Anal. Chem.* **1983**, 55, 1323.
- 24 B. A. Eckenrode, J. T. Watson, C. G. Enke, *Anal. Chem.* **1990**, 62, 1362.
- ²⁵ T. J. Cornish, R. J. Cotter, *Anal. Chem.* **1993**, 65, 1043.
- ²⁶ K. Schey, R. G. Cooks, R. Grix, H. Wollnik, *Int. J. Mass Spectrom. Ion Proc.*, **1987**, 77, 29.

Chapter 2: Time-of-Flight Mass Spectrometry

"Perhaps nowhere in chemistry is the necessity for collaboration more clear than in creative work in instrumentation."

R. G. Cooks

2.1 Advantages of Time-of-Flight Analysis

"The mass spectrometer, in which ions are separated according to mass by passing the beam through a magnetic field, does not lend itself readily to the instantaneous display of the entire spectrum. Observation of the individual ion peaks is too slow when it is desirable to monitor a system in which the composition is changing rapidly as a function of time...(The velocitron) does, however, lend itself to the display of a mass spectrum which can be readily observed even though it changes rapidly as a function of time."[1]

First introduced in 1948 by Cameron and Eggers, the advantages of high acquisition speed possessed by the "velocitron" had been understood 11 years before a chromatograph and mass spectrometer were linked together. The spectral generation speed of time-of-flight spectrometers is limited by the transit time of the ion with highest m/z through the flight tube. Mass spectral generation

rates can be as high as 25 kHz [2]. As reviewed by MSU researchers, the mass spectral generation rates of other available mass analyzers are limited to 1-10 Hz [3]. The scan rate of the quadrupole is limited by the transit time of ions through the quadrupole. For efficient ion transmission the rf and dc potentials should not vary dramatically during the passage of an ion through the quadrupole. The magnetic sector mass spectrometer's spectral acquisition rate is limited by the rate at which the magnetic field can be swept. Limited to a scan rate of approximately 0.1 s/decade and requiring 0.2 s to reset the magnetic field, the magnetic sector can produce only 3-4 spectra/second. Both of these instruments are also limited in scan rate by the ion statistics necessary for useful spectra. The commercially available Saturn II ion trap scans at a rate of 5600 u/second. It can thus yield 9 scans/second when scanning from 30 to 650, but usually averages 3 "micro-scans" resulting in 3 spectra/second.

Interestingly, a time-of-flight mass analyzer was the first to be coupled with gas chromatography [2]. Today, however, quadrupoles are the most popular GC/MS analyzer. With the improvements in chromatographic separations yielding temporally narrower and narrower peaks [4], researchers are once again looking at time-of-flight MS for its high spectral generation rates.

The evolution of gas chromatography into a high resolution separation technique has been achieved mostly through the modification of the GC column. The original packed columns have given way to capillary columns of narrower and narrower width. Today chromatographic researchers are performing separations using capillary columns which have inner diameters as narrow as $10 \,\mu m$ [5]. As the columns become narrower the sample capacity of the columns drops dramatically. The amount of sample to be analyzed is increasingly less and the peak widths are increasingly narrower, placing a demand on both the detection limits of the mass spectrometer and its spectral generation rate. The

detection limits of time-of-flight mass analyzers are much lower than the scanning quadrupole and magnetic sector instruments. In scanning instruments over 99% of the ions produced in the source are not detected because ions of only one m/z value are allowed to reach the detector at any given time (see Figure 2.1). In magnetic sector instruments this inefficient use of ions is even worse due to the narrow slits needed to yield good resolution. Time-of-flight due to its non-scanning mode of analysis, and high ion transmission, yields very low detection limits, quoted to 5 picograms [6]. Ion trap mass spectrometers, also very sensitive, detect a large percentage of the ions produced. Ion traps, however, are limited in ionization duty cycle because the ionization and analysis steps occur in the same region.

High mass desorption/ionization techniques have also rekindled an interest in time-of-flight mass analyzers. The Cf-252 plasma desorption ionization technique introduced in 1974 [7] allows desorption ionization of large biological molecules, and was optimally suited for TOFMS. The fission-triggered ionization source not only allowed easy TOF measurement but, the ion formation occurred on a plane perpendicular to ion acceleration yielding good resolving power. Other high mass ionization techniques including laser desorption [8], secondary ion mass spectrometry (SIMS) [9] and supersonic molecular beam laser ionization also found TOF well suited for mass analysis due to its unlimited mass range, compatibility with event driven ion sources, and mechanical and electrical simplicity.

The numerous and significant advantages of time-of-flight analysis have driven researchers to overcome the limitations of the technique. They included very poor resolving power, low sample utilization duty cycle and inadequate data acquisition electronics.

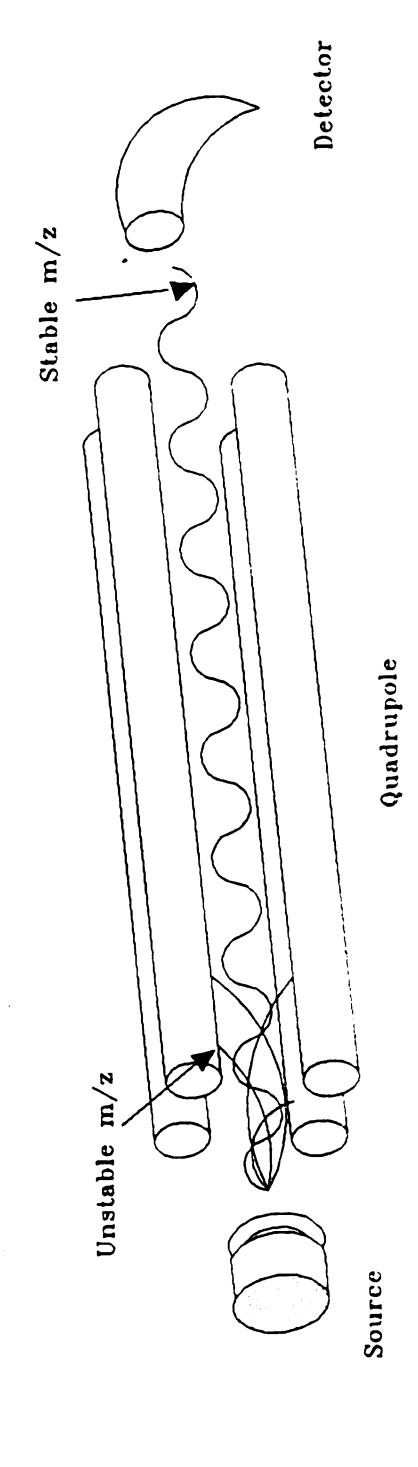


Figure 2.1 Diagram of a quadrupole mass spectrometer, demonstrating the filtering nature of mass analysis.

2.2 TOF Resolution - Problems

The time-of-flight instrument introduced by Cameron and Eggers in 1948 [1] had a flight path of 3 m, used beam deflection to form ion packets, photographs of the oscilloscope screen for data collection and had a resolution of about 2. Wolff and Stephens [10] improved the resolving power to 20 in their instrument which had a 1 m flight path and used a pulsed electron beam to create discrete ion packets. Katzenstein and Friedland [11] introduced a gated ion detector to allow integration of ions from successive cycles in 1955. Resolution was improved to 100 in their instrument which had a flight path of 1 m.

These early TOF instruments were limited in resolving power due to a combination of effects (see Figure 2.2). Ideally, all ions in a TOF source would start at the same point and have no initial kinetic energy. Unfortunately ions produced from gaseous samples start from a finite range of positions in the source, and have different initial kinetic energies. These effects result in a distribution of arrival times for isomass ions. In addition, those ions with initial trajectories away from the source must first decelerate, and turn around before being accelerated from the source. The delay between these ions and those which have an equal initial kinetic energy towards the detector is referred to as the turn-around time. This effect results in an additional spread of isomass ion packets.

2.3 TOF Resolution - Breakthroughs

In 1955, Wiley and McLaren [12] introduced two techniques for improving the resolving power of time-of-flight analysis. Using a two stage ion source,

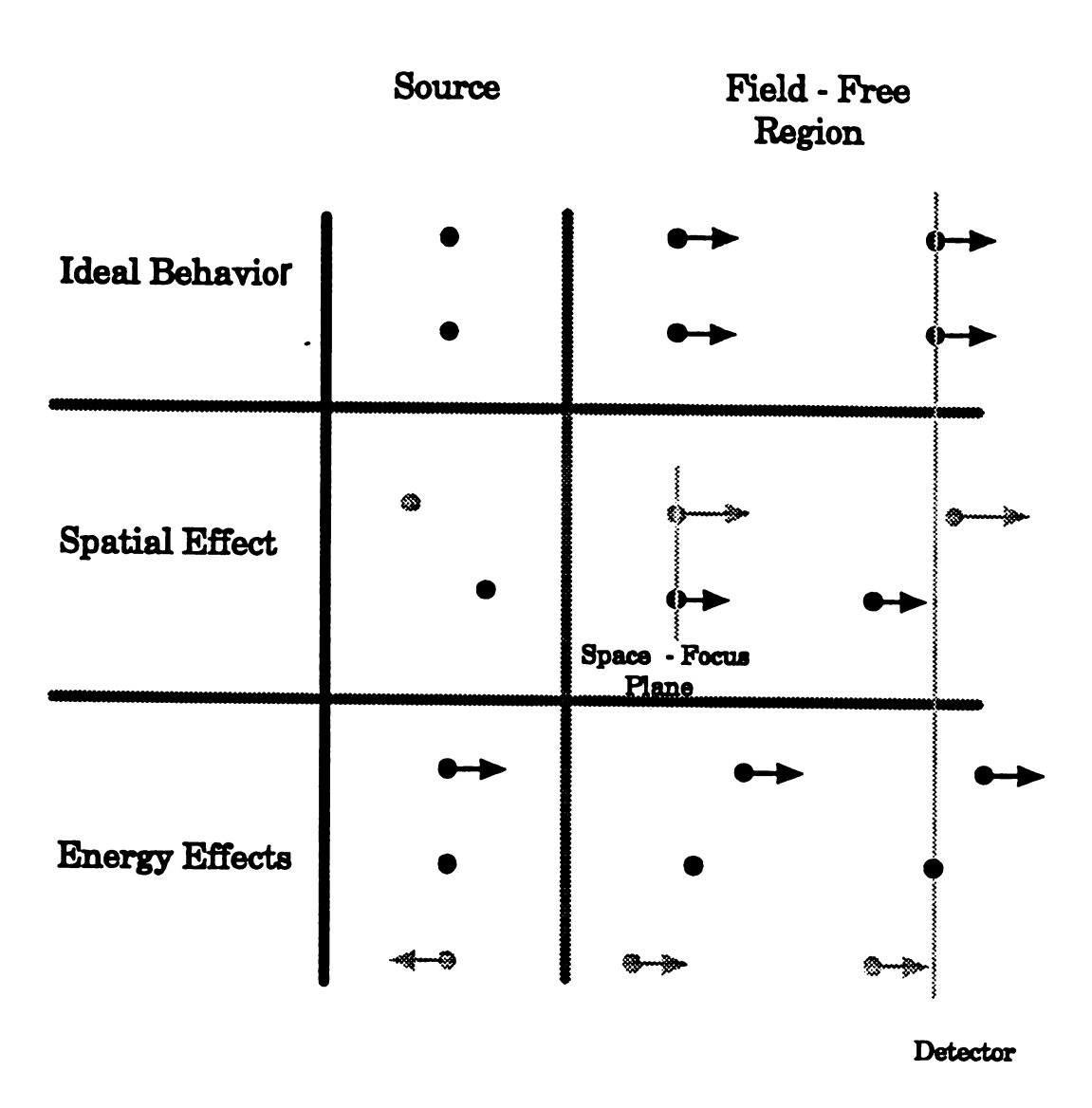


Figure 2.2 Depiction of the ion spatial and energy effects on TOF resolution. lons in the source have a spatial and energy distribution which account for a distribution of arrival times at the detector.

Wiley and McLaren showed both mathematically and experimentally that it is possible to accelerate the ions in the source with a pulse such that ions in the back of the source catch up to ions in the front of the source at a space-focus located at the detector. This technique thus minimizes the spatial contribution to the temporal spread of isomass ions.

Wiley and McLaren also devised a technique termed time-lag focusing which helped to minimize the effects of the turn-around time. A variable delay (time-lag) between the electron ionization pulse and the ion acceleration pulse is used. During this time-lag, ions produced in the electron beam move to new positions in the source. The distance traveled depends upon the initial velocity of each ion. When the acceleration pulse is applied, those ions nearer the exit grid, which are already moving forward, experience a smaller acceleration potential than those moving backward and thus are farther from the exit grid. If the time-lag is correctly adjusted the ions in the back of the source will overtake the ions in the front at the detector and the effects of the initial kinetic energy distribution can be minimized. Incorporated into the commercially available Bendix TOF mass spectrometer, resolutions of almost 600 have been achieved. Despite this improvement in resolution, the time-lag technique is mass dependent and only a small fraction of the total spectrum is in focus.

In 1973 Mamyrin [13] published results of his time-of-flight mass spectrometer capable of resolution to 3500 (FWHM), using a electron impact source. Mamyrin noted that, using the space-time focusing techniques of Wiley and McLaren, an ion packet has a thickness which is proportional to the focal length. If the ions were focused to a detector just outside of the source, ion packet thicknesses of a fraction of a millimeter were possible. He invented an ion-optical system (the mass-reflectron) to reflect the well-focused ion bunch to a detector without allowing expansion of the bunch due to the spread in the initial

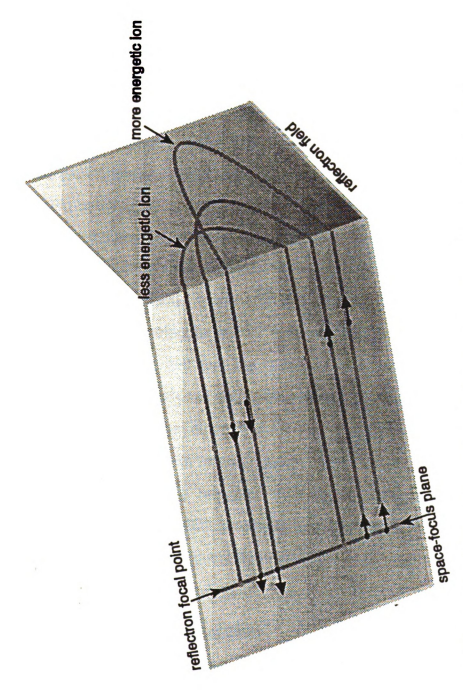


Figure 2.3 Schematic representation of the energy focusing effect of the reflectron. Ions at the space-focus plane have a distribution of energies. An ion with more energy spends more time on the potential hill created by the reflectron than a slower ion. If the reflectron is tuned properly this extra time spent in the reflectron matches the difference in time the ions spend in the field free region, and they come to a temporal focus at the detector.

ion energies. The reflectron's operation is depicted in Figure 2.3. The variations in flight time through the field-free regions due to the variations in kinetic energy are compensated by corresponding variations in transit time in the mass-reflectron. With a mass reflectron system the resolution increases proportionally with the length of the drift region. Using this scheme Wollnik [14] achieved a resolution of 20,000 with a 4 meter instrument. In addition, Wollnik developed a grid-free mirror which yields similar results in resolution, but has improved transmission and radial focusing. Coupled with an ion-storage source, detailed in Chapter 3, Wollnik's time-of-flight instrument eliminated the other problem plaguing TOF; low sample utilization duty cycle.

Oddly enough, not until Wollnik resurrected the idea of using a reflectron to reflect a space-focus image onto a detector did this technique for improving TOF resolution for electron impact sources receive any notable attention. This may be due to the fact that the reflectron was introduced just as high mass ionization techniques were being developed. These techniques produced ions on a plane, and thus did not have the spatial distribution and turn-around problems of the electron impact source. The reflectron was ideal for resolving the energy distribution resultant from these surface ionization techniques. Resolving powers of 3500 for linear instruments could be improved to about 10,000 with the addition of a reflectron [15].

2.4 Time-Array Detection

Although time-of-flight mass spectrometers could produce 25,000 spectra per second, limitations in the acquisition electronics did not allow entire spectra to be acquired at this rate. Researchers had to use a detection technique termed time-slice detection. This technique only allows the integration of ion

current over one narrow (0.1 μ s) time window (slice). To collect a full mass spectrum this window starts at 0 μ s (relative to the extraction pulse) and each acquisition thereafter is successively incremented 0.1 μ s up to 100 μ s. To collect the entire spectrum requires 1000 source extractions. This technique limits the TOF analyzer acquisition to speeds similar to those of scanning instruments.

Prompted by the desire to produce a mass spectral system capable of producing mass spectra at a rate compatible with modern chromatographic methods, researchers at MSU have developed an integrating transient recorder (ITR) [16]. The ITR is capable of recording 80 µs segment of information (transient) with a time resolution of 5 ns. Each transient is read, summed and stored in on of two summing registers. As the contents of one register is processed and stored, incoming transients are summed in the other. The unmanageable volume of data which would be produced in a GC/TOF instrument experiment is thus dramatically reduced by integrating successive transients.

In a TOF review article [17] Campana suggested that the popularity of GC/quadrupole MS was due to the development and availability of computerized data systems to collect and manipulate the GC/MS data. Given the significant advantages of time-of-flight mass spectrometers over other mass analyzers for GC analysis, the commercial availability of a such a system for TOF may be all that is needed for GC/TOF to become the analytical instrument of choice.

References

1 A. E. Cameron, D. F. Eggers, Jr., Rev. Sci. Instrum., 1948, 19, 605.

- 2 R. S. Gohlke, *Anal. Chem.*, **1959**, 31, 535.
- J. F. Holland, C. G. Enke, J. Allison, J. t. Stults, J. D. Pinkston, B. Newcome, J. T. Watson, *Anal. Chem.*, 1983, 55, 997A.
- 4 C. A. Cramers, P. A. Leclercq, *CRC Critical Reviews in Anal. Chem*, **1988**, 20, 117.
- 5 P. A. Leclercq, C. A. Cramers, HRC & CC, 1988, 11, 845.
- R. E. Tecklenburg, Jr., R. D. McLane, R. Grix, C. C. Sweeley, J. Allison, J. T. Watson, J. F. Holland, C. G. Enke, U Gruner, H. Gotz, H. Wollnik, Proceedings of the 38th ASMS Conference on Mass Spectrometry and Allied Topics, Tucson, Arizona, June 3-8, 1990.
- D. F. Togerson, R. P. Skowronski, R. D. Macfarlane, *Biochem. Biophys. Res. Commun.*, **1974**, 60, 616, .
- 8 M. A. Posthumus, P. G. Kistemaker, H. L. C. Meuzelaar, M. C. Ten Noever de Brauw, *Anal. Chem.*, **1978**, 50,985.
- B. T. Chait, K. G. Standing, *Int. J. Mass Spectrom. Ion Phys.*, **1981**, 40, 185.
- 10 M. M. Wolff, W. E. Stephens, *Rev. Sci. Instrum.*, **1953**, 24, 616.
- H. S. Katzenstein, S. S. Friedland, Rev. Sci. Instrum., 1955, 26, 324.
- 12 W. C. Wiley, I. H. McLaren, *Rev. Sci. Instrum.*, 1955, 26, 1150.
- B. A. Mamyrin, V. I. Karataev, D. V. Shmikk, V. A. Zagulin, Sov. Phys. JETP, 1973, 37, 45.
- 14 R. Grix, R. Kutscher, G. Li, U. Gruner, H. Wollnik, *Rapid Commun. Mass Spectrom.*, 1988, 2, 83.

- 15 X. Tang, R. Beavis, W. Ens, F. Lafortune, B. Schueler, K. G. Standing, Int. J. Mass Spectrom. Ion Proc. 1988, 85, 43.
- J. F. Holland, B. Newcombe, R. E. Tecklenburg, Jr., M. Davenport,J. Allison, J. T. Watson, C. G. Enke, Rev. Sci. Instrum., 1991, 62, 69.
- 17 J. E. Campana, *Anal. Instrum.*, **1987**, 16, 1.

Chapter 3: An Electron Impact Ionization Storage Source

"... we all share each others ideas and this is the way that science develops."

Ron D. Macfarlane

3.1 Ion Storage for TOFMS

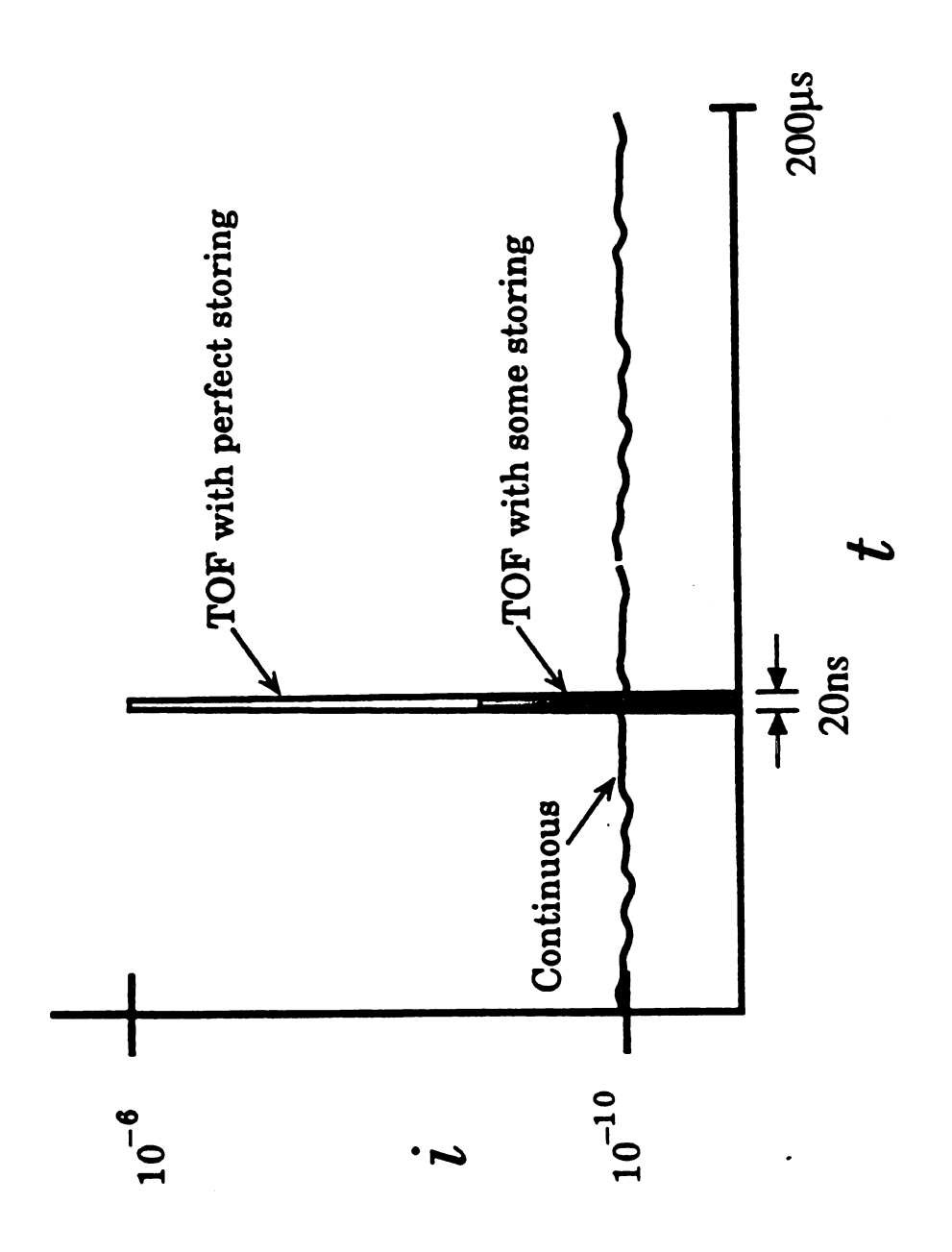
The Bendix TOF mass spectrometer, due to its commercial availability which began in 1957, is commonly used as a benchmark for performance comparison. The Bendix source uses pulsed ionization. Using a 0.25 µs pulse of electrons followed by an extraction pulse, the duty cycle for ion production in this instrument, operated at 10 kHz, is only 0.25%. If a source could be made which stored 100% of the ions produced from a continuous ionization process the sensitivity of TOF could be increased by a factor of 400! In addition, to the sensitivity improvement by ion storage, the ion bunching caused by simultaneous extraction and focusing results in a great improvement in signal to noise ratio compared to continuously detecting filtering instruments. All the ions of each m/z value accumulated in the source over a 2 ms period (extraction

frequency = 500 Hz) arrive at the detector within a 20 ns interval. If 100% of the ions formed were stored, the peak detector current would be about 100,000 times greater than the average ion current (see Figure 3.1).

In 1989 Professor Wollnik et al. [1] published the development of an unique electron impact storage source capable of storing a large fraction ("perhaps 20%") of the ions which are continuously produced. Interest in this tremendous increase in sensitivity, in addition to the high resolution which Wollnik accomplished with electron impact sources led to a collaboration between MSU researchers and Professor Wollnik. I was graciously invited to his Giessen laboratories to undertake fundamental studies of this source. With guidance from George Yefchak, I performed many experiments to probe both the ion storage process, and the resolving power of the instrument. In this thesis, I will discuss the ion storage experiments which began in Giessen and continued on an instrument very similar to the one in Giessen which was built at MSU. A thorough review of the resolution experiments and conclusions can be found in Yefchak's thesis [2].

3.2 The Storage Well

The ion storage source developed in the Giessen laboratories is depicted in Figure 3.2. This source is rotationally symmetric with respect to the ion optical axis. Ionizing electrons are produced continuously by a ring filament (K). Two additional ring electrodes (Pu), are used to direct, or "push", the emitted electrons through the slit created by two grids (G₃ and G₂). G₂ and G₄, are held at slightly positive potentials with respect to G₃. This design was intended to create a potential well about G₃ in which ions are stored between pulsed extractions, and to allow independent variation of the depth of this well. A pulse



A 10,000 fold increase in peak detector current would be achieved in a TOF instrument capable of ion storage over an instrument which could detect all of the ions continuously extracted. Figure 3.1

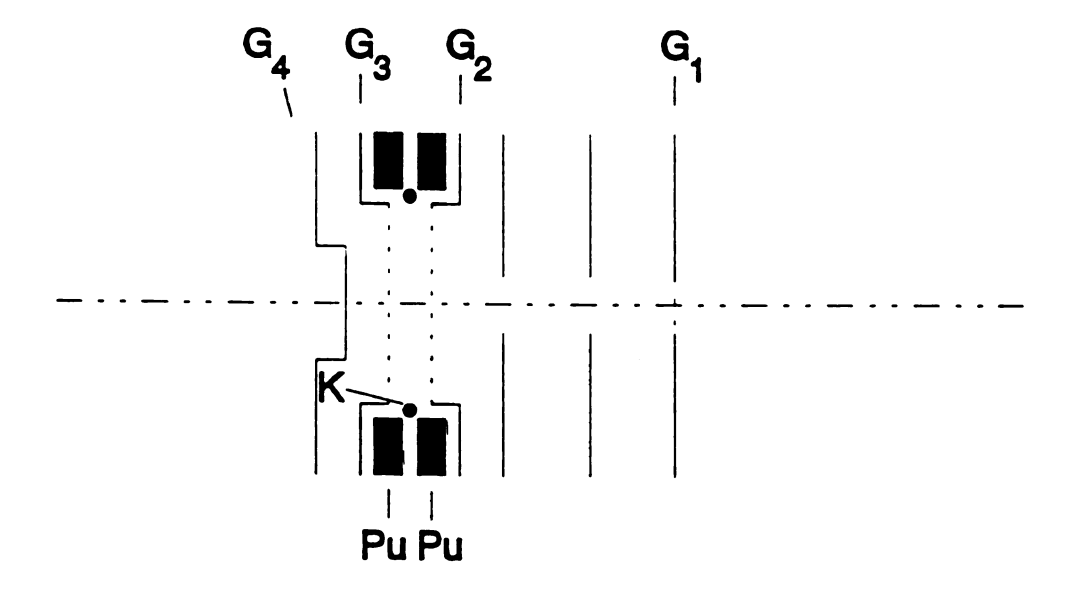


Figure 3.2 Diagram of the storage source developed in Professor Wollnik's laboratory. This source is rotationally symmetric about the ion optical axis. G₄-G₁ are grided electrodes, for acceleration, and storage. Pu are "pusher" electrodes responsible for focusing the electrons generated by (K) the filament into the storage area.

is applied to G₃ to extract the stored ions from the source through G₁, the final grid, and into the field-free flight tube.

One of the first experiments undertaken in Giessen was aimed at measuring the depth of the potential well in which the ions are stored. If Wollnik et al.'s theory that the ion storage capability of the new TOF source is due to a potential well created by the voltages applied to the three source grids: G₄, G₃, and G₂, varying the voltage on the center grid (G₃), even slightly, should cause a significant effect on the ion storage capabilities.

To perform this experiment all of the instrument control voltages were first tuned for optimal sensitivity and resolution. The voltages on G_4 and G_2 were 462.0 V and 451.1V respectively after tuning. The voltage on G_3 was then varied between 451.0 - 455.2 V. The peak intensity for ions of m/z = 18 was measured from the oscilloscope screen as the voltage on G_3 was varied. Figure 3.3 is a graph of peak intensity versus G_3 voltage. The optimal voltage for G_3 was found to be approximately 453.0 V. Instead of forming a potential well between G_4 and G_2 the voltage applied to G_3 was higher than the voltage applied to G_2 thereby forming a potential hill (see Figure 3.4). Another point of interest is that the intensity was at a maximum for a relatively wide range of voltages (452.6 V - 453.6 V). Both of these results contradicted the original hypothesis that the potential well was formed by the potentials applied to the grids. In fact, modified source configurations which do not even incorporate the back-most electrode G_4 have demonstrated similar storage capability.

Another possible explanation for the significant ion storage observed is that the high density of electrons focused into the center of the source from the ring filament forms a space-charge potential well. A strong dependence of the storage effect upon the tuning of the pusher electrodes and filament alignment supports this hypothesis. Support of this theory also came from a thorough,

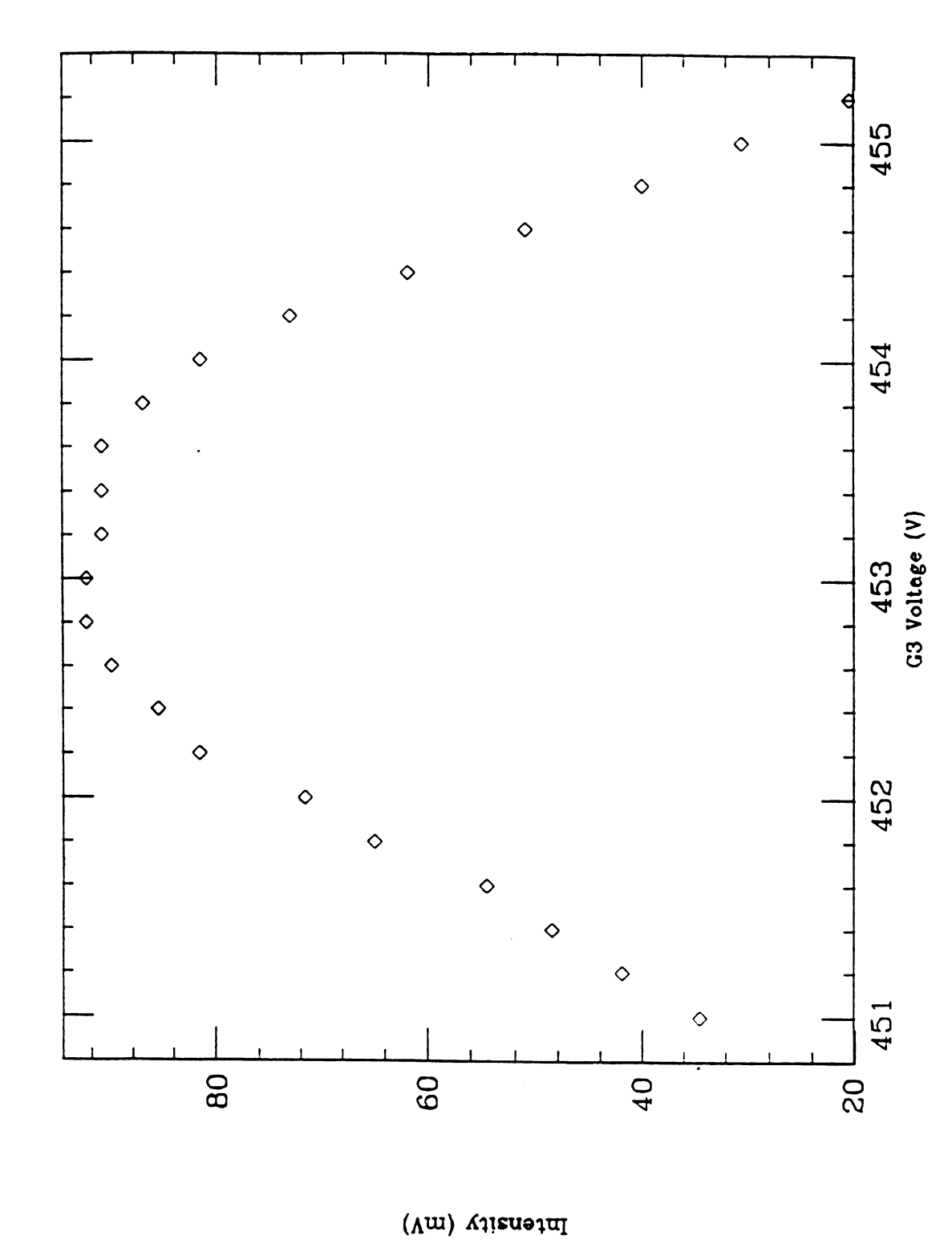


Figure 3.3 Graph of peak intensity (m/z = 18) versus the voltage applied to the center grid (G3)

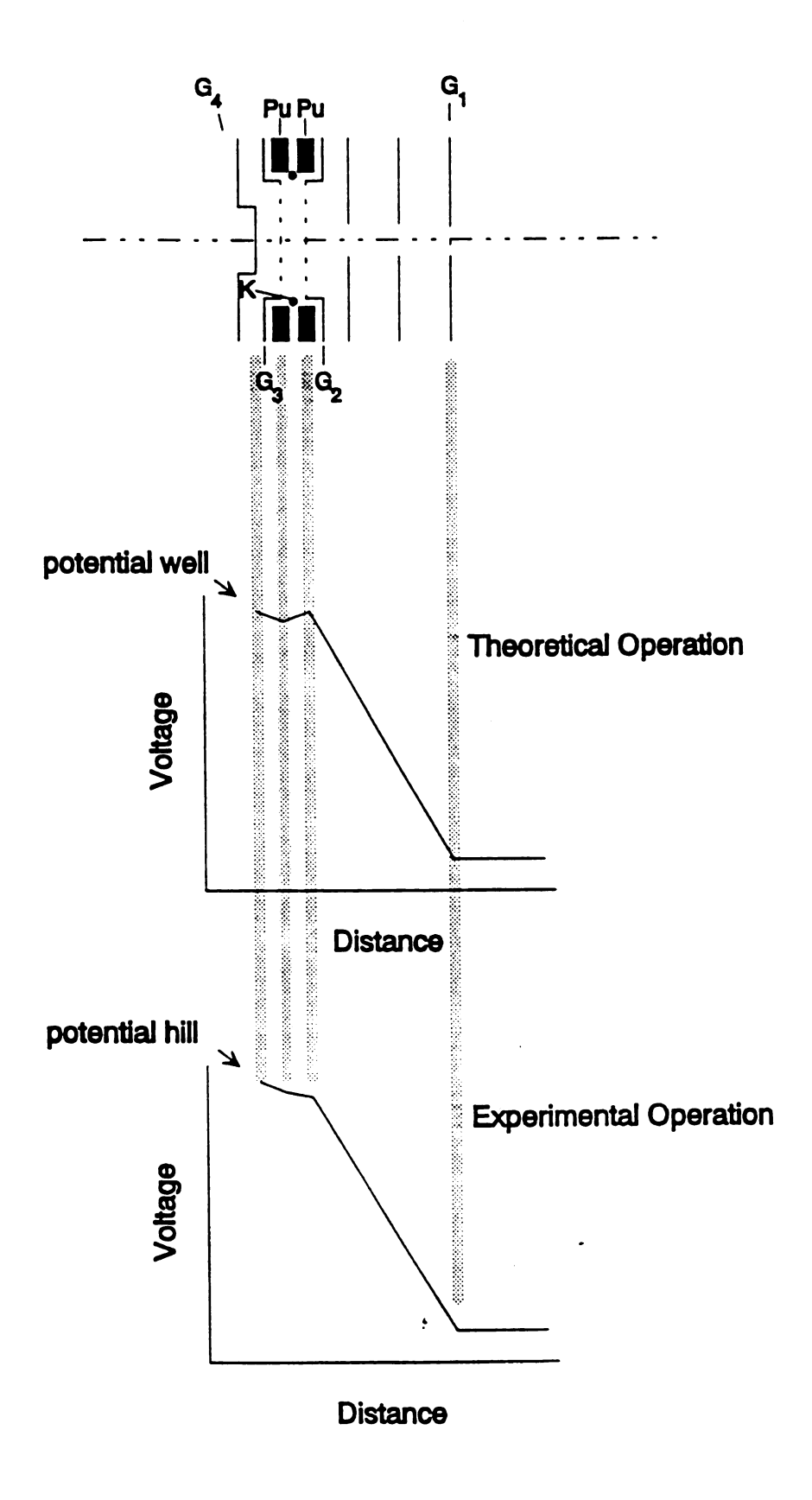


Figure 3.4 Voltages applied to the source electrodes in both theoretical and experimental operation.

albeit dilatory, literature search which uncovered a paper by Studier [3], who in 1963 developed a modified source for the commercially available Bendix time-of-flight instrument. With continuous ionization Studier achieved a factor of 300 increase in sensitivity over that of the pulsed mode of operation by using a focused electron beam to store ions. Curiously, Studier made mention of an alternate source for the Bendix TOF, which was made available for instruments using a continuous source of ions and which utilized three grids. This assembly incorporated a center grid, which is biased 0.2 V lower than the electrodes on either side of it, to "trap" positively charged ions. Despite an ionization duty cycle of approximately 100%, Studier found that this three grid assembly demonstrated little increase in sensitivity over the pulsed ionization source [4]. Unfortunately, the hapless designers of this Bendix source did not incorporate electrodes to focus the electrons into the center region.

3.3 A Mathematical Model of Ion Storage

To characterize the performance of the storage source, a mathematical model of ion behavior was developed by Yefchak, and myself [4]. A model would help us to quantitatively analyze the effects of pressure, mass, instrumental parameters and source designs on storage time in order to fully understand and optimize the storage process.

We hypothesized that ions are formed and lost according to the rate equation:

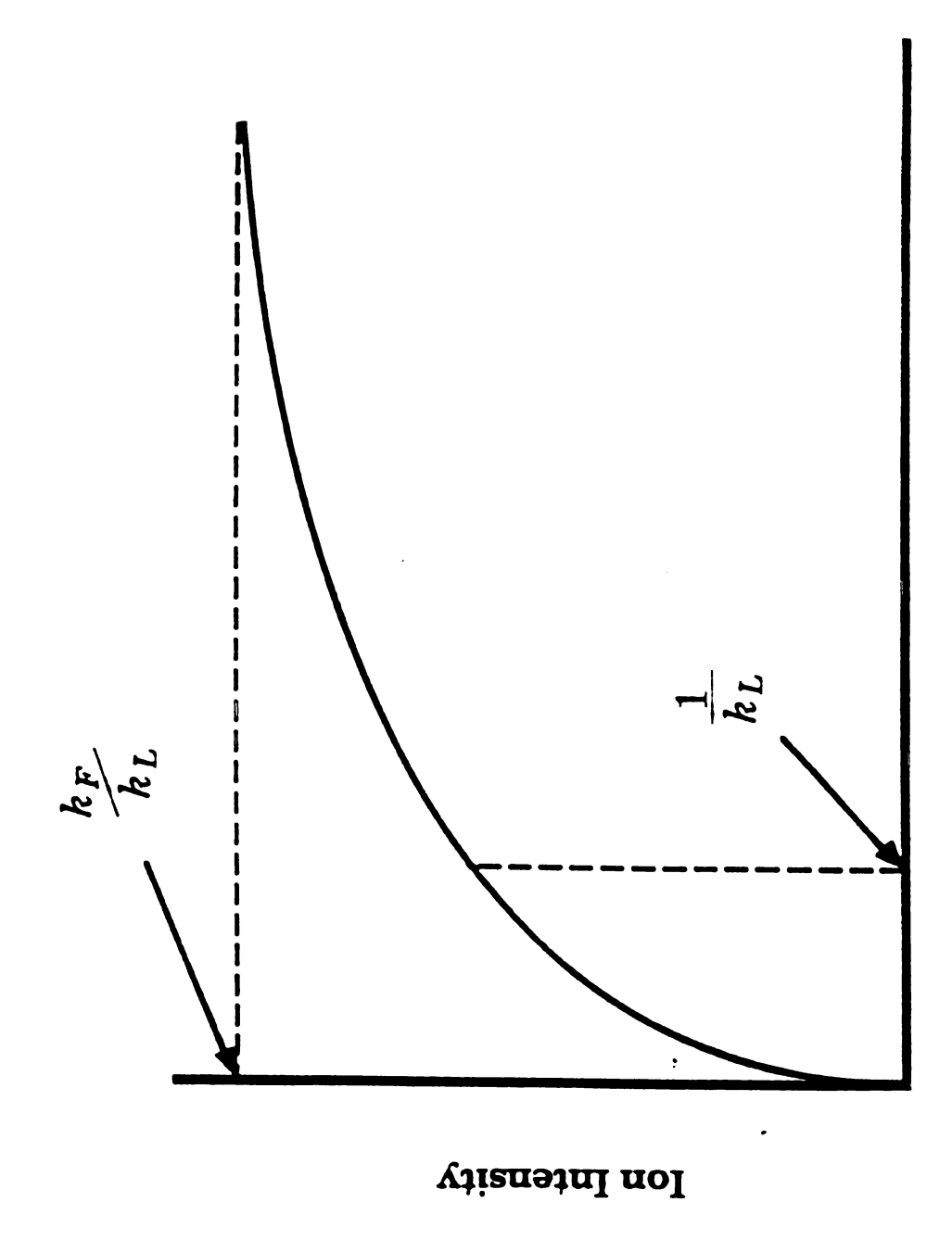
$$\frac{d(n)}{d(t)} = R_F - R_L n. \tag{3-1}$$

where n is the number of ions in the source, t is time, and R_F and R_L are the formation and loss rates, respectively. Integrating equation 3-1, we get the following equation.

$$n(t) = \frac{R_F}{R_I} \left(1 - e^{-R_L t} \right) \tag{3-2}$$

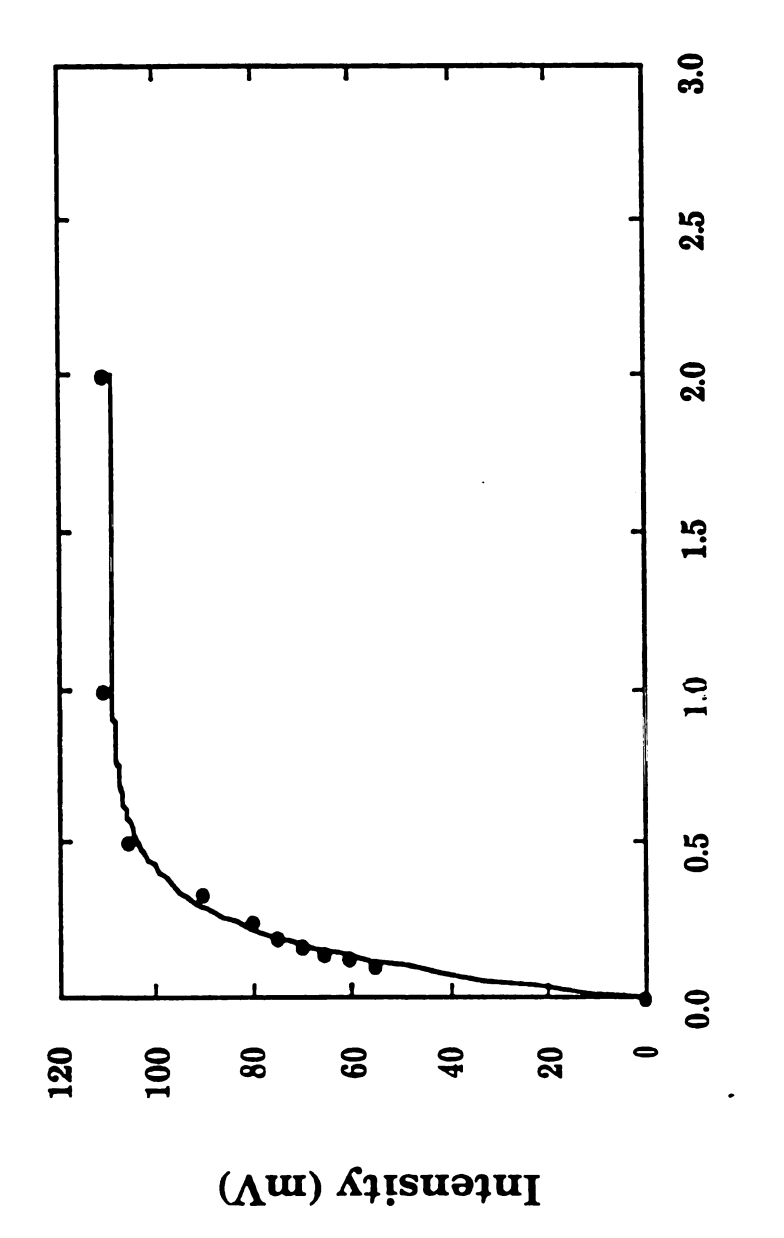
If this model accurately describes the storage process in the source, one would expect that, after the previous ion extraction, as the ionization time *t* increases the number of ions in the source and consequently the number and ion trap mass spectrometers which can actually trap or store an ion for a long, measurable period of time, the "storage" of ions cannot be detected in this source, but only the steady-state level of ions attained. By trying to improving the "storage" effect of this source we actually are trying to minimize the rate of ion loss.

With this mathematical model in hand, we could begin to postulate about the influence of analyte partial pressure, m/z, and carrier gas (in the case of GC/MS) on ion storage. Figure 3.7 demonstrates the expected dependence of storage on analyte partial pressure. We predicted that as the analyte partial pressure is increased the rate of ion formation R_F should increase, while the rate of ion loss R_L should remain constant. Thus the growth curves are expected to rise with similar time constants (1/R_L) but to different population values. Figure 3.8 is a graph of the growth curves for CHBr₃ obtained at 10 mTorr, 20 mTorr and 40 mTorr. As expected the curves reach different plateaus



Ionization Time

Figure 3.5 Theoretical graph of ion peak intensity versus the ionization time.



Graph of peak intensity (m/z=44) versus ionization time. Figure 3.6

Ionization Time (ms)

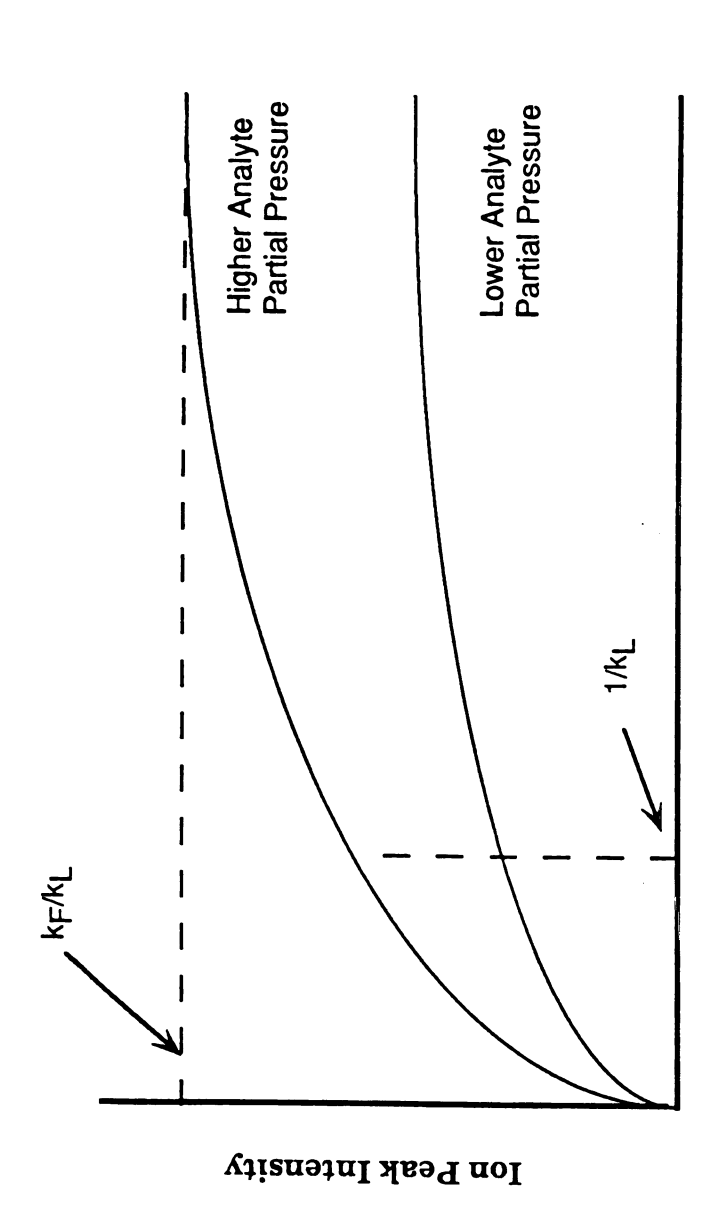


Figure 3.7 Predicted ion population growth curves for different analyte partial pressures.

Ionization Time

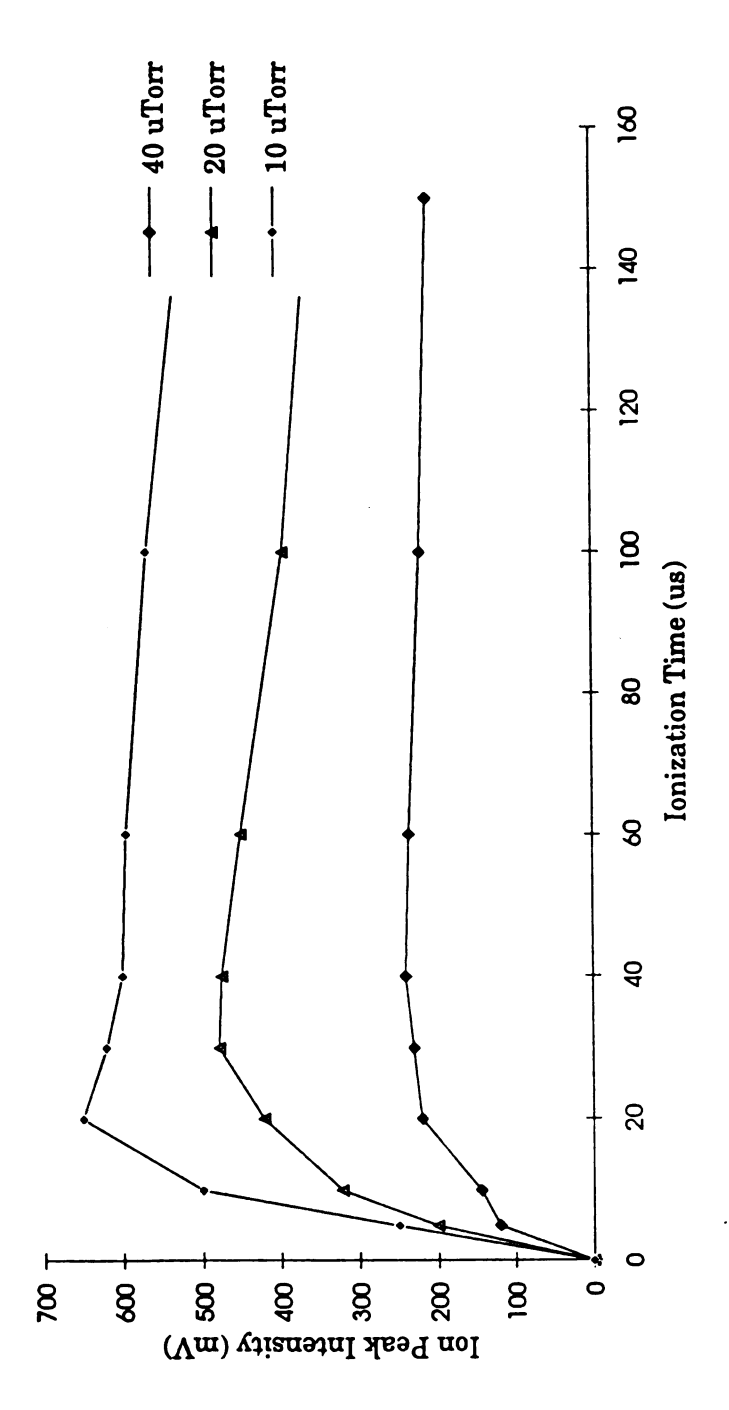


Figure 3.8 Effect of analyte pressure on the ion population growth curves of CHBr3.

but the storage time constants did not change significantly. We also postulated that ion loss rates would be a function of ion velocity. Thus, lighter, faster ions are expected to be lost more rapidly than heavier, slower ions. To directly compare ion loss rates, ionization was terminated at a variable time before extraction. Figure 3.9 is a graph of the normalized peak intensity as a function of loss time for m/z = 58, 43, 18 and 4. As expected, the loss rates were greater for lower masses, and were approximately proportional to $1/\sqrt{m}$.

Preliminary data collected by Tecklenburg in Giessen from samples introduced via a gas chromatographic interface indicated that the presence of the helium carrier gas attenuated the intensity of the background ions compared to lower pressure conditions. This observation indicated that the source pressure also effects the steady state concentration of analyte ions in the source. The extent of this effect is demonstrated in Figure 3.10. This is a graph of ion intensity (m/z = 58) versus ionization time for five different source pressures. Clearly analyte ion storage efficiency is inversely related to source pressure. Under GC conditions, the presence of helium is therefore a detriment to optimal source performance.

3.4 Effects of Helium & High Frequency Field Modulation

To understand the effect of helium on ion storage, a visual model was found to be useful (see Figure 3.11). The storage source can be viewed as similar to a bucket with holes in it. The rate at which the bucket is filled depends upon the ionization rate of the molecules in the source. These rates are dependent upon many factors including the partial pressures of the different analytes, their ionization cross sections, and the electron current. The loss rates are dependent upon ion mass, and also upon the volume of the bucket. Given

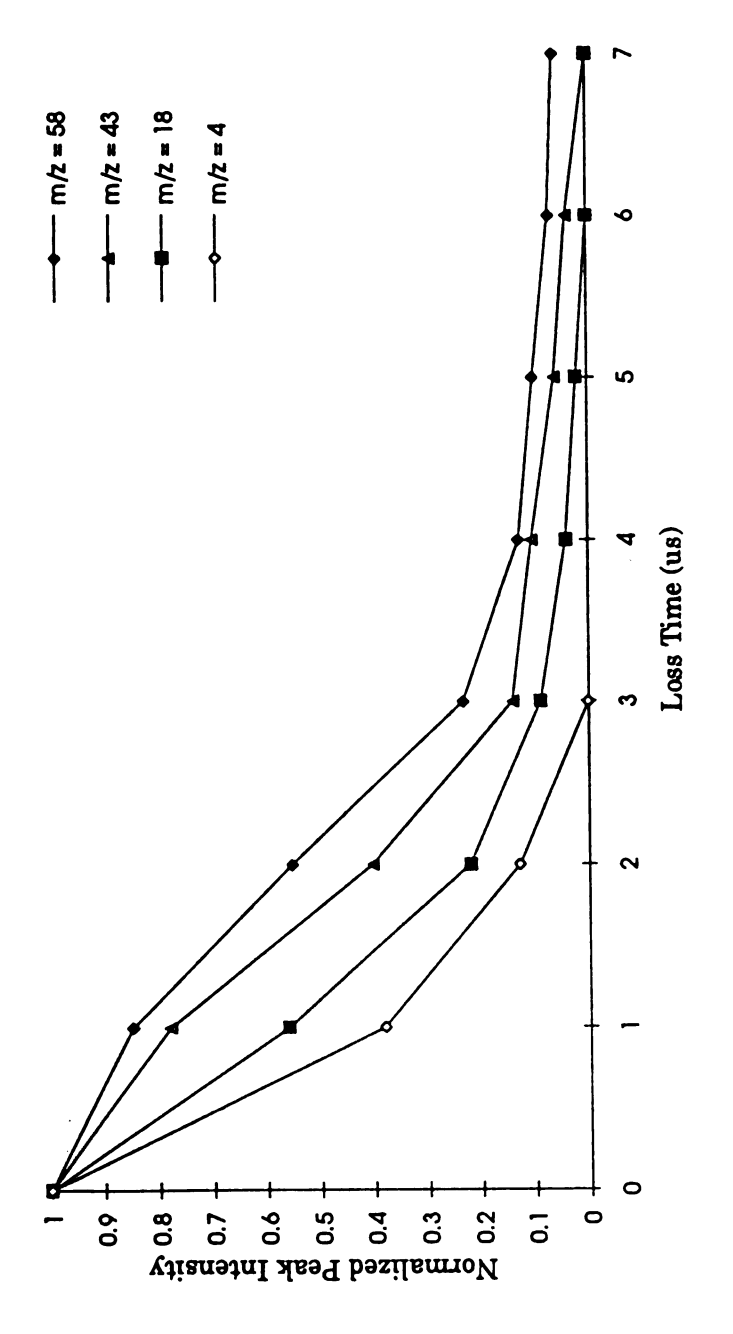


Figure 3.9 Normalized ion loss curves for ions of different m/z.

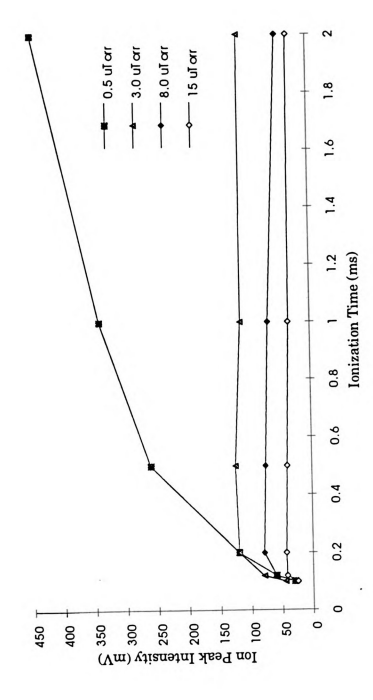


Figure 3.10 Ion growth curves for a background analyte at different helium pressures.

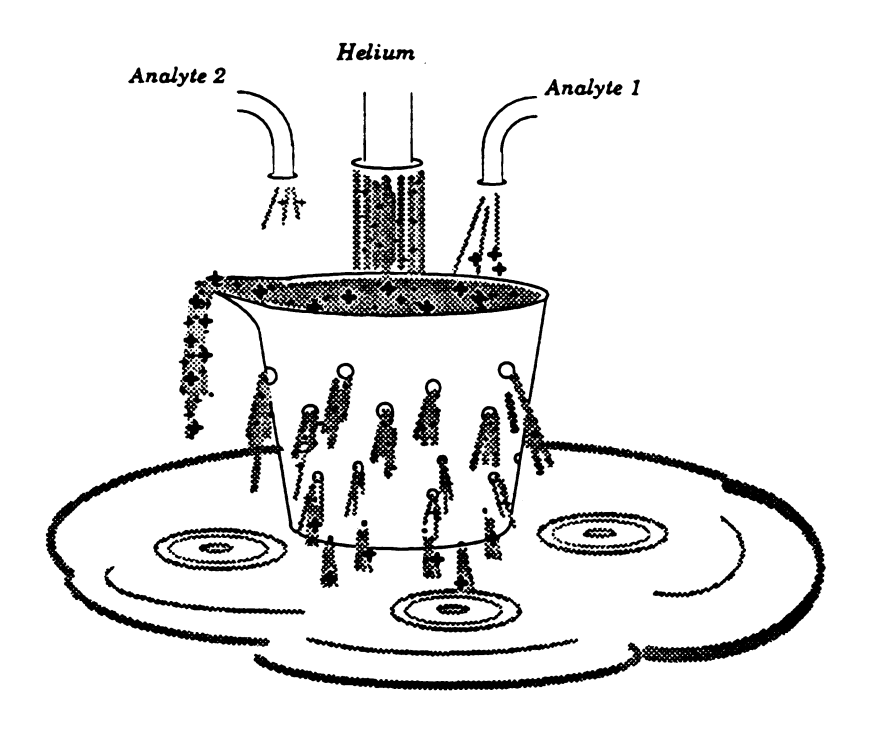


Figure 3.11 Visual model of the process of ion storage and the effect of the tremendous number of helium ions on the loss of analyte ions.

this model, it is clear that if the bucket is filled very quickly with the numerous helium ions produced, the rate of loss for all other analyte ions is very high.

This model would tend to imply that due to the high partial pressure of helium present in the source under GC/MS conditions, the number of helium ions stored in the source would rise very sharply to a maximum indicating that the "bucket" is full. Further storage time, however should yield an increase in the number of heavier ions stored due to their lower velocities and thus lower loss rates. As the source fills with heavier ions the intensity of helium ions should drop. Figure 3.12 demonstrates that this is what is observed under GC/TOF conditions.

Another experiment supporting this model involved lowering the electron energy below the ionization threshold for helium, thereby eliminating the formation of helium ions. If in fact the helium ions, and not the helium neutrals, cause the attenuation of the analyte intensity, an increase in helium pressure should, in such an experiment, not effect the analyte intensity. Figure 3.13 shows that the m/z= 58 peak (background hydrocarbon) drops as previously observed as the pressure of helium is increased when the electron ionization energy is at 70 eV. At an electron ionization energy of 20 eV, however, an increase in helium pressure has no significant effect on analyte intensity.

In order to optimize the storage of higher massed analyte ions, a scheme was developed to enhance the preferential loss of He⁺ ions using an ac voltage applied to one of the source grids (G2). As modeled by SIMION [5] (see Figure 3.14), a 2 MHz, 30 V_{p-p} ac voltage applied to one of the two source grids causes the He⁺ ions to be quickly accelerated from the storage region. The heavier ions, on the other hand, are only slightly disturbed. Experimentally, this removal of helium ions provides more efficient storage and higher sensitivity for

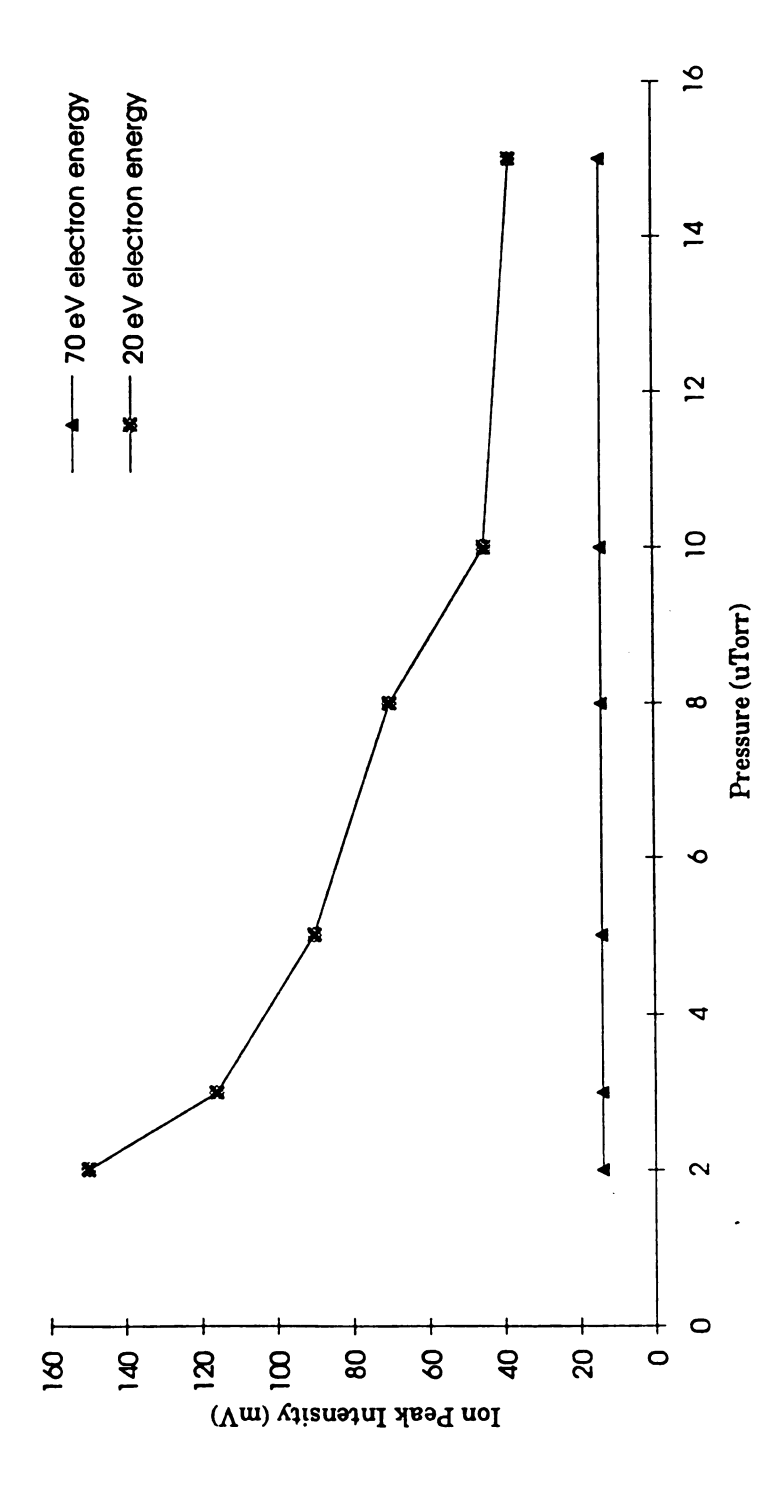


Figure 3.13 Effect of source pressure (due to He flow) on analyte peak (m/z = 58) intensity.

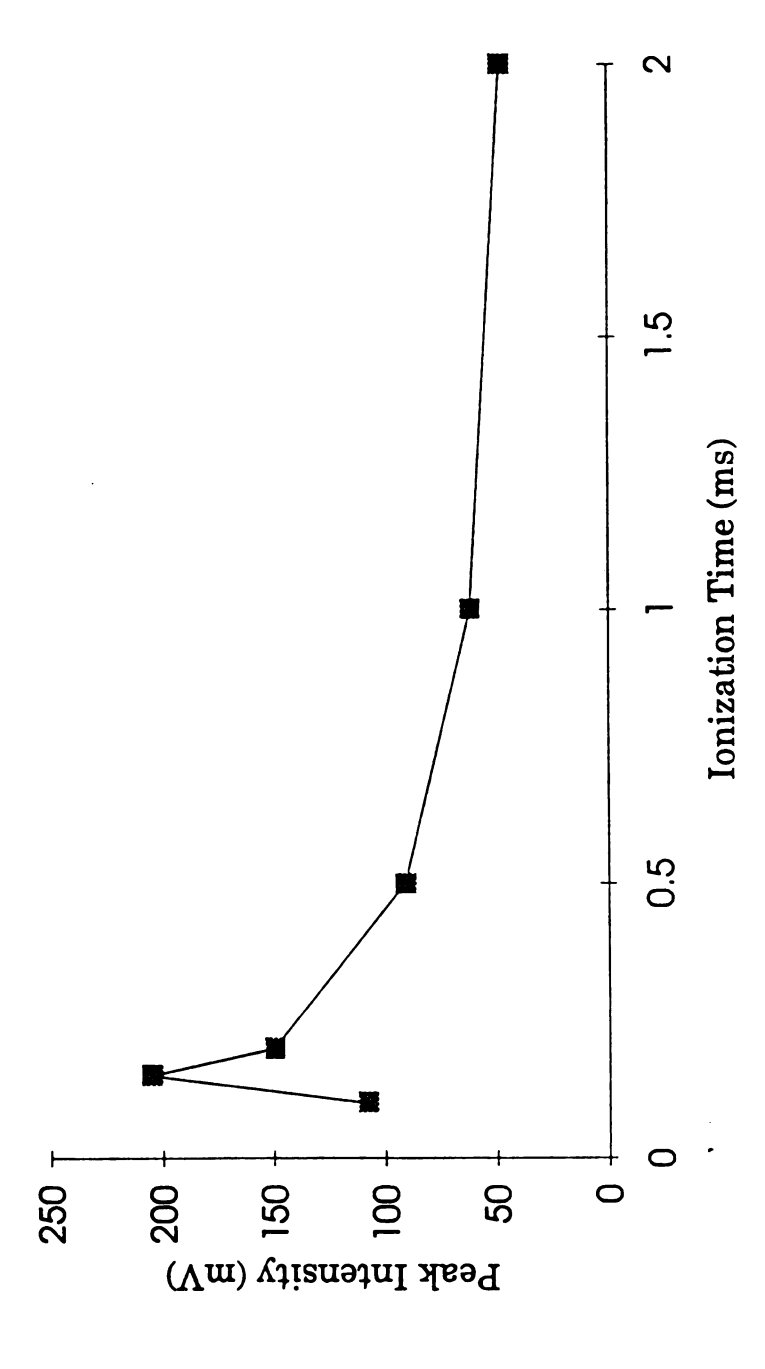


Figure 3.12 Ion storage curve for m/z = 4 (He+).

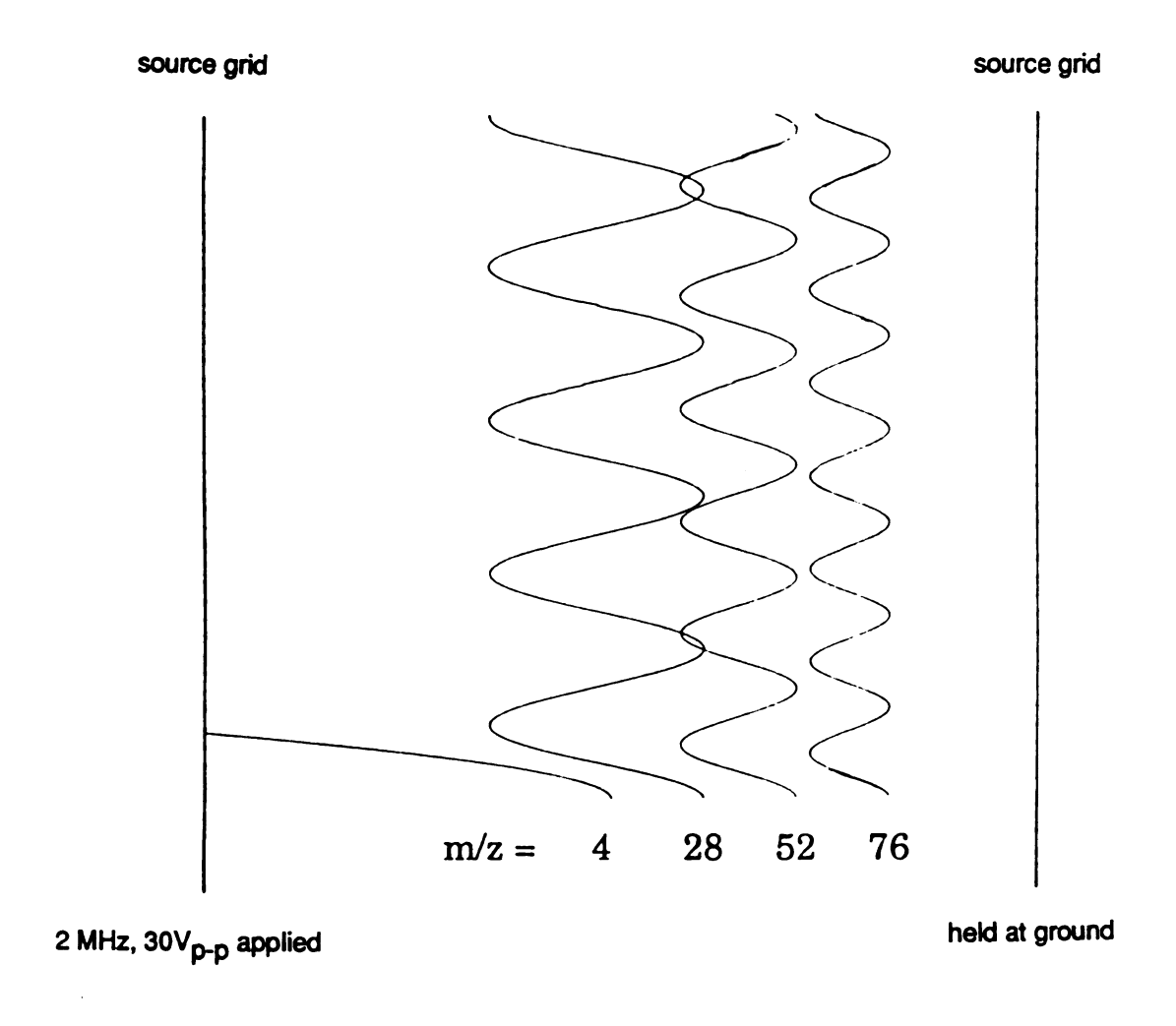


Figure 3.14 Simulated effect of a 2MHz, 30Vp-p ac voltage on the trajectory of ions with m/z=4,28,52, and 76. Ions, starting with 5 eV of kinetic energy and angle = 90 degrees, are oscillated from side to side in the source, causing ions of lower mass to be accelerated out.

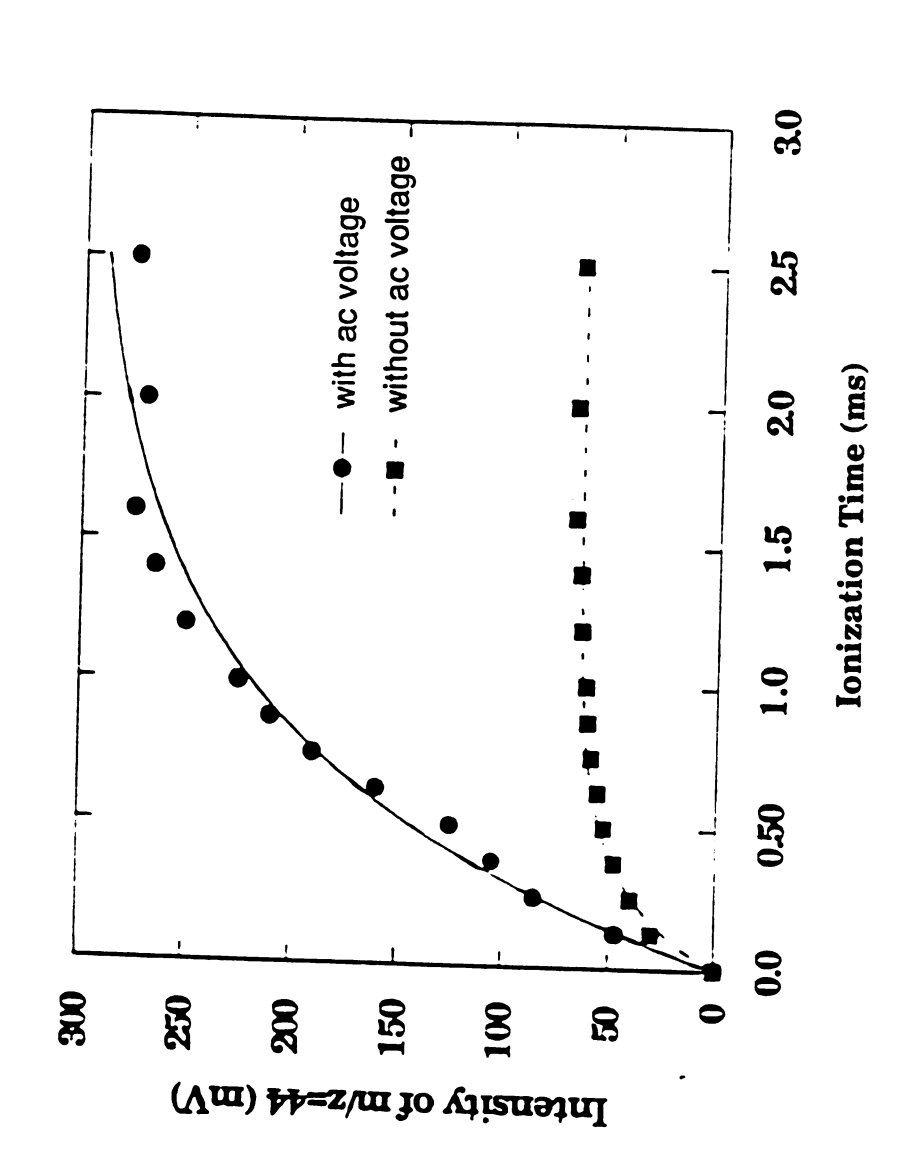


Figure 3.15 Ion population growth curves with and without the application of an ac voltage.

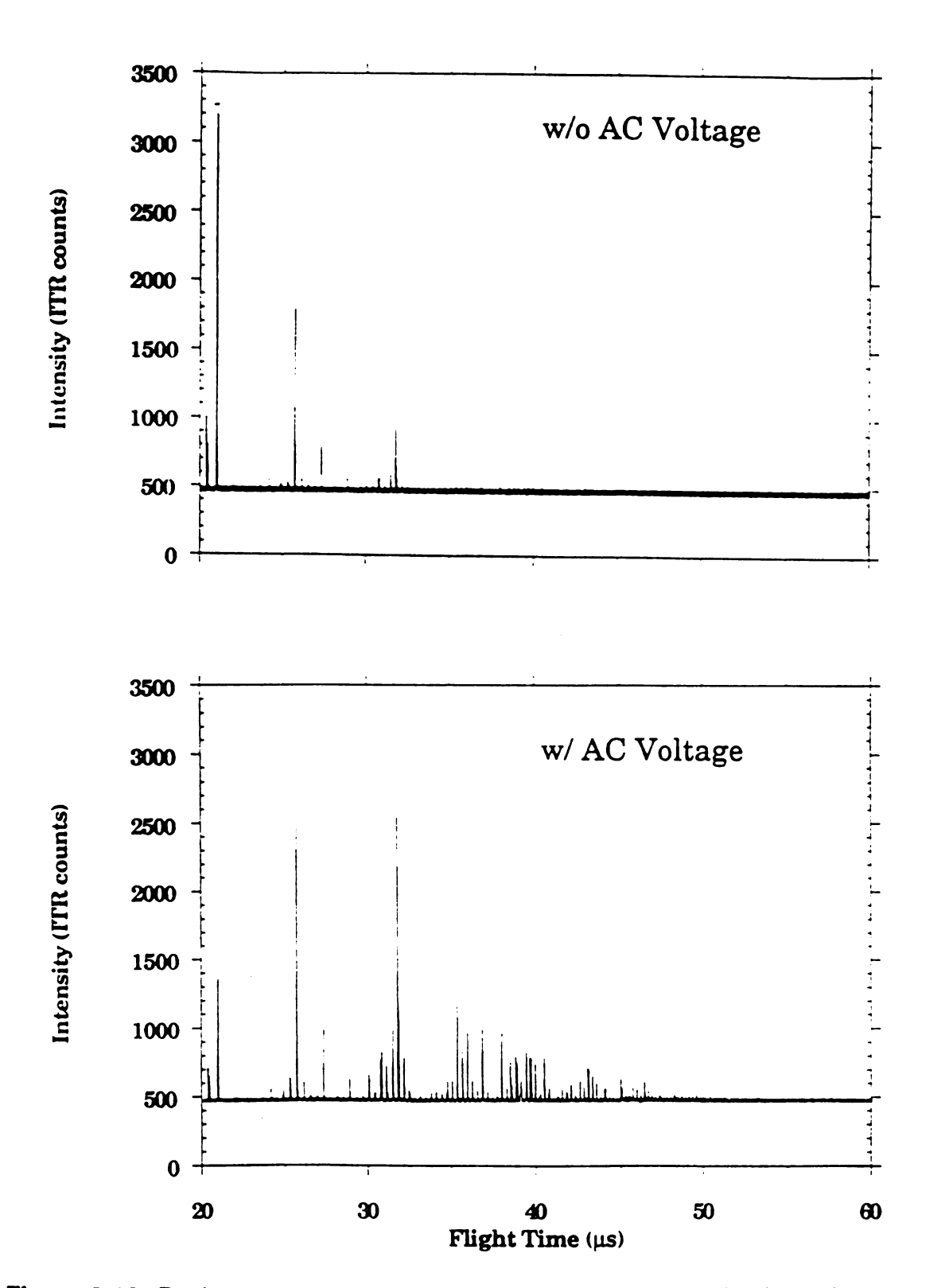
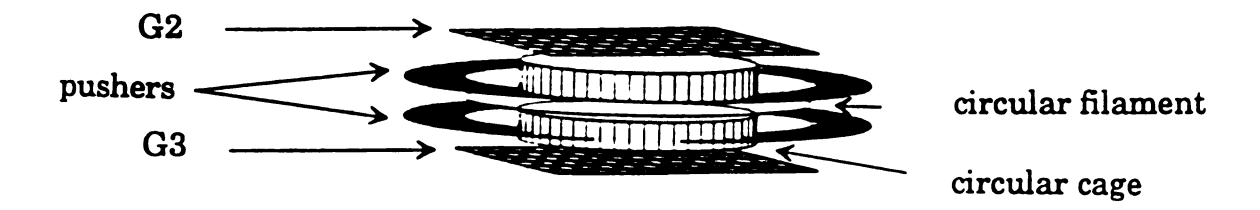


Figure 3.16 Background spectra with and without the application of an ac voltage. Note the increase in intensity for the higher massed ions when the ac voltage is applied.

analyte ions (see Figures 3.15 and 3.16), and is thus very useful under GC/MS conditions.

3.5 Effects of Source Design

Together with Ben Gardner and George Yefchak, I performed a systematic study of source geometry to determine the parameters which are critical for ion storage. Modifications included adding different "cages" between G2 and G3 (see Figure 3.17). The independent voltage applied to the cage(s) is optimized for sensitivity and is typically very similar to G2 and G3. In addition, different filament geometries were tested. For each source tested, the ion storage efficiency was evaluated in terms of the ion storage time constant (1/k₁) and ion formation rate constant k_F. These time constants were obtained by fitting the theoretically derived equation for ion population (Eqn. 3.2) to the experimental ion population growth data. Results from these experiments are tabulated in Table 3.1. These data along with daily observations indicate that the most favorable conditions for ion storage are those which produce source volumes that are essentially field free. Sources A-D, which have symmetric cages were designed to produce such a field free region. The production of a dense electron cloud also was determined to be critical to ion storage. Source B, which has a circular filament, and sources A and D, which have two opposing linear filaments were designed to optimize the electron density. Other significant parameters for source performance are the alignment of the filament with respect to G2, G3, and to the pushers, and the design of the pushers. Modeling of the source with SIMION has indicated that with correct design and voltage adjustment, the emitted electrons have multi-pass trajectories through the source



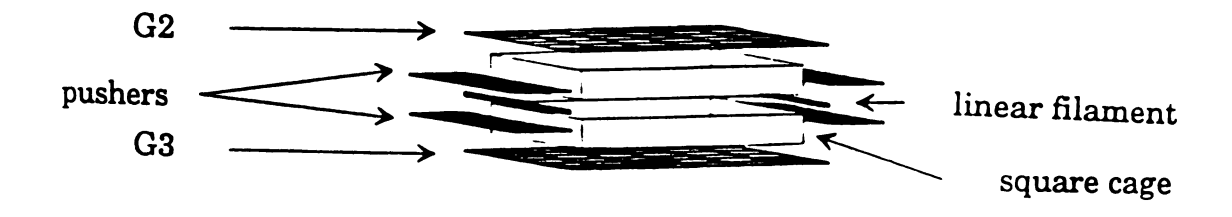


Figure 3.17 Two different source designs depicting the use of a circular cage, and a square cage.

Table 3.1 Ion storage time constants (1/ k_L) and ion formation rate constants (k_F) for six different source designs

| Source | Cage(s) | Filament(s) | 1/k | kг |
|--------|----------------|-------------|------|--------|
| A | Round & Square | 2 Linear | 0.19 | 11,900 |
| B | Round | Round | 0.32 | 1,700 |
| ပ | Square | 1 Linear | 0.17 | 2,420 |
| D | Square | 2 Linear | 0.08 | 650 |
| ш | Segment | 1 Linear | 0.07 | 1,010 |
| Ŀ | none | 2 Linear | | |

region which should yield very high electron densities in the center of the source.

3.6 The TOF/TOF Source

The source for the tandem time-of-flight instrument was designed in light of the information learned about ion storage. Advantageous for GC/TOF, ion storage is *critical* for GC/TOF/TOF. To obtain 10 product spectra per second from a chromatographically eluting compound, a maximum of 50 (limited by laser frequency of 500 Hz) product transients can be summed. To obtain spectra with a statistically sufficient number of ions it is thus critical that for each laser pulse a significant number of ions be present in the interaction region.

The TOF/TOF source is depicted in Figure 3.18. Two linear filaments were used instead of a circular filament. Experience proved that the shaped circular filaments were terribly irreproducible, and often became misaligned. More importantly, the two-filament design performed just as well. A "cage" was incorporated into the source by using lips on G2 and G3. An ion population growth curve for this instrument (Figure 3.19) demonstrates that this source does, in fact, have excellent storage capability. The ion storage constant $(1/k_L)$ was determined to be 1.4 ms, and the ion formation rate constant R_F was 212 (residual water peak, m/z = 18). The approximate number of ions in an ion packet arriving at a detector placed at the interaction region was also experimentally determined. By measuring the peak area of several single ion events at the detector as recorded by the transient recorder, a mean value for peak area resulting from a single ion event was determined. This peak area was divided into the area produced as the result of the arrival of a single ion packet at the detector. The ion packet measured was m/z = 18 (residual water) which

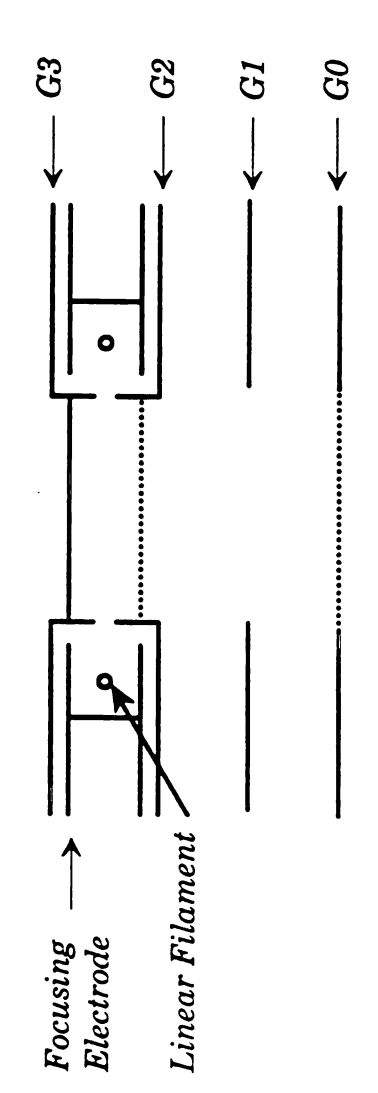


Figure 3.18 Schematic diagram of the TOF/TOF source.

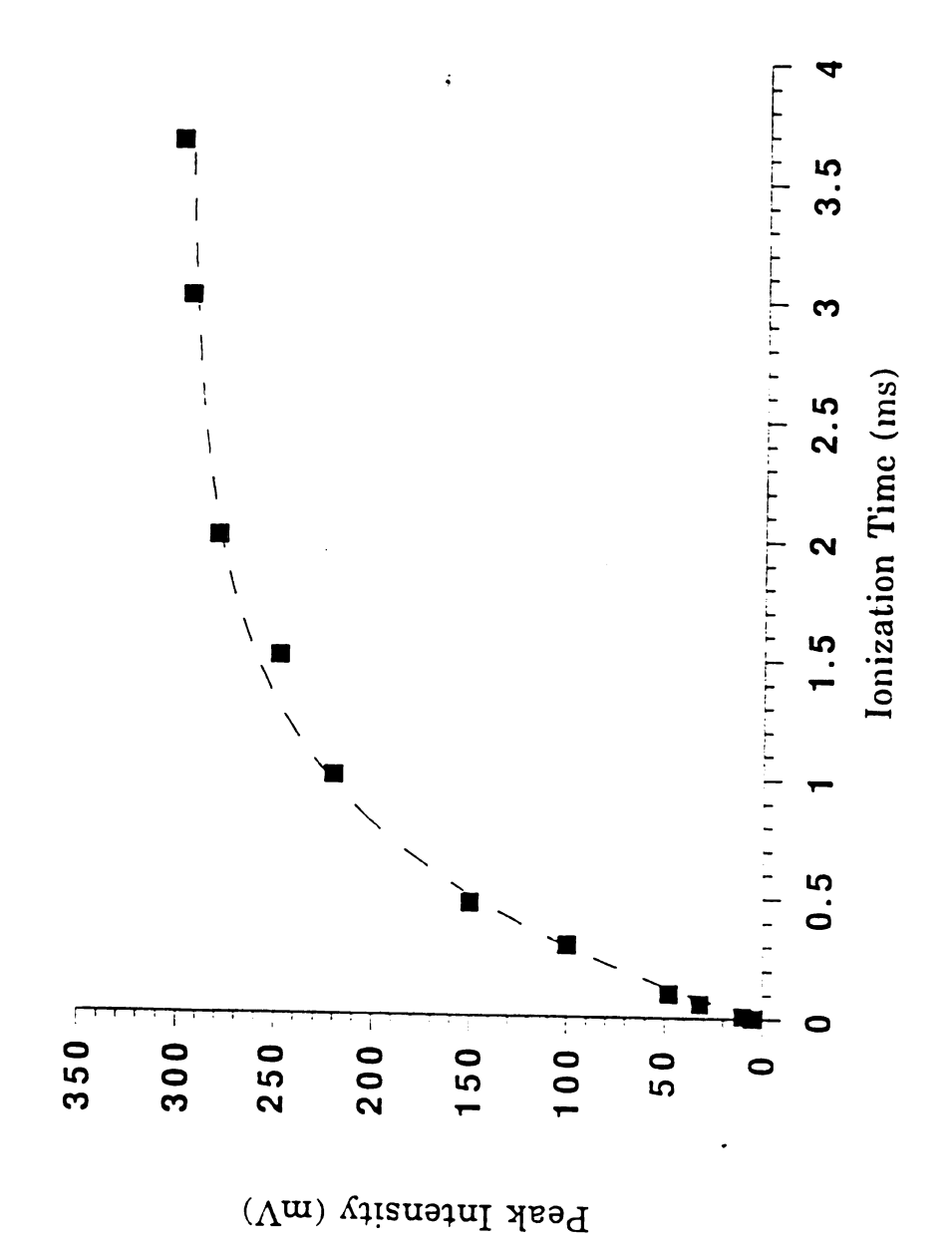


Figure 3.19 Ion population growth curve for the TOF/TOF source.

represented approximately 25% of the total residual gas spectrum for a source pressure of 10⁻⁶ Torr. It was determined that approximately 2000 ions comprise each ion packet.

Although this instrument is designed for GC/MS/MS, the unlimited mass range of time-of-flight, and the high mass potential of laser photo-induced dissociation indicate that it should be ideally suited for techniques such as CZE/MS/MS and LC/MS/MS. In the present source, however, the electrons necessary for ion storage also limit this source to electron impact ionization. A TOF source design which uses an ion trap for storage [6] should not have this limitation, and will be capable of very accurate low mass destabilization to rid the storage volume of unwanted eluent ions.

References

- 1 R. Grix, U. Grüner, G. Li, H. Stroh, H. Wollnik, *Int. J. Mass Spectrom. Ion Proc.*, **1989**, 93, 323.
- G. E. Yefchak, Doctoral Dissertation, Michigan State University, 1985,
 Ch. 5, 107.
- 3 M. H. Studier, *Rev. Sci. Instrum.*, **1963**, 34, 1367.
- G. E. Yefchak, M. A. Puzycki, J. Allison, C. G. Enke, R. Grix, J. F. Holland, G. Li, Y. Wang, H. Wollnik, Proceedings of the 38th ASMS Conference on Mass Spectrometry and Allied Topics, Tucson, Arizona, June 3-8, 1990, 540.
- D. A. Dahl, J. E. Delmore, SIMION PC/PS2 Version 4.0, EGG-CS-7233 Rev. 2, April 1988.

S. M. Michael, M. Chien, D. M. Lubman, Proceedings of the 40th ASMS Conference on Mass Spectrometry and Allied Topics, Washington, DC, May 31-June 5, 1992, 1765.

Chapter 4: TOF/TOF Instrumentation

"Perhaps creative people are those who believe that the impossible can be done and that they are the ones to do it."

Elizabeth Monroe Drews

4.1 Instrument Overview

The tandem time-of-flight mass spectrometer which has been constructed was designed to be capable of obtaining complete MS/MS spectra from compounds eluting from a capillary gas chromatographic column, while maintaining at least unit mass resolution for both precursor ion selection and product ion analysis. The goal was therefore to develop a system capable of acquiring at least 10 product spectra per second. Figure 4.1 is a diagram of the tandem time-of-flight instrument and the system control devices.

The electron impact storage source, detailed in Chapter 3, uses continuous ionization and ion storage between pulsed extractions. A high extraction pulse applied to the back electrode causes a space-focus plane to be formed just beyond the source. Parent ion packets are separated due to their

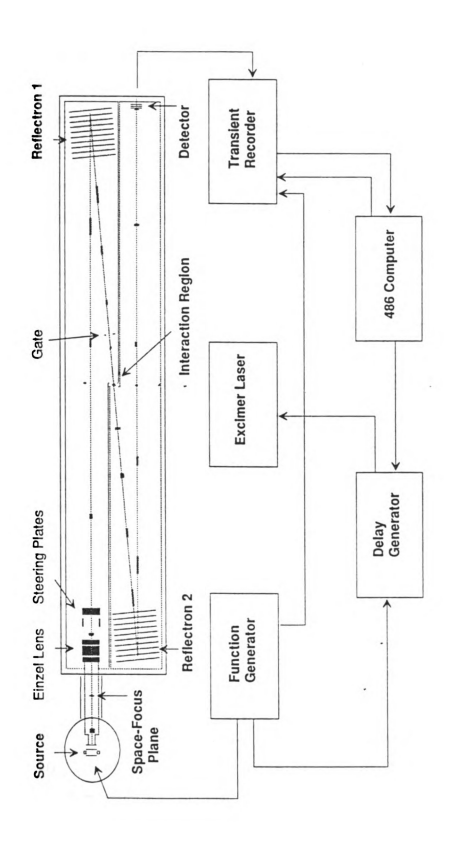


Figure 4.1 Schematic diagram of the TOF/TOF instrument and control system.

mass-dependent velocities. The large distribution of energies the ions acquire in the source are focused by a reflectron. This reflectron is tuned such that the spatial and temporal image at the space-focus plane is focused at the interaction region. A gate located prior to the interaction region can be used to deflect away ions which have m/z values lower than the precursor so that they do not interfere with the product spectra. The arrival time of a 17 ns excimer laser pulse focused at the interaction region selects the desired precursor ion packet. After fragmentation, the product ions formed have the same velocity as their precursor ions, but only a fraction of the precursor ion kinetic energy. Acceleration of the ions just following the interaction region, gives these ions mass-dependent velocities. Product ion packets, as well as the unfragmented precursor ion packet are separated due to their mass-dependent velocities. A second reflectron is used to focus the energy distribution of the isomass ions at Summing successive time-array detected transients using a the detector. LeCroy Transient recorder, and in the future an MSU Integrating Transient Recorder yields the product spectra.

Many functions in this instrument require accurate and precise control. These functions include the timing of the source extraction pulse (± 2 ns), the firing of the laser (± 3 ns), and the triggering of the transient recorder (± 1 ns). To meet these needs a LeCroy 4222 delay generator (± 2 ns) and a Questek 2580 v β excimer laser (jitter and drift ± 2 ns) are utilized and controlled remotely via GPIB interfaces using National Instruments LabWindows software on a 486 computer.

This system will generate 500 product transients per second (limited by the laser). If approximately 50 transients are summed for each product spectrum, 10 product spectra will be produced per second. With this rate of acquisition a substantial amount of MS/MS information can be obtained for a chromatographically eluted component.

4.2 Description

The design and implementation of the complete TOF/TOF system was an effort shared between David McLane and myself, and more recently also shared with both Paul Vlasak and Doug Beussman. Working in parallel, David focused his efforts on all aspects of the laser, gas chromatograph, and system control. Further details on the GC sample introduction, criteria for selection and operation of the laser, transient recorder, delay generator, and documentation of the control software can be found in his thesis [1].

My focus on the other hand was to design and construct the vacuum chamber, source, mass analyzers, and the necessary ion optical elements for the TOF/TOF instrument. These components, their function, and their performance are detailed in this chapter.

4.2.1 Vacuum Chamber

The vacuum chamber for the TOF/TOF instrument was designed to be as versatile and accessible as possible. Figure 4.2 is a blueprint showing the major features. This "coffin" design was patterned after the Finnigan TSQ 700's vacuum chamber in that it is a welded stainless steel box with removable lids providing access to the entire ion optical path. The internal dimensions of this chamber are 60" x 9" x 11" and the walls are 3/4" thick. The entire chamber was electropolished after welding to minimize the surface area upon which water and other molecules can deposit. Such treatment reduces the outgassing rate of unbaked metals by a factor of approximately 20 [2]. All electrical and mechanical feedthroughs are made through flanges allowing for non disruptive modifications. In addition, many tapped holes were included in the interior of the

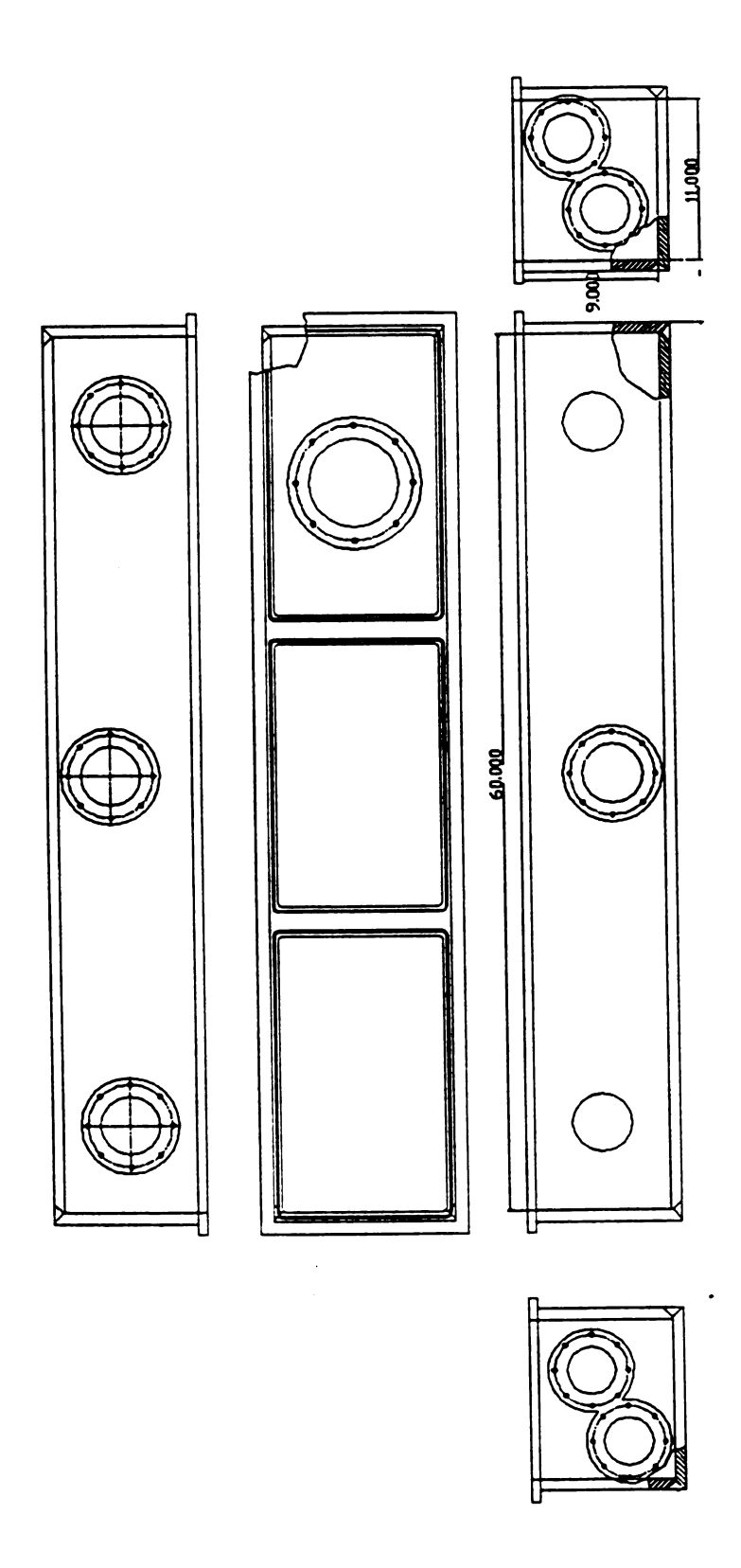


Figure 4.2 Blueprint of the TOF/TOF vacuum chamber.

chamber at various defined locations allowing for accurate positioning of ion optical elements along the flight path.

The source is housed in a separate chamber which is interfaced to the main chamber. This independent, multiport chamber was designed to allow access from multiple directions. This has allowed for different sample introduction systems to be added without major modifications or removal of the GC interface.

4.2.2 Vacuum System

The vacuum system for the instrument consists of two Balzers turbomechanical pumps (TPH270 and TPH510) each backed by a Leybold-Heraeus (Trivac D 16 A) rotary vane rough pump, two standard Bayard-Alpert ionization gauges to measure the source and flight chamber pressures, two thermocouple gauges to measure the foreline pressures, and the necessary controllers, tubing, connectors, and valves. The larger of the two turbo pumps (TPH510) is used on the flight chamber, while the TPH270 is used to pump the source. A 0.5" diameter aperture between these chambers allows for differential pumping so that under GC/MS/MS conditions the majority of the flight path will be under high vacuum conditions.

With this system, the measured source and flight path chamber pressures are typically 5×10^{-7} Torr and 1×10^{-6} Torr, respectively after about 20 minutes of pumping without the GC connected. Still lower pressures are expected if the chambers were to be baked overnight.

4.2.3 Sample Introduction

Currently the tandem time-of-flight instrument is capable of sample introduction from three sources. A direct leak system, which was designed by E. Hemenway, allows for continuous introduction of a pure compound for

extended periods. A Finnigan TSQ 700 heated transfer line has been modified by D. McLane and D. Beussman to interface the GC oven to the ion source. In addition, a Hewlett-Packard direct insertion probe has been modified for TOF use by B. Gardner and has been interfaced to this instrument for nonvolatile compound introduction.

4.2.4 First TOF Analyzer

4.2.4.1 Source Extraction

A nearly linear acceleration field is established during the source extraction pulse. The extraction pulse applied to the back electrode (G3) is 200 V. An additional 500 V potential drop is established between the second grid (G2) and the field-free region (G0). The average energy of the ions, assuming that the storage region is located midway between G3 and G2 is 600 V. Due to the spatial distribution of ions in the source, a kinetic energy distribution is created as ions at the back of the source receive more energy than ions of the same mass near the front of the source. A few inches down the flight tube, a space-focus plane is created where ions originating near the back of the source overtake ions created near the front. The finite widths of isomass ion packets at the space-focus plane (~20-40 ns) are due to the initial kinetic energy spread of the ions in the source, and imperfections in the space-focus conditions.

4.2.4.2 High Voltage Shield

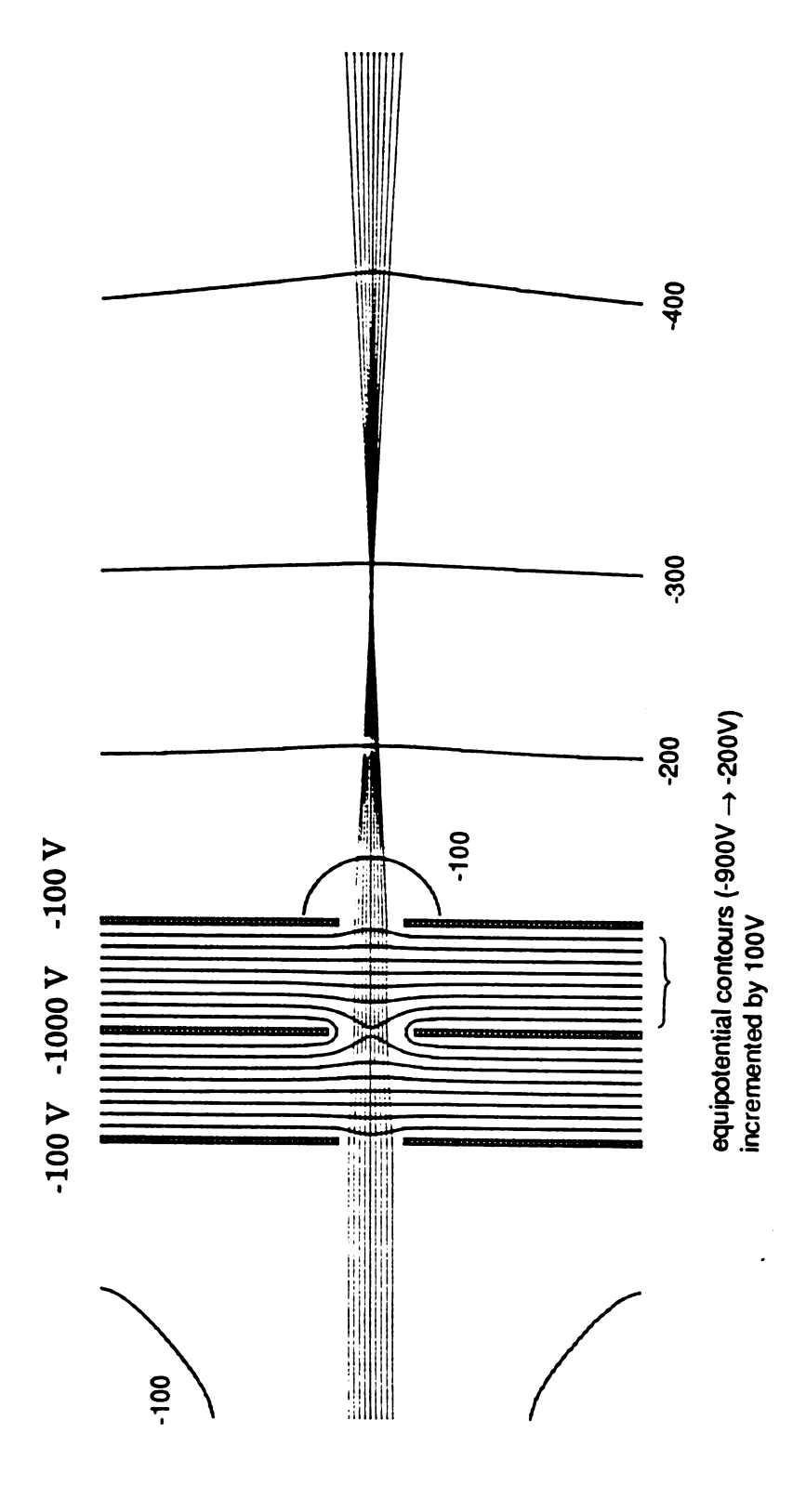
The MTOF instruments built in Geissen and at the MSU Mass Spectrometry Facility, both float the ion source at high voltage (~1000 V), while the flight tube is grounded. In the TOF/TOF instrument, however, the entire TOF flight path is floated. The first TOF region is floated at -500 V and the second

TOF region is floated at -1500 V. This design allows the source electrodes to be at or near ground, and has alleviated the problem of arcing under GC/MS conditions due to the fairly high pressures of helium. The high voltage shields, which establish the field-free flight region were constructed of stainless steel mesh. These are segmented and have easily detachable lids allowing for easy modification and access to the optical elements within them.

4.2.4.3 Einzel Lens and Steering Plates

An Einzel lens and steering plate assembly has been incorporated into the instrument a few inches from the source. An Einzel lens is analogous to a glass lens were the light has the same speed on either side of the lens. This lens has three elements. The outer two elements are held at the same potential and the middle element at another potential. Originally concerned about the effects of spherical aberrations on the temporal resolution, this effect was modeled using SIMION. These studies indicated that for the lens system modeled (Figure 4.3), temporal spreads of up to 9 ns were observed at the focal point (m/z = 500, KE = 500 eV). Another inescapable feature of ion optical lenses is chromatic aberration. In ion optics this means that ions with different energies will be focused at different points. Despite these features, Einzel lens systems have proven to dramatically improve sensitivity. Resolution, which is routinely 1500 (FWHM), is clearly not overly impaired.

Two sets of orthogonally oriented steering plates are used to steer the ion beam. These steering plates consist of two parallel plates. One plate is set at the shield voltage (-500 V) and the other has an adjustable voltage. If each optical element were perfectly aligned, these steering plates would not be necessary. This would be ideal, because the magnitude of deflection in such an electrostatic field is energy dependent. Careful alignment, and motion



energy are focused to a point using an Einzel lens created by the voltages applied to three "washer" electrodes. The outer two electrodes are held at the same potential while the center electrode is held at a SIMION model of an Einzel lens system. Collimated ions of equal either a negative potential (in this case) or a positive potential with respect to the other two. Figure 4.3

feedthroughs on the reflectrons (Section 4.2.8) has minimized the need for high voltages on these elements.

4.2.4.4 First Reflectron

The ion reflectron used in the first stage of mass analysis, is grid-free, and is similar to the reflectron designed by Wollnik et al [3]. (See Figure 4.4) The more energetic and thus faster ions travel further into the reflectron. The extra time spent in the reflectron compensates for their shorter time these higher velocity ions spend in the other regions, and thus the ions of different energy are focused at the interaction region. As modeled by SIMION, (Figure 4.5) the grid-free reflectron constructed for the TOF/TOF instrument does not incorporate "lips" on the first two washers as in Wollnik's design. Considerably more difficult to construct, these were said to establish a better lensing field, considered helpful for radial focusing. Their absence, however, does not significantly change the field produced, or the observed performance.

The reflectron is constructed from a series of large stainless steel washers separated by ceramic insulators. Four of these washers have voltages directly applied to them, while the others, linked by a series of 5 $M\Omega$ resistors, have voltages which are dependent upon the others. The angle of the reflectron with respect to the ion beam is controlled via two linear motion feedthroughs connected at three locations using universal joints. Optimization of the reflectron's angle minimizes the necessity for steering plates.

4.2.4.5 First Detector

Two detectors are used in the TOF/TOF instrument. One of these is permanently mounted on a flange located at the end of the second TOF analyzer. The other, mounted on a stand, is capable of being located throughout the instrument and is helpful for troubleshooting. This detector,

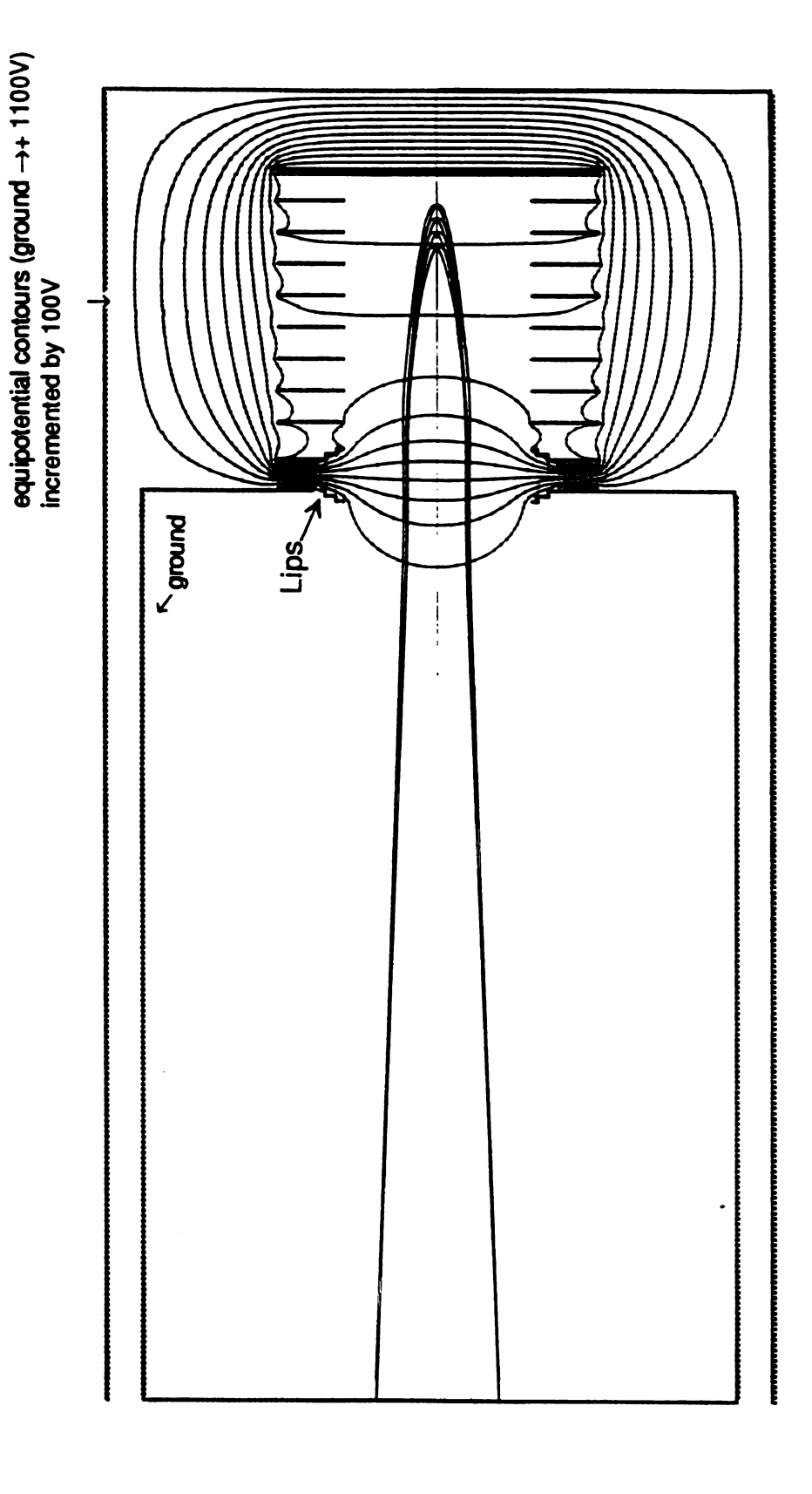


Figure 4.4 SIMION model of Wollnik's grid-free reflectron. The reflectron is made up of large "washer" electrodes which have voltages applied to them. Ions which enter the reflectron will travel up the potential field, stop, and be accelerated out. As depicted in this model ions of greater energy travel further into the reflectron than ions of lower energy.

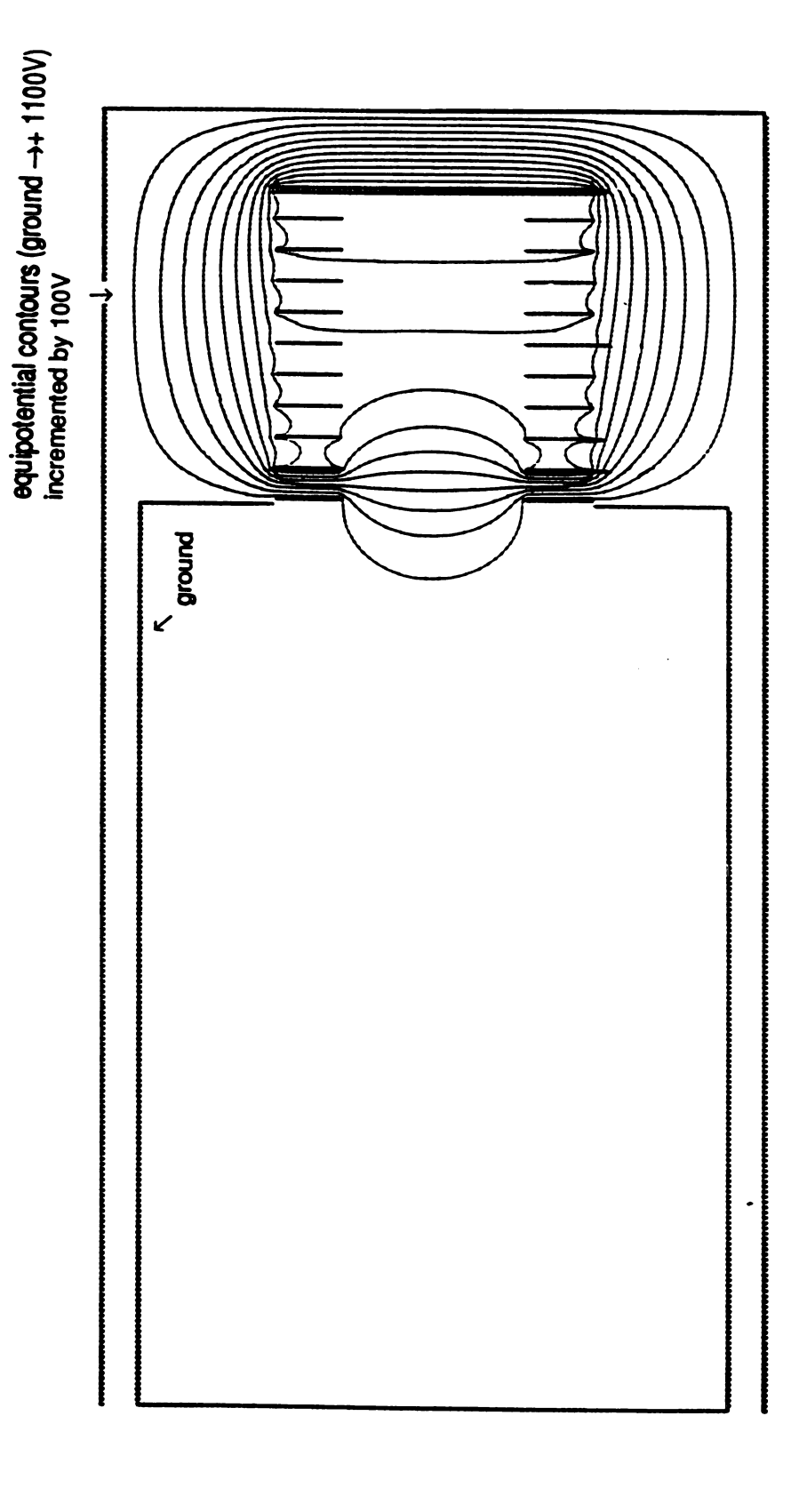


Figure 4.5 SIMION model of the modified grid-free reflectron used in the first TOF analyzer. This reflectron does not have the "lips" in the Wollnik design, yet the contours are not significantly different.

eventually, will be permanently mounted below the interaction region. Deflection of the ion beam in the direction of this detector will allow for very simple measurement of arrival times and focusing of precursor ion packets at the interaction region.

The detectors constructed incorporate two Galileo non-optical grade microchannel plate's (MCP's). These MCP's are thin glass wafers with a honeycomb structure of millions of tiny channels. With a bias voltage applied across these wafers, each channel functions as a single electron multiplier. Two MCP's in series yield a gain of up to 10⁷.

4.2.5 Interaction Region

An isomass ion packet, focused temporally and radially, is selected for photo-induced dissociation by timing a 17 ns laser pulse to intersect it as it enters the interaction region. The interaction region is thus defined by the cross-section of the ion packet and laser pulse.

The top and side views of the ion beam trajectory through the entire instrument is diagrammed in Figures 4.6 A and B respectively. The laser beam is aligned to enter and exit the vacuum chamber through windows in the sides of the instrument. To eliminate the possibility of interaction with the ion beam except at the interaction region a slight angle downward was incorporated into the ion trajectory.

Ideally intended for photo-induced dissociation, the TOF/TOF instrument was also designed to allow for surface induced dissociation (SID) studies, and possibly collisionally induced dissociation (CID) studies. This region thus needs to be very flexible, and many different elements must be accurately positioned in the ion flight path. Together with Paul Vlasak, the necessary elements of this region were designed and constructed.

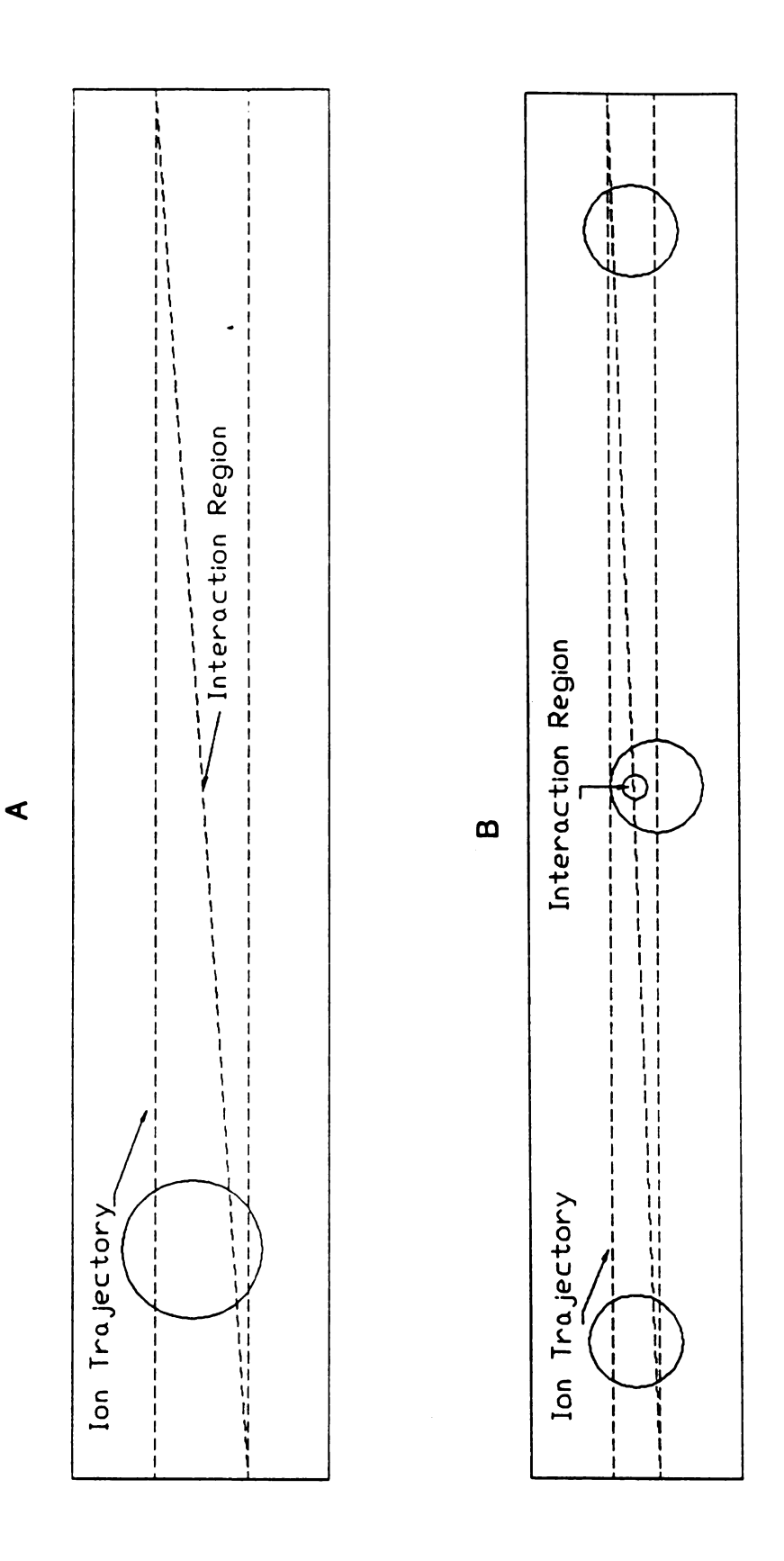


Figure 4.6 The top (A) and side (B) views of the ion trajectory through the TOF/TOF instrument.

4.2.5.1 Optical Rail

A vacuum compatible ion optical rail from Newport Corp. is used in the interaction region to provide a base for aligning the multiple elements in this area. The gate, detector, acceleration grids, apertures, and other elements are all connected to Newport carriers which can be positioned along this rail or easily removed.

4.2.5.2 Gate

When using photo-induced dissociation the implementation of the ion gate will serve to deflect ions of m/z lower than that of the selected precursor. These ions, if not deflected, continue along the flight path and create a background spectrum which is convoluted with the desired product spectrum. Only one precursor ion packet is affected by the laser pulse and thus a "light on" minus "light off" background subtraction algorithm can be used to produce the product spectrum.

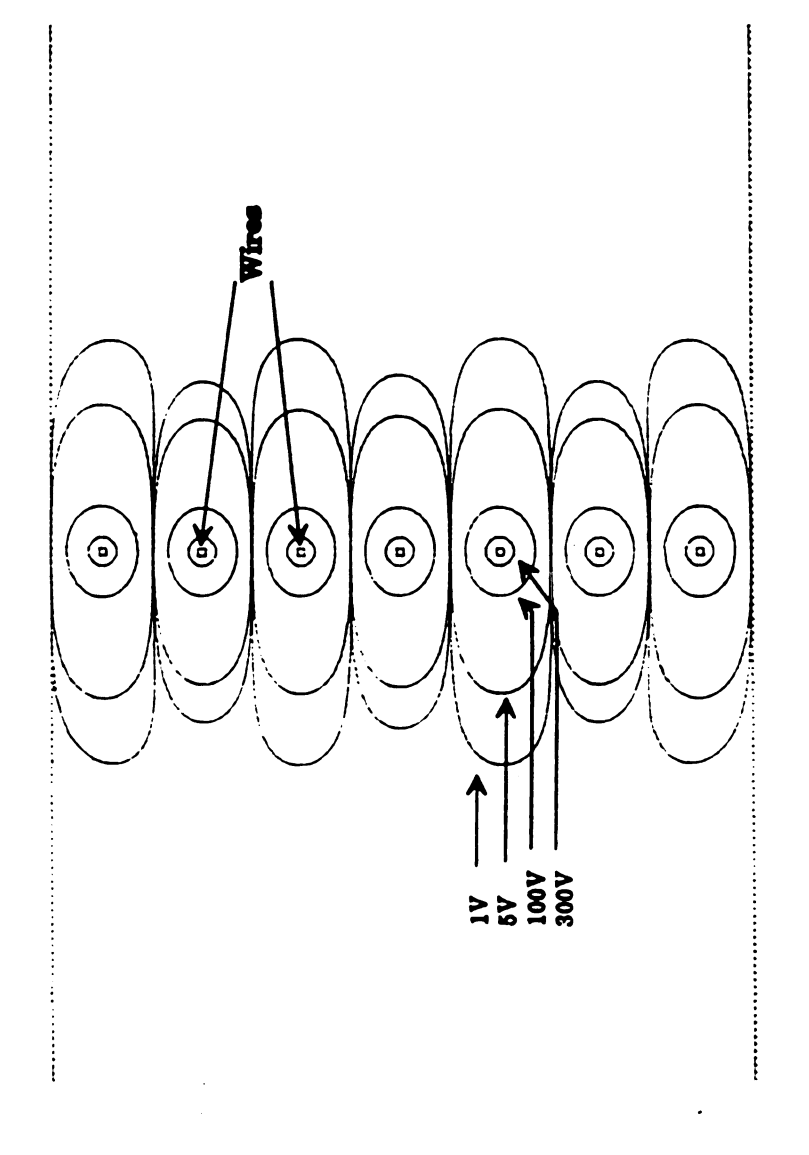
If SID or CID is utilized, however, all precursor ions passing through the interaction region may interact. The result would be a convolution of all product spectra of all precursor ions for the compound(s) ionized. Such a convoluted spectrum would be nearly impossible to decipher. For these experiments, a gate which allows exactly one isomass precursor ion packet to the interaction region and rejects all of the others is necessary.

The gate designed, was patterned after a gate which was only briefly described in a paper by Schlag et al. [4]. This gate uses a plane of thin (.003" thick), parallel wires placed orthogonal to the ion beam about 6 inches prior to the interaction region. With 500 V and -500 V potentials (relative to the shield voltage) applied to alternate wires, ions are deflected to the right or left, depending upon the polarity of the field through which the ions pass. When the

voltage applied to the wires is set at the shield voltage the gate is "open" and ions pass through unaffected. Modeled by SIMION (Figure 4.7), the advantage of this gate design is that the deflection field extends only a short distance down the flight path compared to a parallel plate deflection system, which is typically employed for deflecting ion beams. With this new gate, modeling suggests that unit resolution for precursor ion selection to m/z = 1000 can be achieved if pulsers having very short rise times (~10 ns) are employed (assuming mass resolution of 1500 FWHM).

4.2.5.3 Light Tube

An obstruction free path through the vacuum chamber for the high power excimer laser beam is necessary to eliminate the ionization and volatilization of molecules on any surface. A preliminary experiment in which the laser beam was simply passed through the stainless steel mesh shields caused the ion beam to be reduced to 10% of its original intensity. Although not studied thoroughly we believe that this attenuation in ion signal was caused by ion/molecule, ion/electron, and/or ion/ion collisions with species photo-desorbed off of the mesh shield. A stainless steel tube was designed which extends through both the first and second TOF regions, and has an aperture at the interaction region through which the ions travel. This tube, held at -500 V in the first TOF analyzer and -1500 V in the second mass analyzer allows the laser to pass unobstructed (except for background gas molecules and analyte ions) and maintains a field free drift path in both analyzers.



SIMION model of the ion gate. This gate is made of fine wires (0.003" diameter). Alternate wires are held at +300V and -300V. The potential field generated by these alternating electrodes extends only a few millimeters. This short field allows for the selective gating of closely bunched ion packets and thus high resolution gating. Figure 4.7

The second of th

4.2.6 Second TOF Analyzer

4.2.6.1 Post Acceleration

Product ions produced in the interaction region will retain, approximately the velocity of their precursor ion, but will only have a fraction of the kinetic energy of the precursor. To impart mass dependent velocities, the ions are accelerated immediately following the interaction region. The acceleration field, established by two parallel grids, is mounted on the optical rail.

4.2.6.2 Reflectron 2

The requirements of the second reflectron are different than the first reflectron, because the ions to be focused have a much larger range of energies. The product ions have a mass dependent fraction of energy obtained from the precursor. Two types of reflectrons have been constructed for this second stage of analysis. The first grid-free reflectron is, except for the voltages applied, identical to the grid-free reflectron used for the first TOF analyzer. The second is a gridded, two-stage mirror. To construct this gridded reflectron, a very thin, electrodeposited sheet of grid material was secured to the first and second washers, and 5 M Ω resistors are used between the back eight washers. A more detailed analysis of the requirements and operation of these reflectrons is found in Chapter 6.

4.2.6.3 Detector 2

The final detector, flange mounted at the end of the second TOF analyzer, detects the unfragmented precursor ions and product ions produced. This detector was designed to incorporate three multichannel plate amplifiers if necessary for low current signals. This third MCP has not been necessary due to the ample sensitivity observed.

4.3 Performance

This instrument was built in a stepwise manner. The source, first TOF analyzer, detector, and necessary ion optical elements were built first, and their performance evaluated. Next the second TOF analyzer, and its components were installed and tested. The results of these experiments are reviewed in this section.

4.3.1 Resolution

With a detector placed at the interaction region of the TOF/TOF instrument, mass resolution is measured to be approximately 1500 (FWHM). Figure 4.8 is a mass spectrum of the molecular ion region of bromobenzene, demonstrating the resolution achieved.

Figure 4.9 is a spectrum of bromobenzene (m/z = 158) collected at the final detector. Calculated resolution for this spectrum is over 1700. The ions which produced this spectrum were created in the source, reflected by the first ion reflectron to form a space-focus plate at the interaction region, accelerated by the acceleration grids, reflected and focused by the second reflectron and detected at the final detector position. Unfortunately, the resolution achieved at the final detector is not twice the resolution achieved at the interaction region as would be expected with the extended flight path. The reason for this anomaly is not yet determined.

4.3.2 Beam Image

In order to maximize the photo-induced dissociation efficiency, the ion beam must be both temporally and radially focused at the interaction region. In order to measure the radial distribution of the ion beam, an iris diaphragm which can be controlled via a rotational motion feedthrough was constructed and

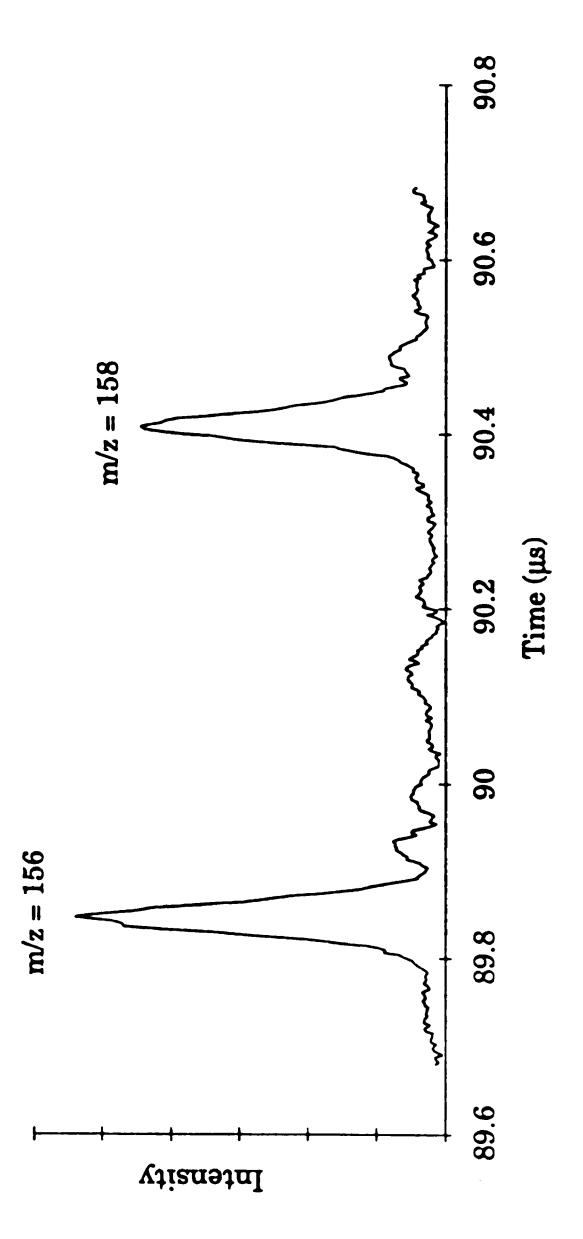
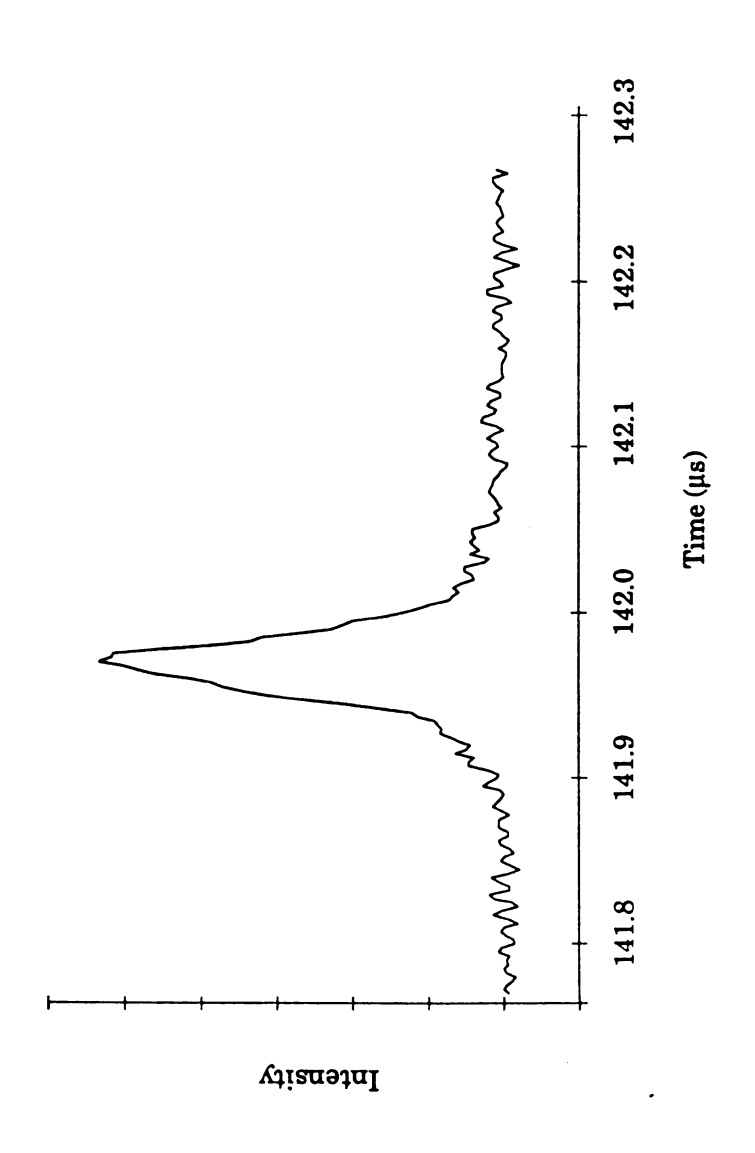


Figure 4.8 Mass spectrum of bromobenzene collected with a detector at the interaction region, showing resolution of 1500 (FWHM) for the molecular ion (m/z = 156 and 158).



bromobenzene collected with a detector placed at the end of the second TOF analyzer, showing resolution greater than 1700 (FWHM). Figure 4.9 Mass spectrum for the monoisotopic molecular ion (m/z = 158) of

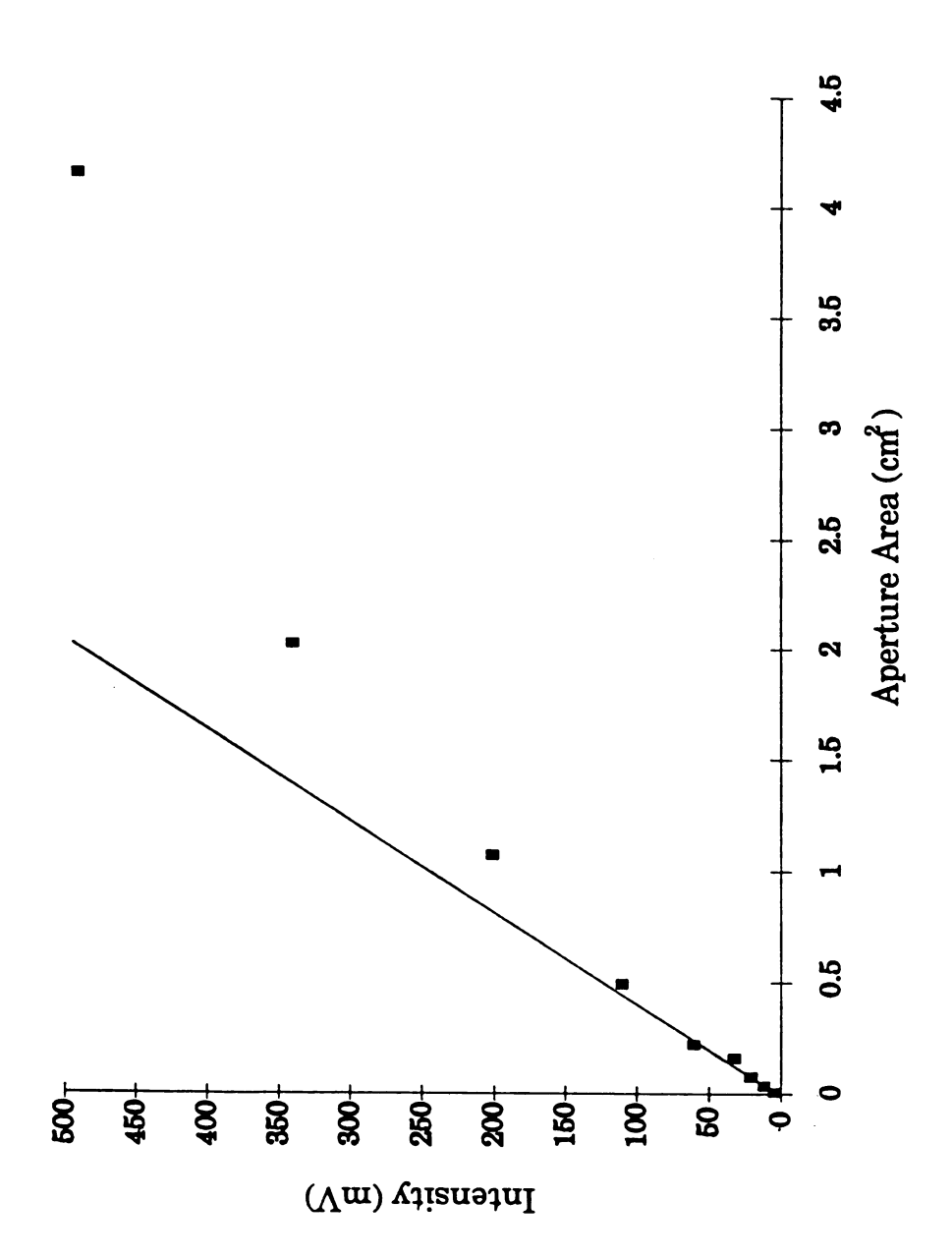


Figure 4.10 Plot of the intensity of m/z = 18 as a function of the iris diaphragm aperture area.

placed in front of the detector at the interaction region. Figure 4.10 is a plot of ion intensity (m/z = 18) versus the area of the aperture opening. The intensity increased linearly until the aperture area was approximately 0.5 cm^2 , and was still increasing, but less rapidly, when the maximum area for the detector was reached ($\sim 4.1 \text{ cm}^2$). This indicates that although the ion beam is more intense in the center, a substantial percentage of the ions at the interaction region are in a less dense outer radius. In addition, a large number of ions are probably not being detected due to their radial energies. Improvements in the source design, to minimize non-linear extraction fields, and in the Einzel lens design, to minimize the aberration effects, may help to tighten the radial focus of the ions and may help reduce the ion loss.

4.3.3 Preliminary Gate Studies

A study of the gate voltage necessary to effect ion deflection was done to establish conformity with the SIMION modeling of this process. Since the dual pulsers needed for this experiment are not yet completed, static voltages were used on the alternate gate wires. The gate was placed 6" in front of a detector located at the interaction region. An 0.5" aperture placed in front of the gate was used to define the diameter of the ion beam. Figure 4.11 is a graph of the relative ion intensity versus the potential difference applied between alternate wires. In agreement with modeling, potentials of 130 V and -130 V, were necessary to deflect the entire beam from the detector. Much larger voltages will actually be used in order to cause deflection of ion packets which only experience a fraction of this deflecting field due to their close proximity to the packet being selected. The amplitude and rise time of this deflecting pulse will ultimately limit the resolution of the gate selection.

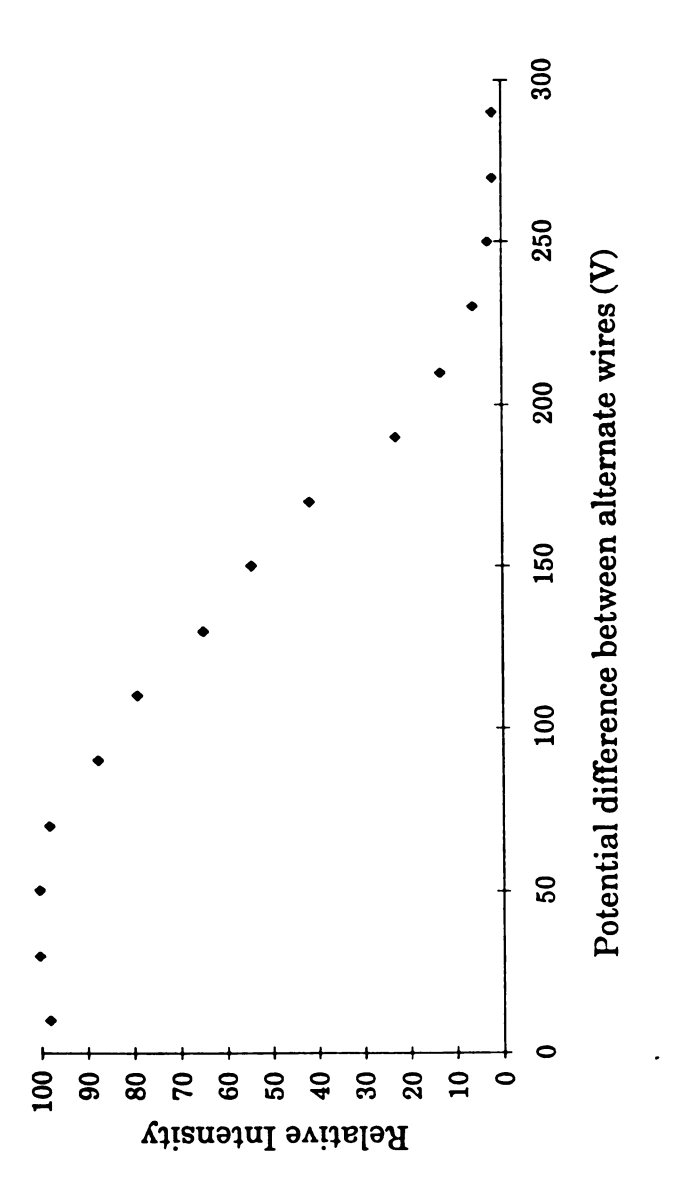


Figure 4.11 Plot of ion intensity versus the potential difference applied between alternate wires of the deflection grid.

References

- D. R. McLane, Doctoral Dissertation, Michigan State University, 1993.
- J. F. O'Hanlon, A User's Guide to Vacuum Technology, John Wiley & Sons, Inc., 1989, 445.
- 3 H. Wollnik, M Przewloka, Int. J. Mass Spectrom. Ion Proc., 1990, 96, 267.
- 4. R. Weinkauf, K. Walter, C. Weickhardt, U. Boesl, E. W. Schlag, Z. Naturforsh., 1989, 44a, 1219.

Chapter 5: Photo-Induced Dissociation

Truth as subject Beauty as means Utility as purpose

Alessandro Manzoni

5.1 Introduction to Photo-Induced Dissociation

Ion photo-induced dissociation is the process:

$$AB^+ + hv \rightarrow A^+ + B$$

The pioneering work in ion photo-induced dissociation (PID) began in the 1960's [1]. These early studies were performed by physicists interested in determining the interaction cross section of very simple species (e.g., H_2^+). In the 1970's, Dunbar [2] began using the ion cyclotron resonance (ICR) mass spectrometer to study photo-induced dissociation of more complex species of chemical interest. PID was shown to provide information about the optical spectroscopy and the electronic and vibrational levels of gas phase ions. Capable of trapping ions for minutes, the ICR was well suited for early PID studies due to the very low PID cross sections and low photon sources available. PID cross-sections have been determined to be between 10^{-17} and 10^{-19} cm²

[2] for ions such as N₂O+, CH₄+, and the molecular ions of trimethylbenzene, butadiene, and hexatriene. In ICR instruments, sufficient photofragment-ion yields were obtained using conventional arc lamp sources. Unfortunately, these experiments are difficult to interpret due to the formation of metastable, CID, and ion-molecule product ions formed during the relatively long trapping time in the ICR [3]. Background subtraction techniques do not eliminate these interferences because the neutral molecules involved in these processes are often desorbed from the ICR electrodes by photon excitation.

In the 1980's Beynon [4] took advantage of the introduction of high-powered continuous-wave lasers and performed PID in a beam instrument. To effect sufficient fragmentation yields, it was necessary to bring the ion and laser beams into axial coincidence.

Morrison [5] used a flashlamp-pumped dye laser with relatively long flash duration (1 μs) oriented perpendicular with respect to the low density ion beam in the interaction region of a triple quadrupole mass spectrometer. Again the low sensitivity with orthogonal excitation observed was improved by the use of a coaxial geometry which exposed a greater number of ions to the laser flash.

With the development of lasers producing short-duration, high-energy, pulses, came the implementation of time-of-flight mass spectrometers in conjunction with PID. Russell has used a hybrid EB/TOF mass spectrometer with PID occurring between the magnetic sector and the TOF mass spectrometer [6]. Using pulsed Cs+ ion liquid SIMS ionization and a pulsed excimer laser, Russel demonstrated an increase in sensitivity of 10³-10⁴ over experiments with a CW laser. Colby and Reilly have performed TOF MS/MS analysis on benzene and aniline [7]. These studies relied on the ability to selectively photodissociate a chosen ion over all others in the source of a TOF mass spectrometer. Duncan [8] has demonstrated the utility of PID in a

reflectron TOF mass spectrometer by exciting gate-selected ions in the turn-around region of the reflectron. Using the reflectron solely to decelerate the ions for interaction was necessary due to the difficulty he experienced in timing the laser pulse. Schlag *et al.* [9] have demonstrated MS/MS using linear TOF separation of gate-selected precursor ions, PID at the space-focus plane, and sequential focusing of the product ions with a reflectron voltage scanning technique.

With the availability of very high-powered, short duration, pulsed lasers which can be operated at frequencies to 300 Hz, photo-induced dissociation is uniquely suited to the fragmentation needs of our tandem time-of-flight mass spectrometer. In this instrument, isomass ion packets are well focused to temporal and spatial dimensions that are very similar to those of our focused laser pulse. The resulting high degree of spatial and temporal overlap not only provides optimal PID efficiency, but high resolution selection of the precursor ion packet of interest is also achieved. In addition, the ability to operate the laser at high frequency allows many product spectra to be produced per second. In this chapter the achievement of high-efficiency PID consistent with the overall instrumentation goals is presented.

5.2 PID in the TOF/TOF Instrument

To maximize the photo-induced dissociation fragmentation efficiency, the maximum number of the desired precursor ions produced in the source must be exposed to as dense a population of photons as possible. In addition, a high percentage of the product ions formed must be detected. Using a storage source and reflectron focusing of precursor ions, the tandem time-of-flight

instrument provides this high overlap of ions and photons and with TOF analysis of product ions detection efficiency is maximized.

For precursor ion selection we rely on the laser pulse interacting with exactly one precursor m/z value. The laser pulse is focused to a width of approximately 1 mm. The isomass ion packets are also focused to 1 mm in length (resolution = 1200 FWHM). At m/z 1000, the trailing edge (FWHM) of the m/z 1000 ion is separated from the leading edge of the m/z 1001 ion by 0.2 mm. During the 17 ns temporal length of the laser pulse, the m/z 1000 ion packet travels 0.2 mm. At higher m/z values, the distance between ion packets becomes smaller than the distance traveled in 17 ns, and unit resolution for precursor selection is not achieved. If greater resolution were required, focusing the laser beam to less than 1 mm or improvements in the precursor resolution (above 1200) could be made.

The laser used in this system is a Questek 2580v β excimer. Operating with ArF (193 *nm*) at 30 *Hz*, this laser was measured to yield between 4-5 *W*, or approximately 150 *mJ* per pulse. When focused by a cylindrical plano-convex lens down to the dimensions of the ion packet (1 *cm* x 1 *mm*), the laser pulse photon density is 1.46 x 10¹⁸ photons/*cm*². Given that PID cross-sections have been determined to be between 10⁻¹⁷ and 10⁻¹⁹ *cm*² [2] the PID efficiency should theoretically be between 100% and 15%.

5.3 Results and Discussion

5.3.1 Precursor Selection

Figure 5.1a is a spectrum of the molecular ion region of bromobenzene. lons in this spectrum have traveled through the entire instrument. With the laser

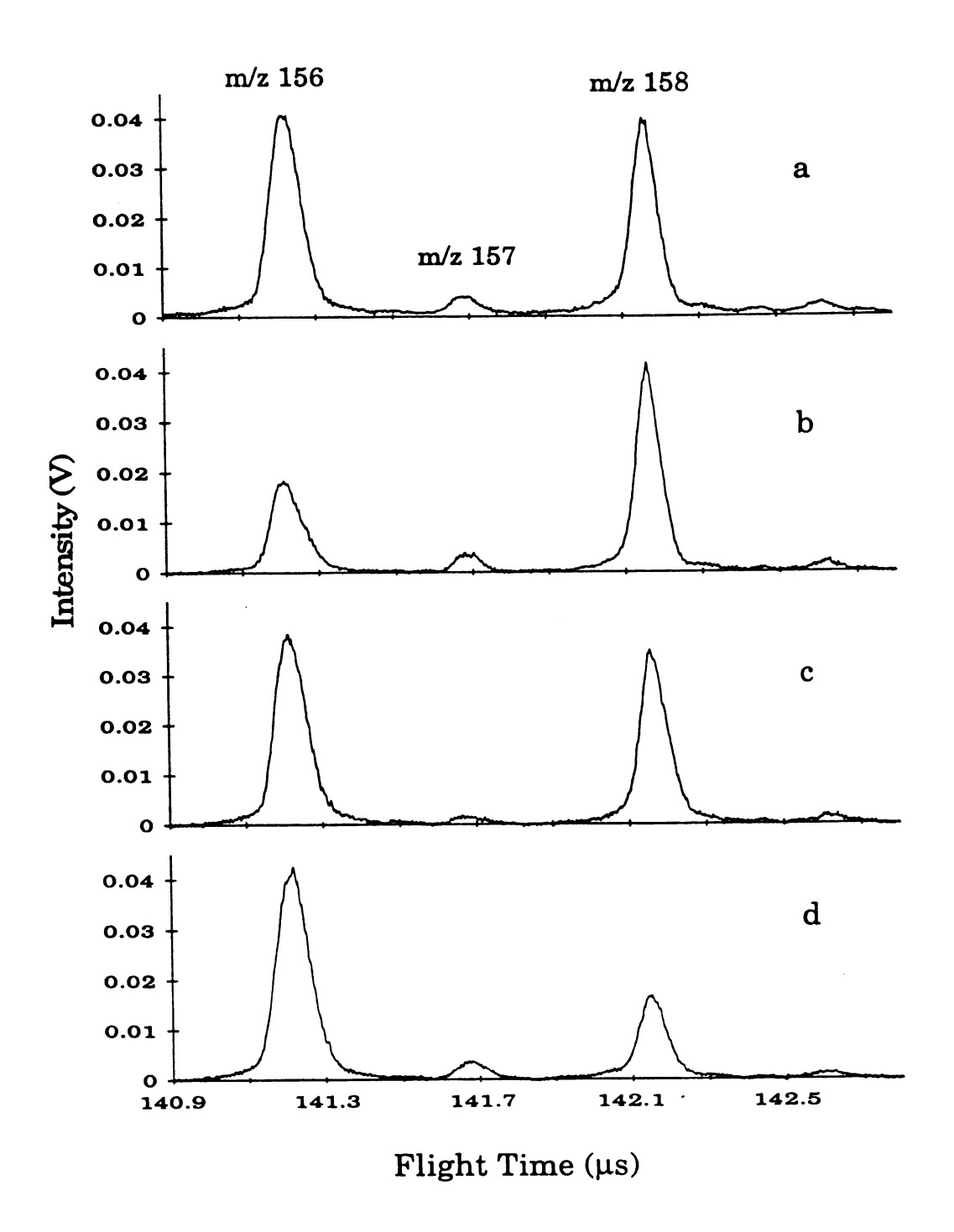


Figure 5.1 Spectra of the molecular ion region of bromobenzene. a. Spectrum with the laser off. b-d. Spectra with the laser delay set at 86.40 μ s, 86.70 μ s and 86.97 μ s, respectively.

on and the delay time between source extraction and laser firing set such that the laser pulse arrives at the interaction region at the same time as the precursor ions, interaction between the ions and photons occurs. Figures 5.1b-d are the spectra obtained when the laser delay times are set at 86.40 us. 86.70 us and 86.97 μ s to coincide with the ion packet arrival times for m/z values 156, 157 and 158 successively. The ion depletion associated with each of these times is limited to the selected ion and demonstrates the effectiveness of precursor selection by laser timing adjustment. Calibration of delay times is easily accomplished due to the linear dependence of flight time on the square root of m/z. The ion arrival time jitter and laser thyratron discharge jitter were both measured to be less than 2 ns. Once the instrument is calibrated, selection of a new precursor ion simply involves changing the laser delay time to the calculated value for the desired precursor m/z value In addition, the day to day arrival time drift is less than 100 ns. Recalibration requires only 3-4 attempted laser delays. Precursor ion areas have been depleted by 55.2%, 56.3%, and 51.8% for m/z = 156, 157, and 158, respectively. This substantial depletion demonstrates that considerable photon-ion interaction is achieved. To prove that the observed fragmentation is due to PID and not CID with laser desorbed molecules, the laser was triggered so that the laser pulse arrives at the interaction region 50 ns before the m/z = 156 ion packet. No depletion was observed. In addition, the fact that we have selectively excited ion packets separated by 300 ns conclusively indicates that only PID is affecting the observed ion intensity.

5.3.2 PID Efficiency

The efficiency of the PID process is determined by the efficiency of fragmentation and the efficiency of collection of the ions. Letting P and Po

represent the precursor ion current with and without laser excitation, respectively, and ΣF_i the total current of all fragment ions, the fragmentation efficiency is $E_F = \sum F_i/(P + \sum F_i)$, the collection efficiency is $E_C = (P + \sum F_i)/P_o$, and the overall PID efficiency is the product $E_{PID} = E_F \cdot E_C = \sum F_i/P_o$ [10].

To perform efficiency studies, a detector was placed approximately 20 cm beyond the interaction region as depicted in Figure 5.2. This arrangement allowed us to study the PID process independent of the effects of the second reflectron. Figure 5.3a-b are product spectra for the molecular ion (m/z = 156) of bromobenzene and for m/z = 91 of toluene. In these cases, the precursor ions have been separated by their m/z-dependent velocities and focused at the detector. These product spectra were obtained by subtracting the Laser Off spectra from the Laser On spectra. In the bromobenzene product spectrum, ion peaks at $t = 93.60 \ \mu s$, $93.39 \ \mu s$, $92.95 \ \mu s$, $92.50 \ \mu s$ and $91.50 \ \mu s$ correspond to product ions with 6, 4, 3, 2 and 1 carbon atoms, respectively. The calculated fragmentation efficiency, collection efficiency and overall PID efficiency are 56%, 116%, and 65%, respectively. Compared to the EI spectrum, the relative intensities of the lower m/z fragment ions are enhanced in this PID product spectrum, indicating that either multiple single photon or multiphoton events are likely to be occurring.

Product spectra from precursor ions for bromobenzene, nitrobenzene, acetophenone, triethylamine, N,N-diethylformamide, N-methylacetamide, and cyclohexene were also collected. Efficiencies for these compounds are given in Table 5.1. The compounds and precursor ions chosen demonstrate PID fragmentation of odd electron, even electron, aromatic and nonaromatic moieties. In most of these studies, the ions were space-focused at the detector rather than at the interaction region to improve product ion resolution. This

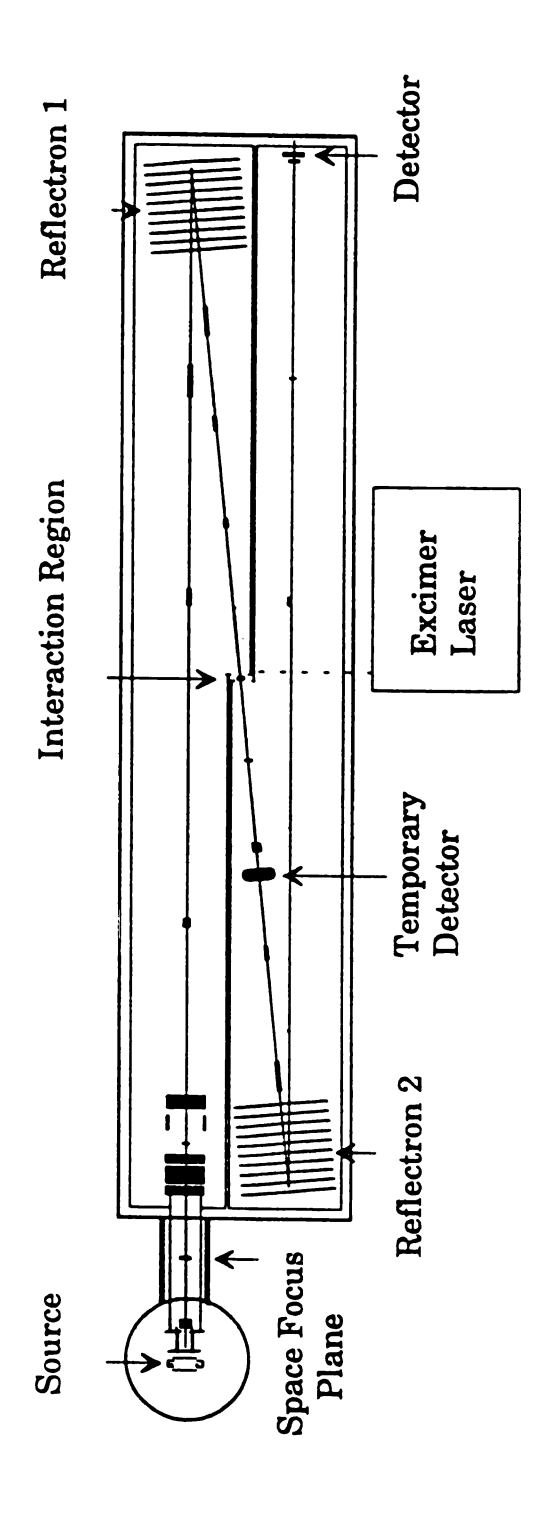


Figure 5.2 Diagram of the TOF/TOF instrument showing the location of the temporary detector approximately 12 inches after the interaction region.

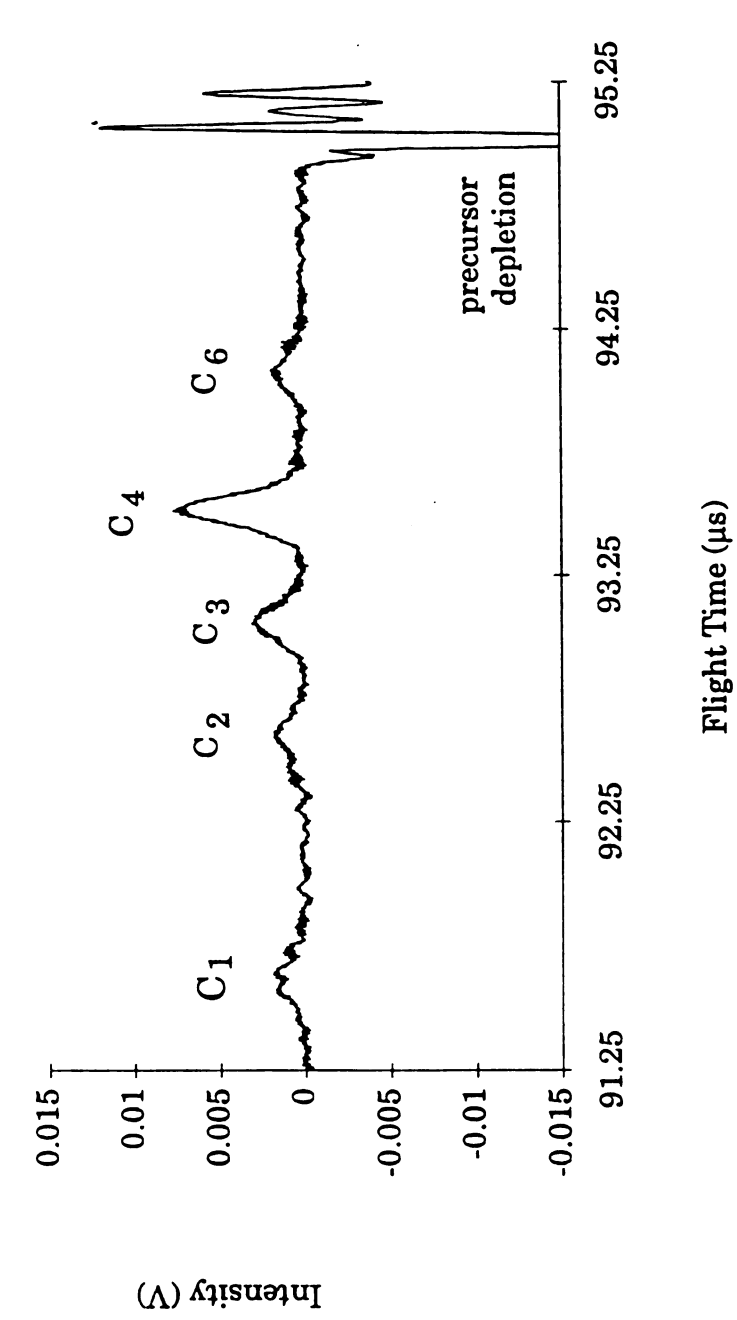


Figure 5.3 A product spectrum for the molecular ion (m/z = 156) of bromobenzene.

| 1 | | |
|--|--|--|
| 7 | | |
| : | | |
| | | |
| | | |
| 1 | | |
| total ferry division construction and an article and article article and article article and article article article article article article article and article artic | | |
| | | |
| | | |
| | | |
| | | |
| | | |
| | | |
| | | |
| | | |
| | | |
| | | |

Table 5.1 PID results for several precursor ion m/z values

| bandamo | Procureor Ion m/7 | I aser Pulse | Fragmentation | Collection | PID |
|---|---|--------------|---------------|------------|------------|
| Collipodina | 100000000000000000000000000000000000000 | Energy | Efficiency | Efficiency | Efficiency |
| | | (m) | (%) | (%) | (%) |
| hromohonzene | 156 | 150 | 56 | 116 | 65 |
| 200000000000000000000000000000000000000 | 77 | 160 | 30 | 93 | 28 |
| | 156 | 130 | 79 | 132 | 104 |
| | 77* | 130 | 44 | 113 . | 20 |
| tolliana | 91 | 110 | 39 | 103 | 40 |
| nitrohonzono | 123 | 140 | 99 | 137 | 91 |
| nii Openzene | 105 | 140 | 54 | 107 | 58 |
| +riothylomino | 88 | 110 | 27 | 119 | 32 |
| N,N-diethyl- | 86 | 100 | 24 | 66 | 24 |
| formamide | | | | | |
| N-methyl- | 73 | 120 | 59 | 94 | 27 |
| acetamide | | | | | 1 |
| cyclohaxana | 29 | 140 | 12 | 91 | |

*Precursor ions were focused at the interaction region instead of at the detector.

resulted in reduced PID efficiencies. To determine the effect of improved focusing on PID efficiency, two precursor ions (indicated by asterisks in Table 5.1) were studied with the space focus at the interaction region. As hypothesized, PID efficiencies were increased. Collection efficiencies of greater than 100% were sometimes observed. This could be the result of greater detector gain for ions with higher velocity (lower m/z) [11].

The overall PID efficiency of 104% achieved for bromobenzene is much higher than the 15% achieved by McIver et al. [12] in an ICR instrument. Furthermore, it is higher even than the efficiency achievable in the CID process in a triple quadrupole instrument (65% for n-hexane) [10]. These results give evidence that PID can be an analytically useful fragmentation technique when implemented in a system with high ion/photon overlap.

5.3.3 Photoionization

In addition to the high efficiency photo-induced dissociation observed, photoionization of residual background molecules present in the interaction region was also observed (See Figure 5.4). The high frequency signal at 67 μs in this spectrum is due to the thyratron discharge of the laser. The three broad peaks located at 71-80 μs are the peaks due to the multiphoton ionization of background molecules. The ions produced in this process must drift from the field free interaction region into the acceleration region. After acceleration they are separated by their mass-dependent velocities and detected after a 12 inch flight. The predominant molecules typically present in the background matrix include H₂O, N₂, and O₂. These molecules have ionization energies of 12.6 eV, 15.6 eV, and 12.1 eV, respectively [13]. The ionization must therefore be a multiphoton process since a 193 nm photon has 6.44 eV of energy. To eliminate the detection of these photoionization ions when collecting product spectra a

repelling grid with a low voltage (10V) applied to it was placed immediately after the interaction region to deflect the multiphoton ionization products.

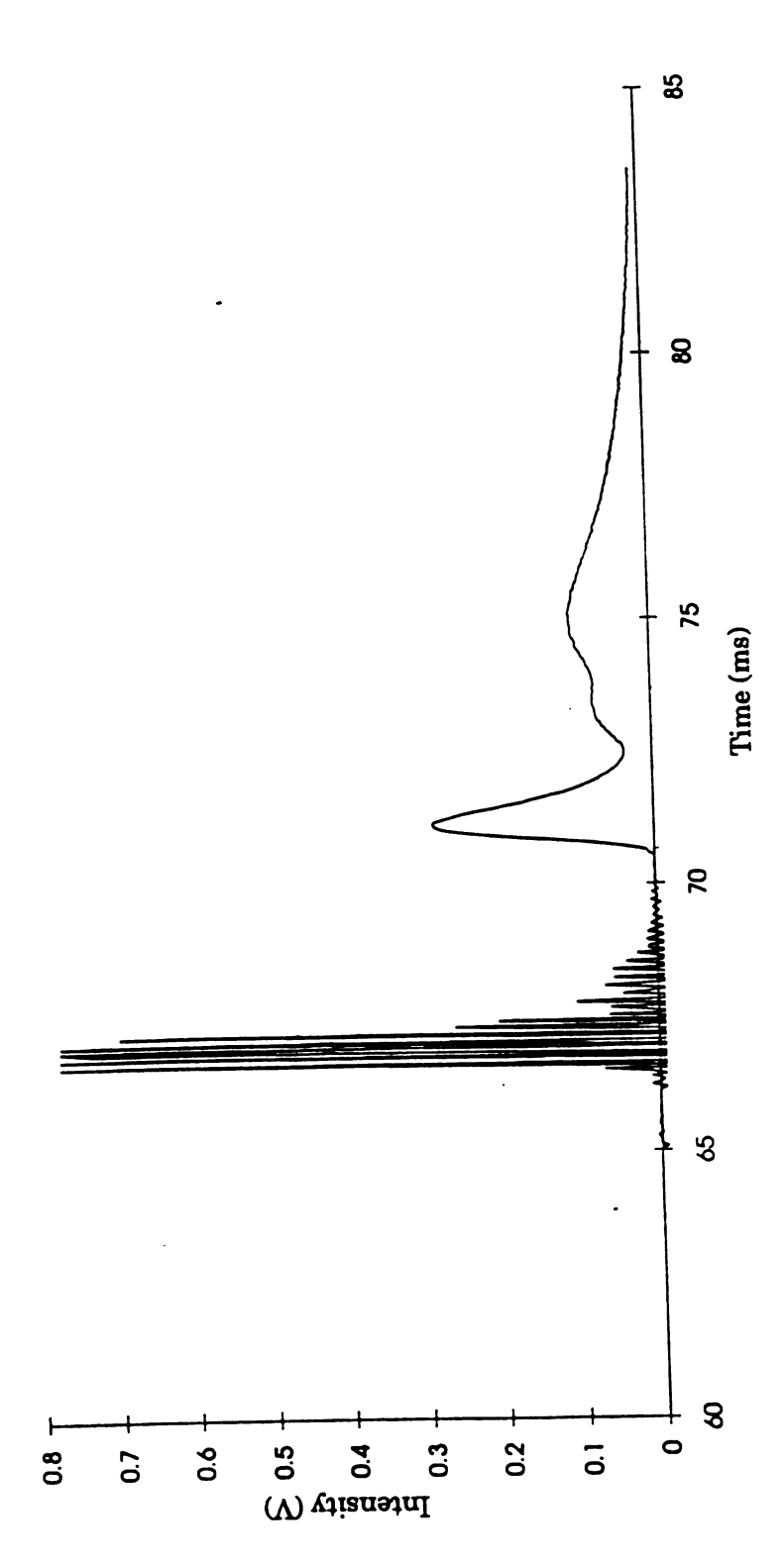


Figure 5.4 The spectrum resulting from the photoionization of residual gas molecules in the interaction region.

References

- G. H. Dunn, *Atomic Collision Processes*, M. R. C. McDowell, ed., North Holland Publ., Amsterdam, 1964.
- Dunbar, R. C. in Gas Phase Ion Chemistry; Vol. 2, Bowers, M. T., Ed. Academic: New York, 1979; p 181.
- 3 R. E. Tecklenburg, Jr., D. H. Russel, *Mass Spec. Rev.*, **1990**, 9, 405.
- 4 F. M. Harris, J. H. Beynon, Gas Phase Ion Chemistry, 1984, 3, 99.
- D.C.McGilvery, J. D.Morrison, *Int. J. Mass Spectrom. Ion Physics* **1978**, *28*, 81.
- R. E. Tecklenburg, Jr., D. H. Russell, *Presented at the Pittsburgh Conference*; Atlanta, GA, March 1989; p 488.
- S. M. Colby, M. Yang, J. P. Reilly, *Presented at the Pittsburgh Conference*; Atlanta, GA, March 1989; p 482.
- K. LaiHing, P. Y. Cheng, T. G. Taylor, K. F. Willey, M. Peschke,
 M. A. Duncan, *Anal. Chem.* 1989, *61*, 1458.
- 9 R. Weinkauf, K. Walter, C. Weickhardt, U. Boesl, E. W. Schlag, Z. Naturforsch 1989, 44a, 1219.
- 10 R. A. Yost, C. G. Enke, D. C. McGilvery, D. Smith, J. D. Morrison, *Int. J. Mass Spectrom. Ion Physics* **1979**, *30*, 127.
- 11 R. Meier, P. Eberhardt, *Int. J. Mass Spectrom. Ion Processes* **1993**, *123*, 19.

- 12 W. D. Bowers, S. S. Delbert, R. T. McIver, Jr., *Anal. Chem.* **1986**, *58*, 969.
- 13 F. W. McLafferty, 1980, <u>Interpretation of Mass Spectra</u>, University Science Books, 278.

Chapter 6: Product Ion Analysis

"The easiest way to lose success is to become convinced that you are successful."

American Express Commercial

6.1 Historical Use of TOF for Product Ion Analysis

The high sensitivity, high speed, low cost and inherent simplicity of time-of-flight analysis have made it an attractive alternative for the analysis of product ions. In 1976 Johnsen *et al.* [1] built a tandem magnetic sector/TOF instrument to study surface induced dissociation (SID). In 1985 LeBeyec and Della-Negra [2] developed a ²⁵²Cf TOF mass spectrometer which utilized a reflectron, and a neutral detector placed behind the reflectron. This instrument was developed to study metastable ions. The decay of a metastable ion in the field free region produced a neutral and a product ion. The time-of-flight of the neutral ion, detected at the neutral detector allows the determination of the precursor ion m/z value, and the reflectron gives the product ion a mass dependent velocity. A similar instrument using Cs+ SIMS was developed by Standing *et al.* [3]. Glish et al. [4], interested in developing a low cost MS/MS instrument built a

quadrupole/ TOF instrument which used CID in an intermediate collision cell, and beam deflection to create a discrete ion packet for TOF mass analysis. Cooks et al. [5] built a tandem TOF/TOF instrument which incorporated SID. The theoretically unlimited mass range and high sensitivity made TOF advantageous for the SID technique which is particularly useful for the fragmentation of large molecules requiring considerable amounts of internal energy to dissociate. More recently, Russel [6] has built a tandem magnetic sector (EB)/TOF instrument, and Schlag [7] has built a tandem TOF/TOF both using laser photo-induced dissociation. Although the instruments built to date have demonstrated some of the advantages of time-of-flight analysis of product ions, none has achieved unit mass resolution of the product spectrum over the full GC/MS mass range.

6.2 TOF Product Ion Analysis in the TOF/TOF Instrument

The tandem TOF/TOF was designed to obtain unit mass resolution for both precursor ion selection and product ion analysis. Achieving unit mass resolution for the production ions, however, is complicated by the fact that the kinetic energy of the product ions is mass dependent.

After photo-induced dissociation in the interaction region has occurred, the product ions produced move with the same velocity as their precursor ion. The product ions also have a fraction of the kinetic energy spread which was obtained by the precursors in the source extraction process as well as the additional kinetic energy acquired in the photofragmenation process. The product ions are not accelerated after photo-induced dissociation, they will all reach the second reflectron at approximately the same time, and the field in this

reflectron will serve to mass separate the ions. Serving as a mass analyzer, however, the reflectron's energy focusing ability is lost.

In order to focus the kinetic energy distribution of the product ions, the products are accelerated just following the interaction region. This acceleration causes the ions to acquire mass dependent velocities, and isomass ion packets separate prior to the second reflectron. The total kinetic energy of the product ion is mass dependent. If the m/z value of a product ion is m_d and the m/z value of the precursor ion is m_p , the kinetic energy of the product ion (K_d) after fragmentation is $m_d/m_p \times K_p$ where K_p is the kinetic energy of the precursor ion. With a precursor ion energy of 500 eV and a post fragmentation acceleration potential of 1000 eV, the range of energies for a given selected precursor and its products is 1000 eV to 1500 eV with the unfragmented precursor ion having the greatest energy.

Unfortunately, for a reflectron to achieve perfect energy focusing, all of the ions should have relatively the same kinetic energy. The second reflectron, if optimized for the energy of the precursor ions, will not achieve perfect focusing of the product ions.

6.3 Theoretically Modeled Resolution

Concerned about the extent to which the resolving power of the second reflectron is dependent upon the energy spread, this reflectron was mathematically modeled.

Using an equation for the resolution of a linear mirror developed by D. Ioanoviciu (Equation 6-1), the effect of the energy spread was theoretically estimated.

$$R = \frac{\left(1 + \frac{C}{L}\right)}{2\Psi} \tag{6-1}$$

where:

$$C = \frac{4d_1}{u_1 \cos \theta}$$

$$\Psi = \frac{l_o}{L} + \frac{S}{L} \tan \theta \left(1 + 2\alpha \tan \theta + \frac{\partial_f}{2} \right)$$

$$+ \frac{1}{L} \left(2\alpha \tan \theta + \frac{\partial_f}{2} + \frac{\beta^2}{2} \right) \left| \frac{\eta}{\eta_{cor}} - 1 \right|$$

$$+ \frac{1}{L} \alpha^2 \left| \tan^2 \theta + \frac{1}{2} \left(1 - \frac{\eta}{\eta_{cor}} \right) \right|$$

$$+ \frac{1}{L} \alpha \partial_f \tan \theta \left(1 + \frac{\eta}{\eta_{cor}} \right) + \frac{\partial_f^2}{8} \left(3 - \frac{\eta}{\eta_{cor}} \right)$$

lo = the ion packet length at the interaction region

S = the ion packet width at the interaction region

 θ = the incidence angle at the second reflectron's entry

 α = the radial half angular aperture of the beam (packet's divergence)

 β = the maximum axial angle normal to the deflection plane

 ∂_f = the relative ion energy spread in the second TOF region

 η = reference energy in the second TOF analyzer. Products of ratio ρ (not energy focused)

$$= U_0 \rho + \Delta U$$

 U_0 = the energy of the precursor before interaction

 ΔU = the additional energy obtained by acceleration after interaction

 η_{cor} = reference energy in the second TOF analyzer. Products of ratio ρ (correctly energy focused)

$$= U_0 \rho_{cor} + \Delta U$$

 ρ = mass product (m_d)/mass precursor (m_D)

 δ_0 = the initial relative energy spread of the precursors

Given the TOF resolving power achieved in Giessen (2000 FWHM), values for the parameters necessary for this calculation were estimated, and the resolution for the second TOF analyzer was calculated for product ions of precursors with m/z values of 500, 1000, and 2000. As seen in Figure 6.1, the product ions formed from precursor ions with m/z values to 1000 were calculated to have at least unit mass resolution. In addition it was determined that improvements in resolution are expected if the range of energy was minimized. For example, resolution should improve if the ions receive an additional 2000 eV after the interaction region giving the product ions an energy spread from 2000 to 2500 eV rather than 1000 to 1500 eV. Another possible method for reducing the relative energy spread would be to decelerate the ions prior to interaction.

6.4 Performance

The reflectron tested in the second analyzer of the TOF/TOF instrument was a grid-free reflectron. This grid-free reflectron was indicated to be capable of resolving a larger range of energies than a gridded reflectron [8].

Initial photo-induced dissociation experiments of the bromobenzene molecular ions (m/z = 156, 157 and 158) showed a dramatic depletion of the precursor ion peaks (Chapter 5, Section 5.3.1) but no product ions were observed. In was anticipated that the predominant product peak would be from the loss of Br· (m/z = 77). As observed in Figure 6.1 the resolution for product ions which retain half of the kinetic energy of their precursors is dramatically less than that of the precursor. It was hypothesized that no product ions were detected in this experiment due to their very poor resolution. Another possible explanation of the absence of product ions is that upon dissociation a significant

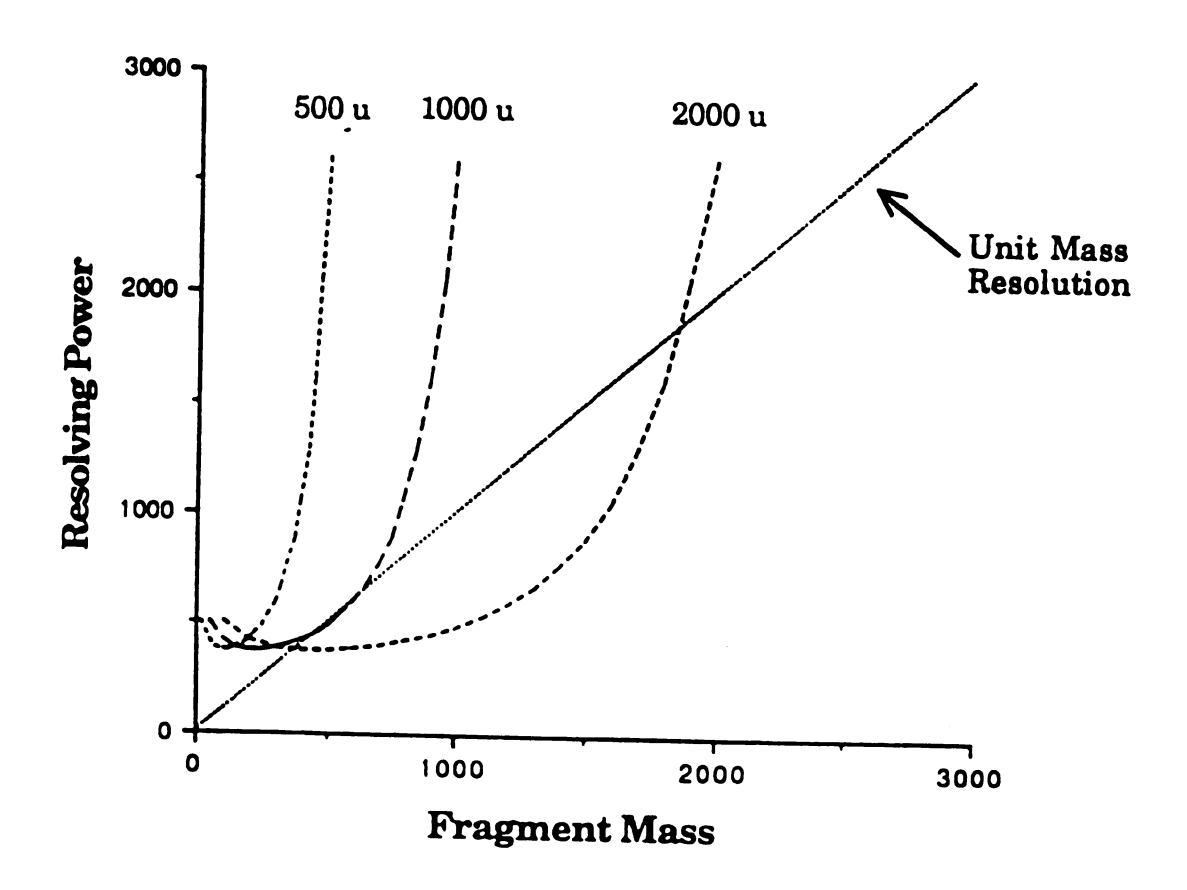


Figure 6.1 Simulated resolution of product ions for precursor ions with m/z = 500, 1000, and 2000. All fragment ions of precursor ions with m/z ≤ 1000 will have at least unit mass resolution.

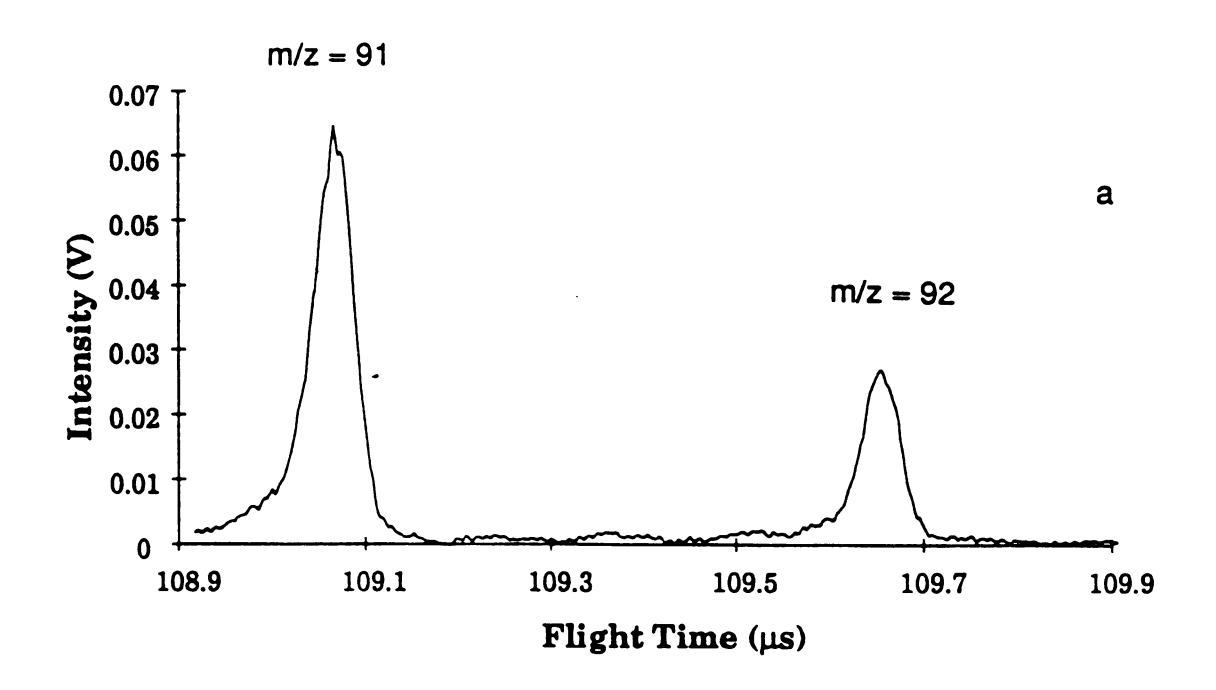
amount of kinetic energy is released causing a displacement of the products from the precursor ion axis [9].

To test these hypothesis, the molecular ion of another compound, toluene, was photodissociated. Toluene was chosen because one of the dominant product ions from the molecular ion (m/z = 92) results from the loss of H· (m/z = 91). A spectrum of the molecular ion region of toluene is shown in Figure 6.2 a. Figure 6.2 b is a spectrum of the same region with the laser timed to interact with the molecular ion. The peak at 109.4 μ s corresponds to the m/z = 91 product ion peak demonstrating that product ions with energies similar to their precursors are focused by the reflectron.

When the second reflectron's voltages were lowered to optimally focus a product ion with 1250 eV (m/z = 77) rather than the 1500 eV of the precursor ion (m/z = 156), a product ion peak was observed (See Figure 6.3). It is thus possible to obtain good resolution for the complete product ion spectra by scanning the reflectron's voltages but the advantages of simultaneous product ion detection are lost. This technique was used by Schlag [7] in his tandem TOF/TOF instrument.

6.5 The Second Reflectron

Ideally, the second reflectron would be capable of resolving a very large range of ion kinetic energies. Mamyrin [10] has shown that second-order time-of-flight focusing for the ions with respect to energy is possible using a two stage reflectron. In addition, Rockwood [11] has developed a method which gives infinite order correction against energy variations. In his "perfectron" the potential field is of the form $\phi = kx^2/2$. Ions start at x=0, travel into the perfectron, are reflected by the parabolic field and are focused at the origin. A



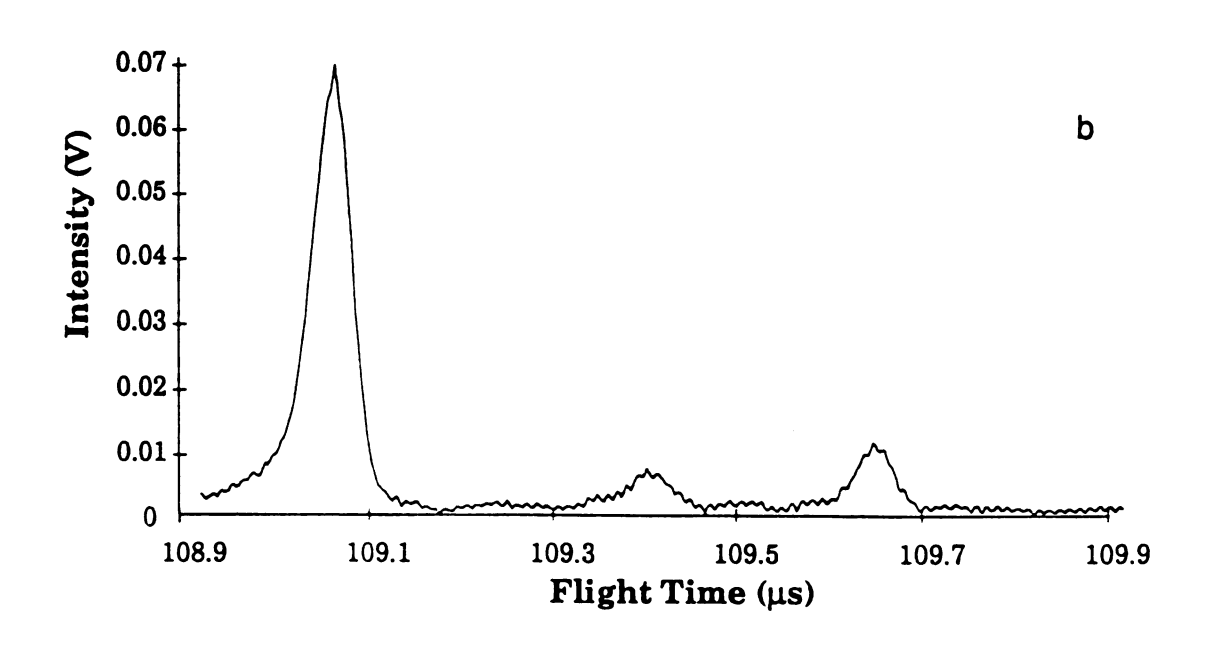


Figure 6.2 a. A spectrum of the molecular ion region of toluene obtained at the final detector. b. The spectrum of the molecular ion region of toluene when the laser is fired to interact with the molecular ion (m/z = 92). The peak at 109.4 μ s is m/z = 91 product ion.

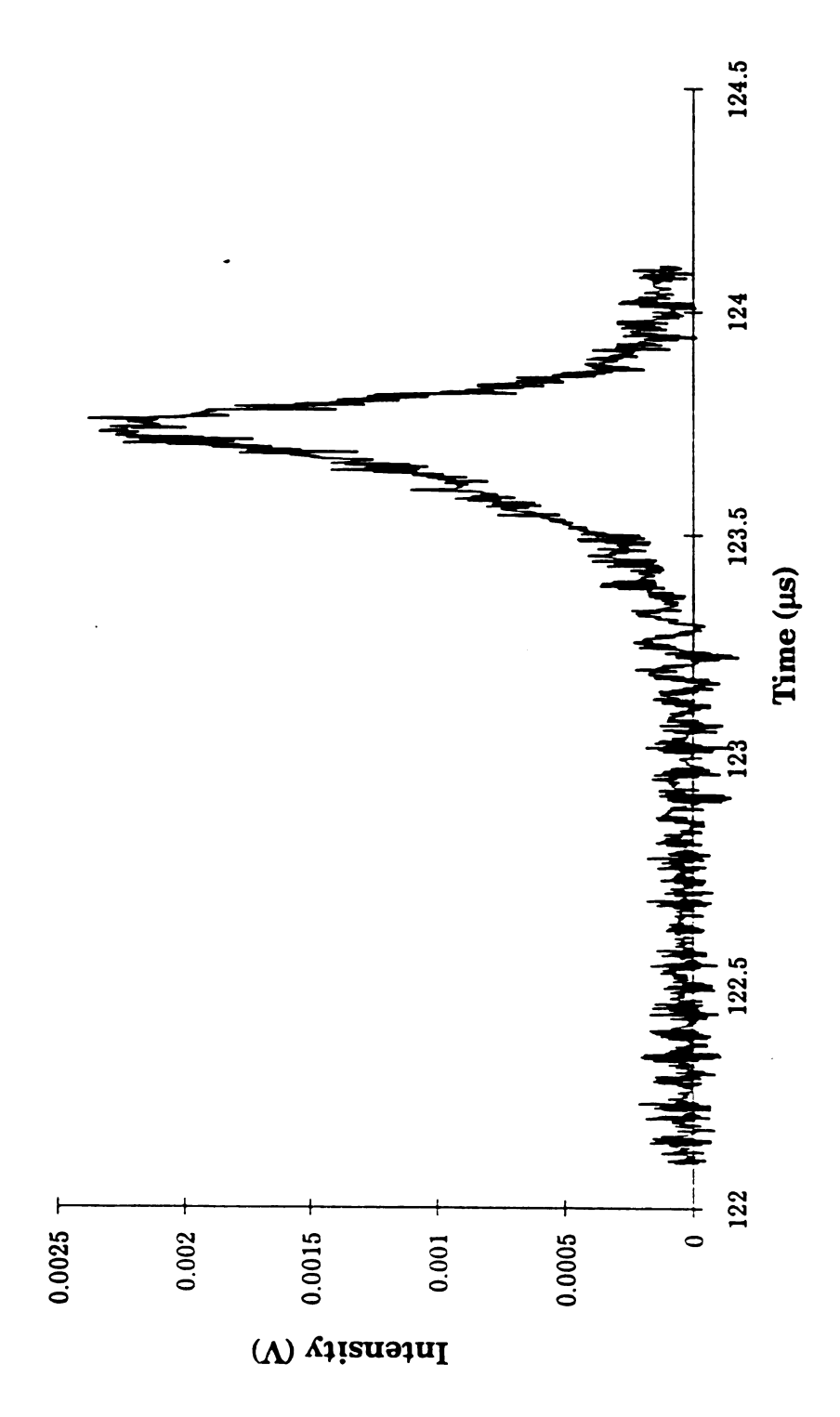


Figure 6.3 The bromobenzene product ion (m/z= 77) obtained after the second reflectron was retuned for lower kinetic energy ions.

detector must be placed at the origin. Knowing that the monopole field is hyperbolic (See Figure 6.4), this focusing ability was modeled with SIMION. As shown in Figure 6.5 the focal point for ions with 100-150 eV as well as for ions with 800 - 875 eV were indeed focused at the origin (x = 75) of this reflectron. Unfortunately, constructing such an extended monopole would be quite difficult. A conical monopole reflectron was modeled to determine if it could achieve the same resolution as an extended monopole system. A conical reflectron has electrodes which are symmetric about the x axis. As seen in Figure 6.6, this reflectron did not achieve energy independent focusing.

The challenge of developing a reflectron capable of focusing a large range of kinetic energies has recently been undertaken by both Qinchung Ji, and Paul Vlasak. Using SIMION, mathematical modeling and a numerical method for achieving a nearly perfect reflectron, they have already achieved very promising results.

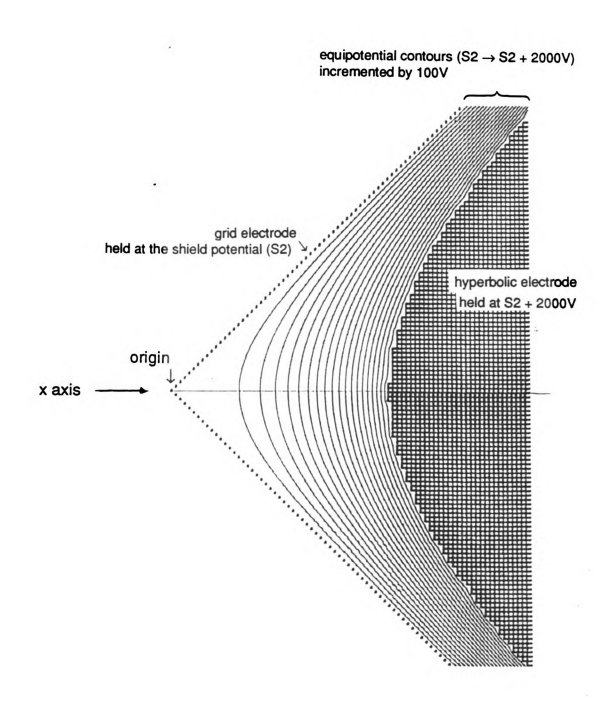
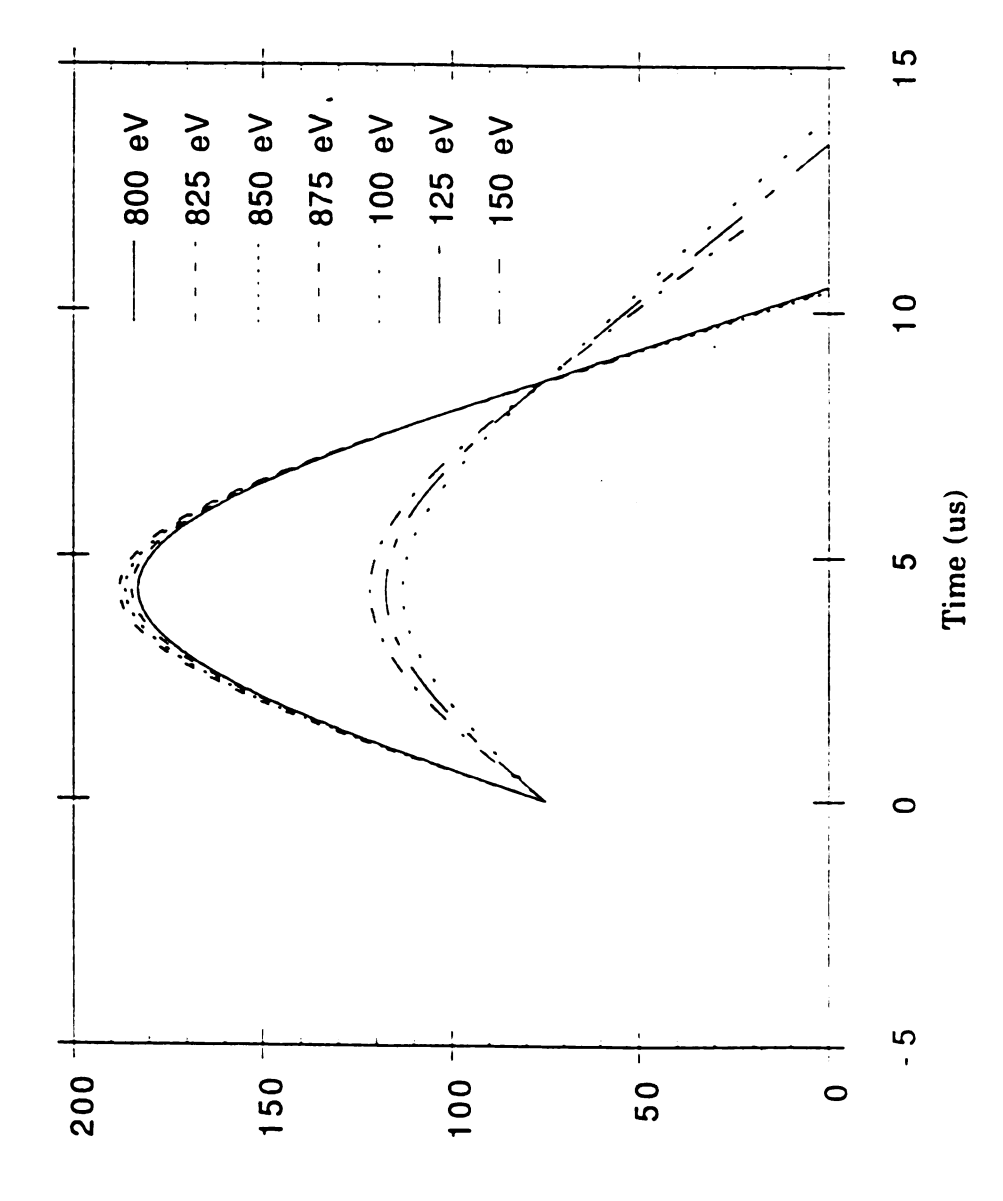
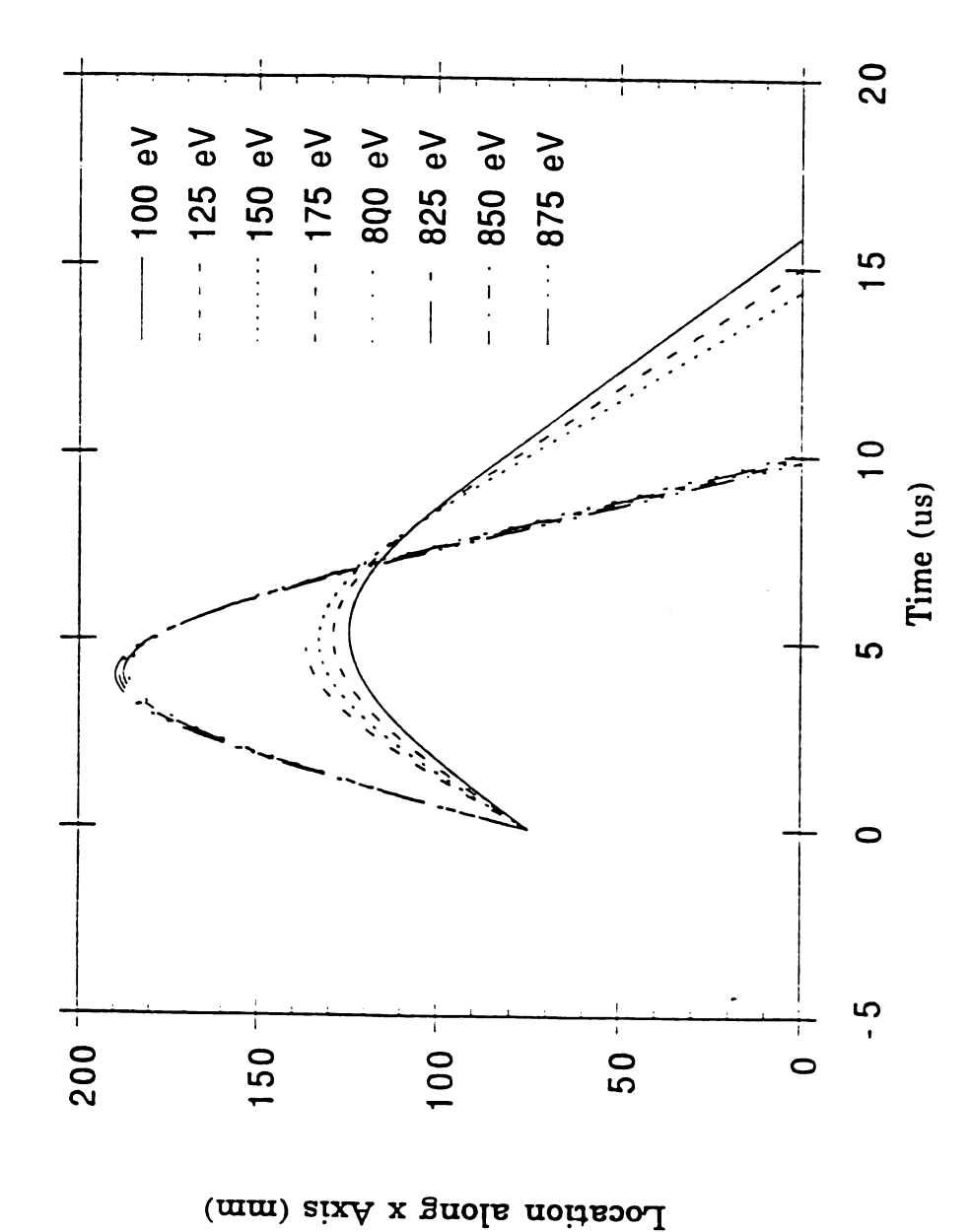


Figure 6.4 SIMION model of a hyperbolic reflectron. The two electrodes used to form this reflectron include a grid electrode and a hyperbolic electrode. In one model both of these electrodes extend perpendicular to this page and are of infinite length, in the other model these electrodes are symmetric about the x axis. Ions enter these mirrors at the origin of the grid electrode and travel towards the hyperbolic electrode with no y velocity component.



Location along the x Axis

Graph of the location an ion along the x axis versus time for ions with a large range of energies. The origin is located at x = 75. Ions which at the origin when they enter the reflectron, exit the reflectron at the origin have a wide range of different energies, and which are temporally focused and are again in temporal focus. This simulation was performed on an extended monopole Figure 6.5



Graph of the location an ion along the x axis versus time for ions simulation was performed on a conical reflectron. Ions which have a wide range of different energies, and which are temporally focused at the origin when they enter the reflectron, are not temporally focused with this The origin is located at x = 75. with a large range of energies. reflectron. Figure 6.6

References

- 1 R. M. Gandy, R. Ampulski, J. Prusaczyk, R. H. Johnsen, *Int. J. Mass Spectrom. Ion Physics*, **1977**, 24, 363.
- 2 S. Della-Negra, Y. L. SeBeyec, *Anal. Chem.*, **1985**, 57, 2035.
- 3 K. G. Standing, R. Beavis, G. Bolbach, W. Ens, F. Lafortune, D. Main, B. Schueler, X. Tang, J. B. Westmore, *Anal. Instru.*, **1987**, 16, 173.
- 4 G. L. Glish, S. A. McLuckey, H. S. McKown, *Anal. Instr.*, **1987**, 16, 191.
- 5 K. Schey, R. G. Cooks, R. Grix, H. Wollnik, *Int. J. Mass Spectrom. Ion Proc.*, **1987**, 77, 49.
- D. H. Russell, Presented at the 37th ASMS Conference on Mass Spectrometry and Allied Topics, Miami Beach, FL, May 21-26, 1989.
- 7 R. Weinkauf, K. Walter, C. Weickhardt, U. Boesl, E. W. Schlag, Z Naturforsch, 1989, 44a, 1219.
- 8 Personal communication with R. Grix, 1989.
- 9 K. LaiHing, P. Y. Cheng, T. G. Taylor, K. F. Willey, M. Peschke, M. A. Duncan, *Anal. Chem.* 1989, 61, 1460.
- 10 V. I. Karataev, B. A. Mamyrin, D. V. Shmikk, *IFT Physics-Technical Physics*, **1973**, 37, 1177.
- A. L. Rockwood, Presented at the 34th ASMS Conference on Mass Spectrometry and Allied Topics, Cincinnati, OH, June 8-13, 1986, 173.

Chapter 7: Conclusions

"The reward for a thing well done is to have done it."

Ralph Waldo Emerson

Throughout the design and construction of the tandem time-of-flight instrument there were numerous instrumental requirements each of which were critical to the goals of achieving MS/MS on the chromatographic time scale with this instrument. Although this instrument was significantly based on existing technology, fulfillment of these requirements was still uncertain. They included:

- The ability to produce a source which could store continuously produced ions and perform reproducibly from one day to the next.
- The ability to focus the ions enough radially such that a significant fraction would interact with the laser pulse.
- The ability to accurately and precisely time the laser pulse to interact with only one m/z value.
- The ability to achieve significant fragmentation with photodissociation.
- The ability to guide ions through two reflectrons without significant ion loss.

 The ability to focus the fragment ions despite the large range of kinetic energies.

One steady step at a time, a new instrument has been constructed, and these instrumentation goals have been met [11,2]. With the instrumentation requirements of the TOF/TOF demonstrated, actually achieving MS/MS acquisition speeds compatible with chromatographically eluting compounds is imminent. There is still, however, the need for an instrument control system, a time-array detection system, and a data control system which are compatible with this instrument. Complete implementation of the GC/MS/MS will require real-time calculation of interaction region arrival times of precursors and real-time laser timing control. Achieving these capabilities, will undoubtedly require significant effort and creativity.

The future of this TOF/TOF instrument is very promising and exciting. The capability of obtaining product spectra at least 100 times faster than current instrumentation will allow researchers to obtain complete MS/MS spectra from chromatographically eluting compounds. In addition, researchers currently limited to single or multiple reaction monitoring in GC/MS/MS applications will be able to monitor all possible reactions of a precursor m/z value with no loss in sensitivity.

Although this instrument was designed for GC/MS/MS, its use with other separation techniques and other forms of ionization including HPLC, CZE, MALDI and electrospray are equally provoking. Some of the most significant advances in mass spectrometry in the last 10 years have been in the ionization of molecules of higher and higher mass. These methods, however, do not provide significant fragmentation for structural interpretation. The unlimited mass range of the TOF/TOF instrument, as well as the high mass fragmentation

capability of photodissociation, may allow the TOF/TOF instrument to provide structural information from such large molecules. Equally significant, these data may be produced from small aliquots of unpurified real samples allowing direct analysis of biological molecules from blood, cell tissue and other samples of limited quantity.

References

- 1 Paul Vlasak, Doctoral Disseration, Michigan State University (in progress)
- 2 Qinchung Ji, Doctoral Dissertation, Michigan State University (in progress)